Characterization of small molecule inhibitors of PINK1

Tara Shomali

Department of Pharmacology and Therapeutics

McGill University, Montreal

December 15, 2022

A thesis submitted to McGill university

in partial fulfillment of the requirements of the degree of

Master of Science

Table of Contents

i. English Abstract

Parkinson's disease (PD) is a devastating neurodegenerative disease which is increasingly affecting our ageing population. The autosomal recessive juvenile form of PD is caused by loss of function mutations in proteins including the PINK1 kinase. Under physiological conditions, PINK1 is responsible for sensing mitochondrial damage and initiating mitochondrial turnover pathways. Modulation of PINK1 through small molecules could help reinstate PINK1's function and provide an important research tool in PD. Here our goal is to characterize small molecule inhibitors of PINK1 as leads for the development of tool compounds. In this project, we used a luminescence-based kinase assay to determine the IC_{50} of PINK1 inhibitors previously identified through thermal shift assays. The IC_{50} of PRT062607, PRT060318, JNJ-7706621, CYC116 and TAK659 were determined to be 1.6 ± 1.2 μM, 2.5 ± 1.2 μM, 30.4 ± 1.2 μM, 76.7 ± 1.1 μM and 7.2 ± 1.1 μM respectively against the insect *Tribolium castaneum* (Tc)PINK1. Crystal structures of TcPINK1 bound to PRT062607 and CYC116 were determined by our laboratory and confirmed that they bind in the adenosine triphosphoate (ATP) binding site. Since active *Homo sapiens* (Hs) PINK1 cannot be purified in *Escherichia coli*, we developed a surrogate humanized TcPINK1 construct, in which human-like mutations were introduced in the ATP binding domain, where the inhibitors bind. We determined that the ATP binding pocket might differ between orthologues as the IC_{50} values obtained are 1.5 ± 1.1 μM for PRT062607 and 18.1 ± 1.3 μM for PRT060318. This work provides the baseline for development of PRT062607 derivatives with higher potency. Furthermore, the humanized TcPINK1 construct provides a basis for HsPINK1 specific modulators, a method which has not been explored before for PINK1.

ii. Résumé

La maladie de Parkinson (MP) est une maladie neurodégénérative dévastatrice qui touche de plus en plus notre population vieillissante. La forme juvénile autosomique récessive de la MP est causée par des mutations de perte de fonction dans des protéines, dont la kinase PINK1. Sous des conditions physiologiques, PINK1 est responsable de la détection des lésions mitochondriales et du déclenchement des voies de renouvellement des mitochondries. La modulation de PINK1 par de petites molécules pourrait aider à rétablir la fonction de la kinase et constituer un outil de recherche important dans la MP. Notre objectif est de caractériser des petites molécules inhibitrices de PINK1 comme points de départ pour le développement de composés chimiques plus puissants et sélectifs. Au cours de cette thèse, les CI50 des inhibiteurs de PINK1 ont été déterminées. Les CI50 de PRT062607, PRT060318, JNJ-7706621, CYC116 et TAK659 sont 1,6 ± 1,2 μM, 2,5 ± 1,2 μM, 30,4 ± 1,2 μM, 76,7 ± 1,1 μM et 7,2 ± 1,1 μM respectivement envers l'isoforme de PINK1 dérivé de l'insecte *Tribolium castaneum* (TcPINK1). Après avoir déterminé les CI50, l'activité de ces inhibiteurs devait être mesurée contre l'isoforme *Homo sapiens* (HsPINK1). Cependant, HsPINK1 ne peut pas être purifié à partir de *Escherichia coli*. Ce défi a été surmonté en développant une construction TcPINK1 humanisée, dans laquelle des mutations ont été introduites dans le domaine de liaison à l'ATP, où les inhibiteurs se lient. Nous montrons que ce domaine pourrait différer entre l'espèce humaine et insecte, car la valeur de CI50 obtenue est 18,1 ± 1,3 μM pour PRT060318, mais 1,5 ± 1,3 μM pour PRT062607. La construction humanisée de TcPINK1 servira de modèle pour le développement de dérivés de PRT062607 plus puissants envers PINK1.

iii. Acknowledgements

I would like to express my gratitude towards Dr. Jean-François Trempe who has helped me throughout the past several years by providing me with a learning environment and amazing support. Dr Trempe has shared his excitement and passion for science and helped navigate me towards being a better graduate student.

I am sincerely thankful to Shafqat Rasool, Simon Veyron, Andrew Bayne and Nathalie Croteau for generously providing their expertise and knowledge. I would also like to thank Mark Hancock and Kim Munro, members of the CRBS, for all their help.

I would also like to thank all the members of my committee, including my advisor Dr Terrence Hebert, Dr Jason Tanny and Dr Jerry Pelletier who helped guide my project.

Special thanks to my parents, Arya Shomali, Jimmy Ibarra, Christina Guluzian and Emma Wilson for helping me every step of the way. I would also like to thank Jerry Dong, Sabrina Romanelli, Stefanie Kouzas, Hanna Bahsa.

iv. Contribution of Authors

The Thermal Shift Assay shown in figure 3, the in organello assay in methods 2.11 and figure 16 were performed by Nathalie Croteau. Figure 16 was adapted from Dr Trempe's figures as part of a CIHR grant submission. The design of the 6-aromatic TcPINK1 protein was done by Shafqat Rasool. Figure 1 was adapted from Rasool et al 2022. The crystal structures of TcPINK1 bound to CYC116 and PRT062607 were determined by Shafqat Rasool and Simon Veyron. All other experiments presented were performed by me and designed by Dr Trempe.

v. List of Abbreviations

1NM-PP1 1-tertbutyl-3-naphthalen-1-ylmethyl-1H-pyrazolo[3,4-d] pyrimidin-4-ylemine

ACN Acetonitrile

ADP Adenosine diphosphate

ATP Adenosine triphosphate

AUC Analytical ultracentrifugation

CamKII calcium/calmodulin-dependant protein kinase II

CCCP Carbonyl cyanide m-chlorophenyl hydrazone

CDK Cyclin dependant kinase

CLL Chronic lymphocytic leukemia

CTE C-terminal extension

ER Endoplasmic reticulum

F.A. Formic Acid

FLTK3 FMS-like tyrosine kinase 3

FT Flowthrough

GST Glutathione S-Transferase

HCN hyperpolarization-activated cyclic nucleotide-gate

HDX Hydrogen deuterium exchange

Hs *Homo sapiens*

IMM Inter mitochondrial membrane

Ire1 inositol-requiring enzyme 1

KO Knock out

KTP kinetin triphosphate

LB Lysogeny broth

LRRK2 Leucine rich repeat kinase 2

MAO-B monoamine oxidase B

MFN2 Mitofusin 2

MPP Mitochondrial processing protease

MPP+ 1-methyl-4-phenylpyridinium

MPPP Desmethylprodine

MPTP 1-methyl-4-phenyl-1,2,3,6-tetrahydropyridine

MQC Mitochondrial quality control

mtDNA Mitochondrial DNA

MTS Mitochondrial targeting sequence

NT N-term

OMM Outer mitochondrial membrane

OPTN Optineurin

OTC Ornithine transcarbamoylase

PAM Presequence translocase-associated motor

PARL Presenilin-associated rhomboid-like

PD Parkinson's Disease

Ph *Pediculus humanus corporis*

PINK1 PTEN-induced putative kinase 1

PKA Protein kinase A

pUB Phosphorylated Ubiquitin (at residue serine 65)

SAXS Small-angle X-ray scattering

SEC Size exclusion chromatography

SNARE SNAP receptors

SNpc Substantia nigra pars compacta

SYK Spleen tyrosine kinase

TBS Tris buffered saline

TC *Tribolium castaneum*

TIM Translocase of the inner mitochondrial membrane

TMD Transmembrane domain

TOM Translocase of the outer mitochondrial membrane

Ub Ubiquitin

Ub_4 tetraubiquitin

Ubl Ubiquitin like

UPR(mt) Mitochondrial unfolded protein response

WT Wild type

vi. Table of Figures (subtitles)

vii. List of tables (titles)

1. Introduction

Parkinson's disease (PD) is the most common movement disorder in our population. PD is characterized by many motor symptoms including resting tremor, bradykinesia, postural instability, as well as rigidity. Many patients also experience non-motor symptoms such as autonomic dysfunction, difficulty sleeping, loss of olfaction and mental health issues namely psychosis and dementia (Grimes et al., 2012; Poewe, 2008). Despite the increasing incidence in the ageing population, there is still no disease-modifying treatment for PD. Therapeutic avenues to alleviate PD symptoms involves the administration of levodopa (L-Dopa) alongside carbidopa, deep brain electrical stimulation and ablative surgeries (Cotzias et al., 1969; Grimes et al., 2012). The lack of treatment options stems from the complex pathology behind PD and its elusive neurological molecular mechanisms. The pathology of PD points us to the brain, an organ which requires high levels of energy obtained though oxidative phosphorylation by the mitochondria (Erecinska & Silver, 1989). Numerous studies have furthered our understanding of the selective vulnerability of dopaminergic neurons based on their pacemaking ability, broad action potentials, the presence of CaV1.3 channels and increased arborization (Surmeier, 2007).

The distinct electrophysiological and morphological characteristics of dopaminergic neurons increase mitochondrial bioenergetics and create higher levels of redox stress (Guzman et al 2010; Pacelli et al, 2015). Mitochondrial health and function play critical roles in PD and accordingly, the balance of mitochondrial degradation and biogenesis is critical for neuronal health (Van Laar & Berman, 2009). Interest in the mitochondria

in relation to PD was mainly sparked after the discovery that 1-methyl-4-phenyl-1,2,3,6-tetrahydropyridine (MPTP) administration in humans caused mitochondrial damage and Parkinsonian symptoms (Langston, 1987). Brains of PD patients also exhibit lower Complex I activity (Schapira et al 1989). The association with mitochondria was confirmed by identification of risk loci and genes contributing to PD. In particular, loss of function mutations in *PRKN* and *PINK1*, encoding the proteins Parkin and PTEN-induced putative kinase 1 (PINK1), cause the majority of early-onset (below 50 years old) recessive cases (Chang et al., 2017; Hardy, 2010). Parkin and PINK are important players in a mitochondrial quality control (MQC) pathway (Clark et al., 2006; Narendra et al., 2008).

Although we have dedicated years of research to PD, there is still a gap of knowledge in relation to pathophysiology of PD and the lack of treatment. The proteins involved in MQC pathways could be utilized in the progress towards finding disease modifying treatment. Of the aforementioned proteins, PINK1 is a kinase implicated in the MQC pathway, thereby making it a good pharmacological target. However, there are many constraints regarding our understanding and our ability to utilize PINK1 in vitro, in vivo and as a target. In this thesis, I will be presenting potential strategies to address these constraints, specifically the lack of PINK1 tool compounds, and the inability to obtain recombinant human PINK1 protein.

1.1 Treatment for PD

A study conducted between 1990 and 2016 by the Global Burden of Disease determined that the prevalence, disability-adjusted life-years and deaths associated with PD had increased by 20% in each of these categories. Other neurological diseases such as Alzheimer's disease and multiple sclerosis did not see such a drastic change (GBD 2016 Neurology Collaborators, 2019). Given that age is the primary risk factor for this illness, it is predicted that the incidence of PD will double in the next 30 years (Tolosa et al., 2021).

Despite the increase in prevalence, there is still no diagnostic tools or readily accessible biomarkers available for diagnosis of PD. Most clinicians will diagnose PD based on the four cardinal signs including tremor, bradykinesia, rigor and postural instability, and based on how well patients respond to levodopa treatment (Bereczki, 2010). However, the diagnosis can only be confirmed post-mortem as the brain of PD patients display degeneration of their substantia nigra pars compacta (SNpc) or display the presence of abnormal α-synuclein aggregates called Lewy pathology (Dauer & Przedborski, 2003; Maries et al., 2003).

One of many challenges surrounding PD research is the lack of disease-modifying treatment. Patients who are diagnosed with PD are prescribed levodopa alongside carbidopa to supress unwanted motor symptoms (Cotzias et al., 1969). Levodopa is an amino acid precursor which gets converted to L-tyrosine and is used by the central nervous system to make dopamine. Since levodopa is decarboxylated in the periphery

by dopa-decarboxylase, most of the drug is unable to reach the brain as L-tyrosine does not cross the blood brain barrier. To bypass this, levodopa is co-administered with carbidopa, a peripheral inhibitor of dopa-decarboxylase, resulting in a higher concentration of levodopa reaching the brain ("Sinemet," 1974).

A concern that arises with the administration of levodopa is the diminishing responsiveness to drug treatment over time as well as increased dyskinesia with prolonged treatment (Contin & Martinelli, 2010). Levodopa increases dopamine levels; however, it needs to be taken several times, in between doses there is a drop in dopamine levels. The fluctuation in levels of dopamine in plasma and the altered pre- and post-synaptic levels of nigrostriatal neurons seem to mediate levodopa induced dyskinesia (Pandey & Srivanitchapoom, 2017). Another treatment option for those patients would include deep brain stimulation of the subthalamic nucleus or the globus pallidus internus and ablative lesions (Grimes et al., 2012). These treatment options do not come without concern, as they have been found to lose efficacy over time, and in some instances, worsen the progression of the disease by increasing the rate of degeneration of the neurons (Kasemsuk et al., 2017).

1.2 Selective vulnerability of dopaminergic neurons

In PD, the motor symptoms arise from the loss of dopaminergic neurons in the substantia nigra pars compacta (SNpc) of the midbrain, which disrupts signal relay to the striatum leading to the impairment of motor function. The appearance of parkinsonian symptoms would only begin once about 60% of the neurons had been

deteriorated (Surmeier, 2007). The rationale regarding the localized loss of neurons arises from the selective vulnerability of dopaminergic neurons in that region. The SNpc neurons are pacemakers, however they differ from other pacemakers because they rely on L-type calcium and hyperpolarization-activated cyclic nucleotide–gated (HCN) cation channels in addition to sodium channels (Ping & Shepard, 1996). These brain calcium channels are also different from the calcium channels found in the heart as the neuronal ones are formed by the CaV1.3 subunit while those in the heart are mainly CaV1.2 (Striessnig et al., 2006). Following an action potential, calcium flows into the cells and needs to be quickly pumped extracellularly in order to maintain membrane potential. The channels in these neurons however display slow kinetics, they are open for long periods of time and are slower in closing the channels (Wilson & Callaway, 2000). Contrary to most neurons, the affected SNpc dopaminergic neurons also lack calbindin which is responsible for buffering calcium (Guzman et al., 2015). Increased intracellular levels of calcium burdens these cells and potentially leads to quicker ageing and thus neuronal death (Surmeier, 2007).

In order to compensate for this extra calcium, SNpc neurons deploy a variety of mechanisms. Firstly, membrane transporters, which consume ATP, will transport calcium out of the cells, however they are slow to do so. Another mechanism is through sequestering of calcium by the mitochondria and endoplasmic reticulum (ER) (Szabadkai et al., 2006). The calcium is transported with ATP-dependant transporters from the cytosol into the ER lumen. However, when the internal levels of calcium are too high in the ER, the calcium is released back into the cytoplasm via calcium

channels which are in proximity to mitochondria (Berridge, 1998). This will lead to increased mitochondrial uptake of calcium through uniporters present on the mitochondrial membrane, causing electrochemical imbalance in the mitochondrial matrix which is very energetically expensive for the mitochondria (Rizzuto & Pozzan, 2006). This increased use of ATP leads to overworked neurons and faster ageing. Oxidative phosphorylation produces free radicals and reactive oxidative species which when accumulated, could damage the mitochondria (Guo et al., 2013). Blocking the calcium import from L-type calcium channels with isradipine and measuring dendritic versus somatic recording of calcium currents show an L-type calcium channel dependent current influx in SNpc dopaminergic cells (Guzman et al., 2015). Blocking the mitochondria uniporter with a selective inhibitor also shows decreased levels of oxidative stress in the mitochondria, linking increase in calcium concentrations to oxidative stress accumulation (Guzman et al., 2015). Some of the accumulating stress is dealt with using the ubiquitin-proteasome system and autophagic vacuoles, dysfunctions in which would lead to accumulated stress in mitochondria as well (Betarbet et al., 2006; Surmeier, 2007).

1.3 Mitochondrial damage in Parkinson's Disease

The etiology of PD is still undetermined, however there are some indications leading researchers to focus on the mitochondria. The first hint arose between 1976 and 1983, when several young individuals were found to have developed parkinsonian-like symptoms. A commonality between these individuals was the use of a synthesized drug, desmethylprodine (MPPP), which was found to be contaminated with MPTP

(Langston, 1987). This compound is converted by monoamide oxidase (MAO-B) to 1-methyl-4-phenylpyridinium (MPP^+), an inhibitor of complex I of the mitochondrial electron transport chain (Langston, 2017). Complex I disruption by MPP^+ can cause inability of the cell to produce ATP and accumulation of reactive oxygen species which can in turn lead to DNA damage and disruption in ion homeostasis such as calcium (Rizzuto & Pozzan, 2006). Researchers thereby started investigating the role of the mitochondrial damage in PD.

Another indication of the involvement of SNpc neuronal mitochondrial dysfunction arose from PD patient autopsies. Post-mortem analysis of patient brain tissues revealed complex I deficiencies and mitochondrial DNA (mtDNA) damage (Bender et al., 2006; Schapira et al., 1989). The implication of complex I and mtDNA damage guided researchers to investigate other compounds which might negatively affect these pathways. They found two compounds which increased risk of PD, the pesticide rotenone and the herbicide paraquat, were complex I inhibitors as well (Dick et al., 2007). These discoveries further confirmed the implication of mitochondria dysfunction in disease pathology.

1.4 Genetics of Parkinson's Disease

Recent loci mapping and genome wide association studies have provided a precise understanding of the main genes involved in the onset and progression of PD. Over 90% of all cases of PD as sporadic, whilst 10% can be attributed to genetic etiology (Thomas & Beal, 2007). Autosomal dominant PD is caused by mutations of *SNCA* or *LRRK2*, while

autosomal recessive cases are caused by mutations in *PRKN* and *PINK1* (Puschmann, 2013).

A hallmark of PD is the presence of Lewy bodies in the brain of patients, which are composed of α-synuclein protein aggregates, encoded by the *SNCA* gene (Conway et al., 2000). In normal physiological conditions, α-synuclein is thought to be interacting with synaptobrevin to stimulate the formation of SNAP receptor (SNARE) vesicles and the release of neurotransmitters (Diao et al., 2013). Synucleinopathy has been found in 90% of PD cases, but loss of function of the protein does not lead to any PD symptoms or striatal degeneration in mice (Abeliovich et al., 2000; Riederer et al., 2019; Singleton et al., 2003). Large quantities of unfolded α-synuclein tend to aggregate and form oligomers and fibrils and lead to impairment of neuronal communications and is believed to spread to healthy neurons (Burke et al., 2008; Sian-Hulsmann et al., 2015).

The spread of Lewy bodies across the brain is associated with disease severity. Spreading areas have been categorized into ‘Braak staging’ which first begins at the olfactory bulb, vagus nerve and enteric plexus. The second part involves spreading to the medulla oblongata, raphe nuclei and locus coeruleus which correspond to autonomic and olfactory disturbances. Thirdly, they are found in the central subnucleus of the amygdala, substantia nigra pars compacta and temporal mesocortex which are related to sleep and motor disturbances. Finally, they reach the

insular and cingulate mesocortex and the primary neocortex which account for emotional and cognitive disturbances (Braak et al., 2004).

Leucine rich Repeat Kinase 2 (LRRK2) has both a serine/threonine protein kinase domain and ROC-type GTPase domain (Li et al., 2014). LRKK2 mutations account for the majority of the hereditary cases of PD (Dauer & Ho, 2010). LRRK2 has been found to be involved in several different signaling cascades such as Rab phosphorylation, immune cell response and even MAPK signalling pathways (Dzamko et al., 2012; Gloeckner et al., 2009; Madero-Perez et al., 2018; Steger et al., 2017). Gain of function mutations of this protein have been closely linked to familial autosomal dominant late onset forms of PD (Paisan-Ruiz et al., 2004; Zimprich et al., 2004). Most mutations in LRRK2 are found within its kinase domain or its GTPase domain and increase the protein's activity (Cookson, 2010). The most common activating mutation is the G2019S mutant, found in a large number of Ashkenazi Jews and north Africans and accounts for nearly 29% and 37% of hereditary PD cases in these populations respectively (Lesage et al., 2005; Ozelius et al., 2006).

PRKN and *PINK1* genes are associated with autosomal recessive early onset PD cases (Kitada et al., 1998; Valente, Abou-Sleiman, et al., 2004). Taken together, Parkin and PINK1 mutations account for over 50% of the recessive cases of PD, but only about 1-2% of the overall disease (Ibanez et al., 2006). These affected genes are not completely alienated from the Lewy body pathology, as some patients with Parkin/PINK1 mutations were also found to have Lewy body disease (Samaranch *et*

al., 2010). Despite their accounting for a low number of cases, Parkin and PINK1 mutations have shown definitive implications in PD pathology in which mutations cause loss of function of the protein (Lucking et al., 2000; Valente, Abou-Sleiman, et al., 2004). These association to PD makes them candidates for research into understanding the pathology in association with mitochondrial damage and into deciphering a mechanism with clinical utility (Martin et al., 2011).

The *PRKN* gene, encodes the E3 ubiquitin ligase Parkin, and mutations leading to PD are found in almost all domains of Parkin and result in loss-of-function of Parkin (Shimura et al., 2000). To further narrow the pathway which Parkin influenced, knock-out models of *Drosophila* were generated and found to have muscle degeneration, flight defects and sterility issues, which are linked back to abnormalities in their mitochondria (Greene et al., 2003). The physiological function of Parkin in relation to PD will be further discussed in latter sections.

On the other hand, *PINK1* was initially discovered as one of the genes upstream of the PTEN (tumor suppressor) pathways in ovarian cancer (Unoki & Nakamura, 2001). PINK1 is a serine/threonine kinase expressed in the cytosol of cells and localized to the mitochondria (Okatsu et al., 2015). Loss of function mutations of PINK1 were deemed to increase cells to stress and were found to be expressed throughout the body (Shimura et al., 2000). Others have found that PINK1 loss of function tends to increase the susceptibility of cells to stress and dysfunction (Valente, Salvi, et al., 2004). PINK1 knock-out (KO) models in drosophila also display similar defects as the

Parkin model, suggesting that PINK1 and Parkin might be affecting the same pathway (Clark et al., 2006). This was validated as overexpression of Parkin did rescue PINK1 deficient drosophila, while PINK1 overexpression in Parkin deficient drosophila did not rescue the phenotype. This corroborates that the two proteins converge on a single pathway and suggests that PINK1 is an upstream effector of Parkin and a defendant of mitochondrial health (Park et al., 2006). Taken together, the mitochondrial localization and its involvement in oxidative stress links PINK1 to mitochondrial quality control.

1.5 Parkin and PINK1 mediated clearance of damaged mitochondria

1.5.1. PINK1 structure in relation to its activation and activity

PINK1 is a 63 kDa serine/threonine bi-lobular kinase whose structure has been recently elucidated by X-ray crystallography and enhanced our understanding of the association between PINK1's structure and its activity. Five years ago, the first structures of PINK1 were published. The first structure was the apo structure of *Tribolium castaneum* PINK1 (TcPINK1) (Kumar et al., 2017). The second structure included AMP-PNP (a non-hydrolysable form of ATP) bound to TcPINK1 (Okatsu et al., 2018). The third important structure was that of a nanobody and ubiquitin^{TVLN} (Ub^{TVLN}) (Thr66Val and Leu67Asp mutant ubiquitin (Ub) which confers the minor conformation of Ub) bound to Pediculus humanus corporis (PhPINK1) protein (Schubert et al., 2017). In addition to these structures, small-angle X-ray scattering (SAXS) modelling and hydrogen-deuterium exchange spectrometry (HDX) performed on TcPINK1 revealed more about the dynamics of the protein. More specifically, it

revealed that phosphorylation of Ser205 induces conformational change of the kinase, and revealed flexibility of certain domain of the protein (Rasool et al., 2018). It is by virtue of these structures and modelling that much of the molecular dynamics of PINK1 in relation to bound and un-bound states were determined.

PINK1's structure has an N-terminal mitochondrial targeting sequence (MTS), followed by a transmembrane domain (TMD) harbouring the Ala103-Phe104 cleavage site for presenilin-associated rhomboid-like protease (PARL) (Deas et al., 2011). The MTS contains known PD mutations which were revealed to impair the ability of PINK1 to stabilize on the outer membrane (I111S, C125G, Q126P) (Sekine et al., 2019). The MTS is followed by an N-term (NT) linker which houses two PD mutations, C125G and Q126P, and is important to stabilize the αK helix of the C-terminal extension (CTE) through interactions (Rasool et al., 2022). These interactions involve hydrophobic contacts between Ile133 and Ile137 of the NT helix, and Leu507, Leu508 and Leu515 of the αK helix. Indeed, mutations of these residues abolished the ability of the two regions to bind to each other (Rasool et al., 2022). The final region is the CTE, which sits on the back of the C-lobe and away from the active site. Its αK helix binds back to N-terminal helix (NT) and forms stabilizing interactions which are critical for the stability of the protein. Surprisingly, the CTE region of the protein is amongst the most non-conserved regions of PINK1 amongst its homologues.

Following the NT linker, PINK1 has its first lobe, referred to as the N lobe which contains 3 unique inserts as well as the αC helix. Insert 1's structure remains unsolved

as it is the most disordered of the inserts and the most non-conserved between insect and human homologues (Cardona et al., 2011). Despite not knowing the structure or function of this insert, it is likely important as the mutation P196L it harbours leads to PD (Song et al., 2013). Insert 2 is required for the autophosphorylation of PINK1 as it contains the αi helix which binds and stabilizes the αC helix (Figure 1). The αi helix bound to αC, activation loop (A-loop) from the hinge region and αEF helix together form the autophosphorylation interface which accommodates the opposing PINK1's A-loop (Rasool et al., 2022). Insert 3 is critical for Ub and UbL phosphorylation and is the most conserved amongst the inserts. Insert 3 can only bind its substrate after a conformational shift in PINK1 following its autophosphorylation (Rasool & Trempe, 2018).

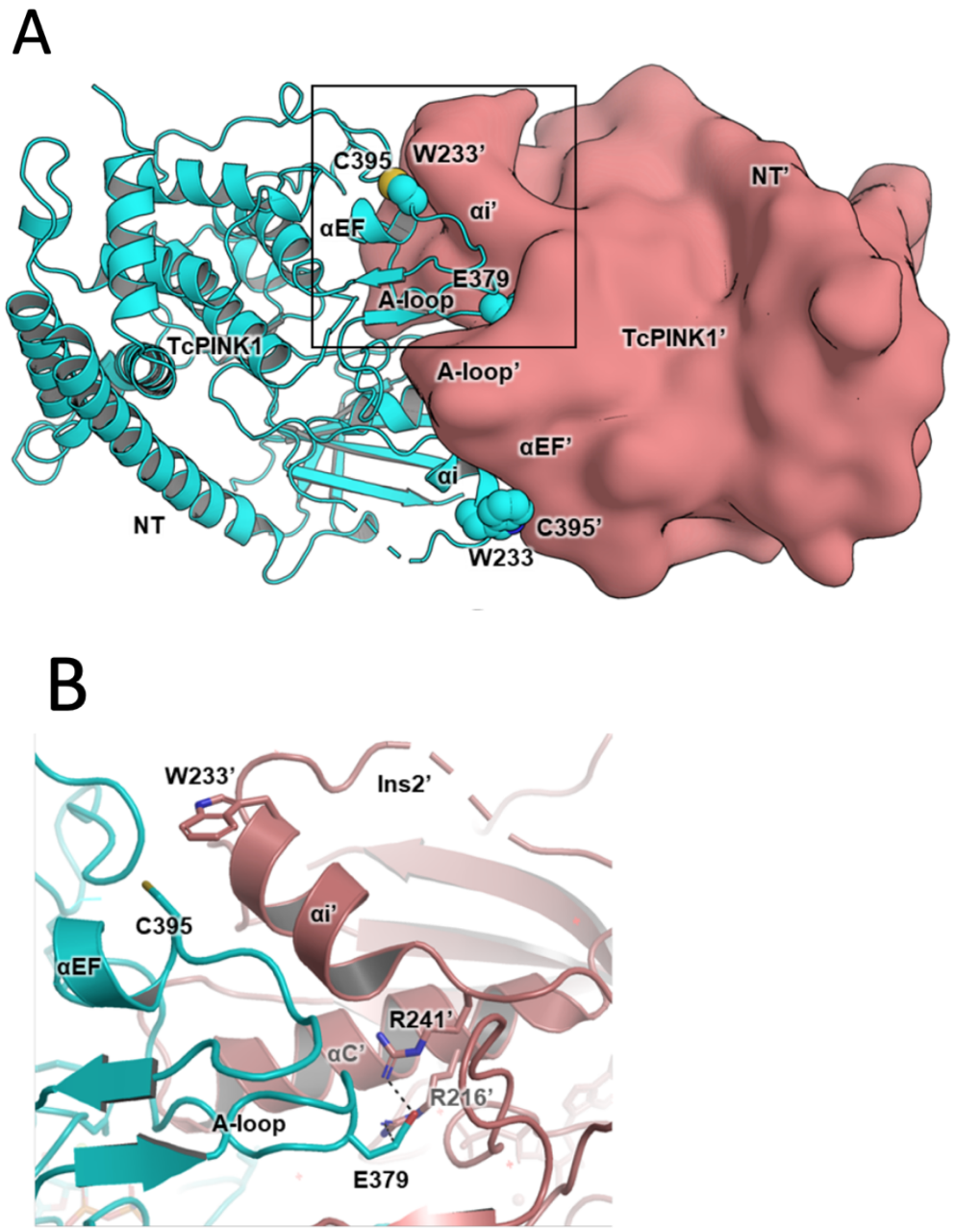

Figure 1. Dimer of TcPINK1 and autophosphorylation interface.

(A) Depiction of two PINK1 in a dimer conformation. The monomer shown in salmon has its domains annotated with a prime to differentiate them from the domain of the cyan monomer. (B) Zoomed in section of panel A shows the cyan A-loop residue Glu379 interacting with Arg241' of the αi and Arg216 of the αC'. This figure was adapted from Rasool et al., 2022.

The region following the N-lobe and prior to the C-lobe is referred to as the “hinge” region and corresponds to the catalytic kinase domain of PINK1, which contains its ATP binding pocket. Interestingly, the kinase domain of PINK1 holds structural similarity with the calcium/calmodulin-dependant protein kinase II (CamKII), otherwise, PINK1 is unique from any other kinases (Trempe & Fon, 2013). This region also houses the A-loop which mediates the Mg^{2+} ion required for catalysis, and a catalytic loop containing an Asp337 which mediates phosphoryl transfer from ATP (Cardona et al., 2011; Sim et al., 2012). The “hinge” is followed by the C-lobe consisting of 4 main alpha helices. The C-lobe is a very ordered region of PINK1 and mediates stabilizing interactions with the CTE (Kumar et al., 2017).

1.5.2 Detailed mechanism of autophosphorylation

Dimerization at the OMM is essential for PINK1’s activity as it allows transphosphorylation to take place at Ser228 in HsPINK1 (Ser205 in TcPINK1, and Ser202 PhPINK1). In the dimer, the C-loop forms an interaction with the opposing A-loop and is stabilized by residue Lys339 (HsPINK1) in the catalytic loop (Rasool et al., 2022). Phosphorylation will occur on the opposing PINK1’s C loop of the N-lobe. This is unusual for kinases as autophosphorylation site usually lies within the A-loop and is mediated by an αG helix, while in PINK1, it is located in the C-loop (Rasool et al., 2022). This transphosphorylation will allow PINK1 to shift confirmation by creating a 90˚ kink in the αC helix, the C-loop moves from an “in” to an “out” state. When in the “in” state, the C-loop creates a stable interaction with the αi and the αC helix, when in the “out” state, this interaction is abolished (Rasool et al., 2018). This conformational

shift also reconfigures the insert 3, as it adopts a partial helix conformation and pushes the glycine rich loop (G-loop) into the active site. In unphosphorylated PINK1, the G-loop would clash with Ub or Ubiquitin like (Ubl) binding, thus requiring PINK1 autophosphorylation to prime substrate interactions. This primed PINK1 will now be able to accommodate ubiquitin and the Ubl domain of Parkin in its insert 3, this step is critical as inhibition of autophosphorylation will yield inactive PINK1 (Rasool et al., 2018).

1.5.3 PINK1 and Parkin in mitochondrial quality control

Given Parkin and PINK1's involvement in MQC pathways, we will dive deeper into the mechanism used by these proteins to ensure mitochondrial health. PINK1 is a ubiquitin kinase found in the cytosol and localizes to the mitochondrial membrane by its N-terminal mitochondrial targeting sequence (MTS) and its transmembrane segment (Okatsu et al., 2015; Silvestri et al., 2005; Valente, Salvi, et al., 2004). Under physiological conditions, PINK1 will localize to the outer mitochondrial membrane (OMM) and insert its MTS into the pore of the translocase of the outer mitochondrial membrane (TOM) complex formed by the TOM40 subunit (Okatsu et al., 2015). Indeed, there is a triad of glutamic acids (Glu112, 113, 117, or 3E motif) which are critical for the arrest and stabilization of PINK1 in the TOM complex in depolarized mitochondria (Sekine et al., 2019). Overall, PINK1 has previously been found on BN-PAGE to form a ~700 kDa complex with subunits of the TOM complex, amongst which are TOM20, TOM22, TOM40 and perhaps TOM70 (Lazarou et al., 2012; Okatsu et al., 2013). TOM20, TOM22, and TOM70 are subunits designed to recognize MTS

presequences on a preprotein (Brix et al., 1997). PINK1's MTS is then further pulled down through the translocase of the inner membrane (TIM) pore into the inner mitochondrial membrane (IMM) by the presequence translocase-associated motor (PAM) complex situated in the matrix (Caumont-Sarcos et al., 2020).

When mitochondria are not under stress, PINK1 will get sequentially cleaved at two locations, once by PARL and once by the mitochondrial processing peptidase (MPP) (Greene et al., 2012; Jin et al., 2010). While the exact cleavage site of MPP is to be determined, PARL cleaves PINK1 within its TMD between Ala103 and Phe104 (Deas et al., 2011; Greene et al., 2012; Jin et al., 2010). This 52 kDa truncated PINK1 will be released from the OMM and get degraded according to the N-term rule by E3 ligases UBR1, UBR2 and UBR4 (Narendra et al., 2010; Tasaki et al., 2012; Yamano & Youle, 2013).

Alternatively, if PINK1 localizes to damaged mitochondria, it will start to accumulate and dimerize on the surface of the OMM by sensing damage such as membrane depolarization (Kondapalli et al., 2012). PINK1 can also sense damage independently of depolarization. Other damage includes the accumulation of mutant ornithine transcarbamoylase (OTC), or knockdown of LONP1 protease (housekeeping AAA+ protease) resulting in unfolded protein response in the mitochondria (UPR(mt)) and leads to PINK1 buildup on OMM through accumulation of peroxidative stress, independently of any membrane depolarization (Burman et al., 2017; Jin & Youle,

2013; Thomas et al., 2014). This suggest that UPR(mt) is also sensed by PINK1, but their exact mechanism has not been elucidated yet.

As previously stated, dimerization of PINK1 is critical as it is required for the activation of PINK1. This activated form of PINK1 will phosphorylate neighbouring ubiquitin tethered on membrane proteins present on the mitochondrial outer membrane. Phosphorylated ubiquitin is found to be the signal which recruits Parkin (Shiba-Fukushima et al., 2012). Parkin is then recruited and when in proximity to PINK1, gets phosphorylated on serine 65 (Ser65) of its UbL domain, this pSer65 is critical for the activation of Parkin's ubiquitin ligase activity (Kondapalli et al., 2012; Narendra et al., 2010; Shiba-Fukushima et al., 2012).

Activated Parkin will start to ubiquitinate surrounding proteins, such as Mitofusin 2 (MFN2), thus providing more substrate for PINK1 and results in a feedforward loop leading to accumulation of many phospho-ubiquitin chains on the damaged mitochondria (Ordureau et al., 2014). MFN2 under physiological conditions would tether the ER to the mitochondria, but when ubiquitinated, it will let go of the ER and drive mitophagy (de Brito & Scorrano, 2008; McLelland et al., 2018). MFN2's strategic localization near PINK1 leads to selective recruitment and activation of Parkin and leads to rapid activation of mitophagy (Vranas et al., 2022).

Furthermore, polyubiquitin chains also recruit cargo receptor proteins such as optineurin (OPTN) and NDP52 to the mitochondria, which can also initiate mitophagy

(Lazarou et al., 2015). This pathway can be activated by PINK1 independently of Parkin although at a much slower rate. This again fortifies our decision in targeting PINK1 as a potential therapeutic for PD by increasing MQC and damaged mitochondrial clearance.

1.6 Kinases as therapeutic targets

1.6.1 Kinases as therapeutic targets

Kinases have recently gained popularity as pharmacological targets for their broad roles in regulating many pathways in the body. In the past 5 years, the number of small molecule kinase inhibitors approved by the FDA between 2016 and 2021 accounts for 15% of new approvals (Attwood et al., 2021). These kinase inhibitors are used to target a multitude of biological processes, targeting transcription, kinase signalling and proto-oncogenes in cancer, T cell checkpoint inhibitor, inflammation and vaccine adjuvants in the immune system, or ER stress (Ire1), angiogenesis and kinases involved in neurodegeneration (LRRK2) in degenerative diseases (Ferguson & Gray, 2018). Out of 538 known eukaryotic protein kinases, there are only 68 FDA approved small molecule inhibitors of kinases which treat 18 different diseases across 19 targeted kinases (Fabbro et al., 2015; Roskoski, 2022). Despite the increasing interest in kinases as drug targets, the field holds untapped potential as only a small percentage of kinases have so far been explored as targets (Botta, 2014; Fedorov et al., 2010).

1.6.2 Paradoxical agonists

Current work surrounding the use of kinase inhibitors as therapeutics involves proteins which regulate cell proliferation, differentiation and viability involved in oncogenesis (Fabbro et al., 2015). A review of kinase inhibitors and their molecular mechanisms has identified several inhibitors which through conformation modification can induce changes in protein localization, protein-protein interactions and enhancement of catalytic activity (Dar & Shokat, 2011). Amongst them is the RAF family of kinases, composed of the three RAF paralogues ARAF, BRAF and CRAF (Udell et al., 2011). These inhibitors were developed with the intent of reducing the activity of BRAF, but instead induced a paradoxical activation by promoting the dimerization of the RAF kinase domains (Lavoie et al., 2014). Similarly to PINK1, RAF isomers need to reposition their αC helix in order to adopt a catalytically active conformation and carry out phosphorylation of its substrates (Cheng & Niv, 2010). Through the binding of the inhibitor, the isomers would dimerize and the αC helix would thus adopt an active conformation on both proteins (despite only one monomer having the inhibitor bound). One such compound is Zm-336372, which was identified as an inhibitor of multiple RAF isoforms, but in vivo data alternatively shows activation of the CRAF isoform (Hall-Jackson et al., 1999).

Similarly, inositol-requiring enzyme 1 (Ire1) is also activated by the small molecule inhibitor 1-tertbutyl-3-naphthalen-1-ylmethyl-1H-pyrazolo[3,4-d] pyrimidin-4-ylemine (1NM-PP1). Ire1 is an ER transmembrane protein involved in the activation of the UPR (Papa et al., 2003). When Ire1 sense signals, its attached chaperones will dissociate

and instead engage with unfolded proteins (Patil & Walter, 2001). Surprisingly, inactive mutants of Ire1 were rescued by 1NM-PP1 and produced a full UPR response. Researchers have found that the occupancy of the active site by the inhibitor, even in the absence/inability of phosphorylation, was able to change conformation and lead to active protein response (Papa et al., 2003).

1.7 PINK1 kinase as a therapeutic target

1.7.1 Thermal shift screen identifies thermal stabilizers of PINK1

Given our current understanding on PINK1's role in MQC pathway and damaged mitochondrial clearance, this kinase has become a therapeutic target for the treatment of PD. The strategy would be to activate the PINK1 kinase in order to maintain the balance between biogenesis and degradation of mitochondria, as the accumulation of damage in mitochondria is linked to disease pathology (Bender et al., 2006). It is a good target because it has direct link to disease onset and kinases are a highly druggable class of enzymes. In the context of PD, PINK1 would need to be activated to reinstate the MQC pathway and maintain mitochondrial balance within neurons. In support of this idea, studies have shown that selective degeneration of SNpc neurons can be rescued by overexpressing PGC-1a, which reinstates mitochondrial biogenesis (Siddiqui et al., 2016). To this effect, one group discovered that a precursor of kinetin triphosphate (KTP) called kinetin binds the nucleotide domain of PINK1 with a higher affinity than ATP and can thus activate it in cells (Orr et al., 2017). This compound, as seen in Figure 2, has a furfurylamine group attached to the pyrimidine ring. However, despite being able to increase PINK1 activity in cells, kinetin was unable to rescue α-

synuclein induced neurodegeneration in rodent models (Orr et al., 2017). Nevertheless, the company Mitokinin submitted a patent on a class of molecules that can activate PINK1-dependent mitophagy in cells under sub-threshold levels of mitochondrial damage (de Roulet and Devita, 2015).

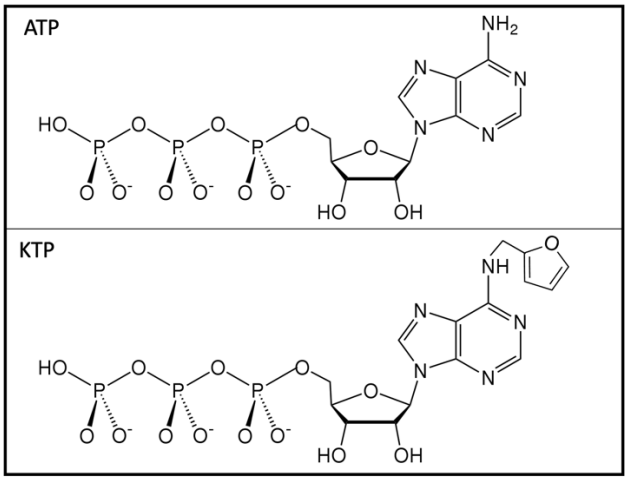

Figure 2. ATP and KTP structures.

The chemical structure of ATP is shown at the top of the figure while the structure of KTP is shown below. The only chemical difference between ATP and KTP is the addition of a furfuryl group on the nitrogen attached to the benzene ring. The affinity of PINK1 is 3-4 times higher compared ATP.

Instead of finding kinase activators, another potential strategy could be to find paradoxical activators. PINK1 is similar in many ways to kinases which have been paradoxically activated. PINK1 is a dimer, it localizes to membrane and is an unstable enzyme with a fast turnover rate. Therefore, PINK1 could potentially be paradoxically activated by an inhibitor.

An efficient and robust method used to identify kinase inhibitors is the thermal shift assay (TSA). Importantly, the data obtained through a TSA screen has been deemed

reproducible and correlated well with other means of ligand binding determination (Fedorov et al., 2012). The TSA of a kinase library previously helped to identify several small molecules which induced an increase in the thermal stability of TcPINK1 by at least 2.5˚C (Truong, 2019; Figure 3). A previous student in our laboratory has investigated some of these stabilizing compounds and found that one of them (PRT062607) inhibits TcPINK1 in vitro. Addition of PRT062607 to U2OS cells treated with CCCP decreases the amount of phosphorylated ubiquitin compared to CCCP alone while PINK1 levels remain constant. Furthermore, it was shown that PRT062607 was able to decrease CCCP-induced mitophagy. The compounds which were highly destabilizing the protein, on the far right of Figure 3, have not yet been investigated for their interaction with TcPINK1 as they highly destabilized the protein and would thus unlikely be paradoxical agonists. In this thesis, I will be focusing of the inhibitors which stabilized the protein, seen on the far left of Figure 3.

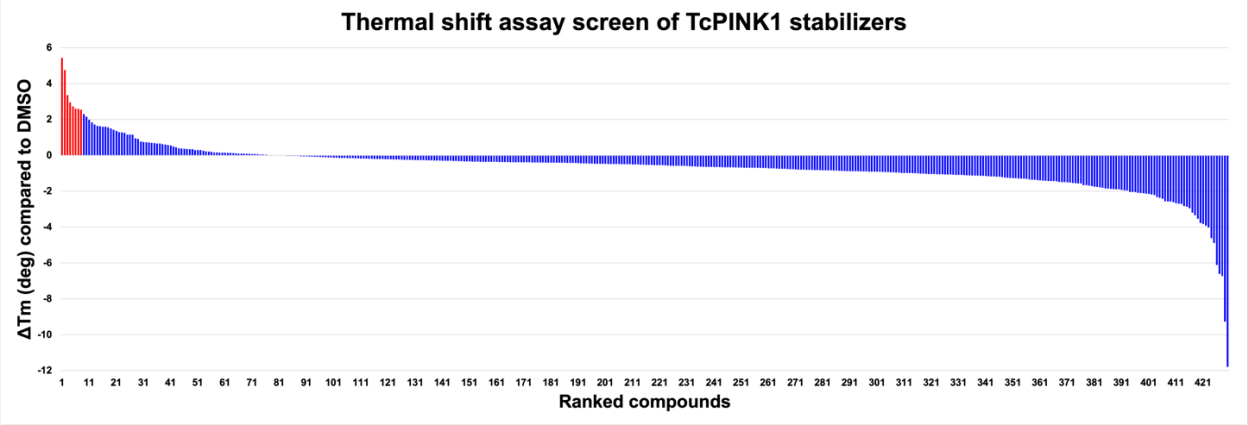

Figure 3. Thermal shift assay of SelleckChem kinase library against TcPINK1.

A ranking based on the 430 compounds in the SelleckChem known small molecule kinase inhibitor library against TcPINK1. In red are the compounds which increase Tm by at least 2.5˚C.

1.7.2 Humanization of insect PINK1

Currently, researchers are unable to express substantial quantities of active *Homo sapiens* PINK1 (HsPINK1), whether through bacteria expression or in insect cells (Woodroof et al., 2011) or with yeast (Wu et al., 2016). To overcome this issue, researchers have instead turned to insect homologues of this protein including TcPINK1 as well as *Pediculus humanus* (Ph)PINK1, which produce high yield of active and folded protein upon expression in *Escherichia coli* (Kumar et al., 2017; Rasool et al., 2018; Schubert et al., 2017; Woodroof et al., 2011). Therefore, in vitro research and crystal structures were generated using these homologues. However there would be merit in obtaining recombinant human PINK1 as the insect variants of PINK1 only share about 40% sequence homology with the human sequence (Figure 4). This would be especially crucial for the development of drugs, as small changes in the composition of the binding site could lead to dramatic changes in potency.

	Description	Total Score	Query Cover	E value	Per. Ident	Acc. Len
☑	HsPINK1	1172	100%	0.0	100.00%	581
☑	TcPINK1	277	81%	2e-89	36.74%	570
☑	PhPINK1	280	79%	9e-91	36.83%	575

Figure 4. Sequence homology between HsPINK1, TcPINK1 and PhPINK1.

Sequence homology obtained by Blastp and the alignment were obtained by performing Clustal alignment and shown in Jalview. As seen at the top of the figure, TcPINK1 and PhPINK1 have less than 40% sequence homology (percent identity) with HsPINK1.

Solubility and expression issues can be overcome by “humanizing” proteins, i.e. by introducing human amino acids in an ortholog from another species. Humanization of proteins is not new to the field of PD, as LRRK2’s ATP binding pocket from ameba has also been mutated to the human ATP binding domain, which they refer to as mosaic (Liu et al., 2014). With their new hybrid protein, they were able to provide a resource for the development of new small molecule inhibitors against LRRK2.

We adopted the same strategy towards the development of a humanized PINK1 protein. TcPINK1 was chosen to be the vector on which the human ATP binding domain will added, given that we can purify large amounts of this protein. Despite only needing to mutate few amino acids, the intricacies of bond formation, bond length and slightest shift in structure could prove a striking difference between homologues.

1.8 Research Objectives and Rationale

The goal of my project is to find and characterize a chemical probe to aid in the ongoing search towards fundamentally understanding PD and to provide a potential therapeutic approach for the treatment of the disease. Currently, compounds such as oligomycin A, an ATP synthase blocker, antimycin A, an inhibitor to the electron transport chain, or Carbonyl cyanide m-chlorophenyl hydrazone (CCCP), an uncoupling agent used to study mitophagy, are used to induce PINK1 accumulation on the mitochondrial membrane. However, these methods disturb the entire mitochondria in various ways, also affecting other cellular pathways and possibly leading to non-physiologically relevant responses to membrane potential disturbance. It is imperial that we find chemical probes which could modulate the activity and localization of PINK1 to further investigate its role in mitochondria and PD. Despite the low number of individuals displaying PINK1 dysfunction, increasing the MQC pathway could also beneficial to alleviate other pathological processes in PD, such as decreased concentrations of soluble Parkin with increasing PD severity (Wang et al., 2005). Moreover, it is critical to use a humanized variant of the PINK1 protein, as sequence homology with TcPINK1 is low, and key residues lining the ATP binding

domain of the homologues could greatly affect the discovery and optimization of inhibitors and modulators of PINK1. My research will thus be divided into finding chemical probes against PINK1, determining their IC_{50}'s and designing a humanized PINK1 protein which would allow us to better screen for HsPINK1 specific modulators and allow us to take a look at the differences between the ATP binding domains.

2. Methods

2.1 Protein expression

2.1.1 Protein co-expression with lambda-phosphatase

The TcPINK1 plasmid used spans residues 121 to 570 and is codon optimized (Rasool et al., 2018). The TcPINK1^{humanized} was ordered from GenScript with codon optimization and spanned residues 121-570, with the addition of 6-aromatic mutations (W131A, W142A, Y225A, Y378A, F401A and F437A) and 12 humanizing mutations (A169G, T172C, N173S, G174A, V175A, V251I, R296N, D298P, N300T, Q302R, S303Q, S358A) (Rasool et al., 2022). TcPINK1-WT (121-570) and the 6-aromatic humanized TcPINK1 (121-570) ampicillin resistant plasmids were co-expressed in BL21 DE3 E. coli with lambda phosphatase spectinomycin resistant plasmid (Addgene plasmid #79748) as per the New England Biolabs protocol. Plasmid maps are shown in Figures 5-8.

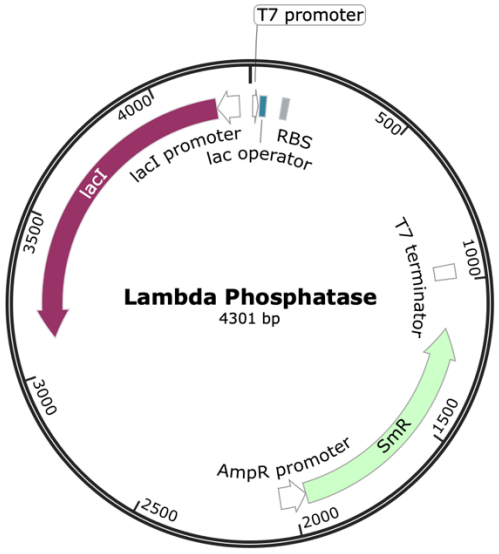

Figure 5. pET 13S-A vector containing Lambda Phosphatase.

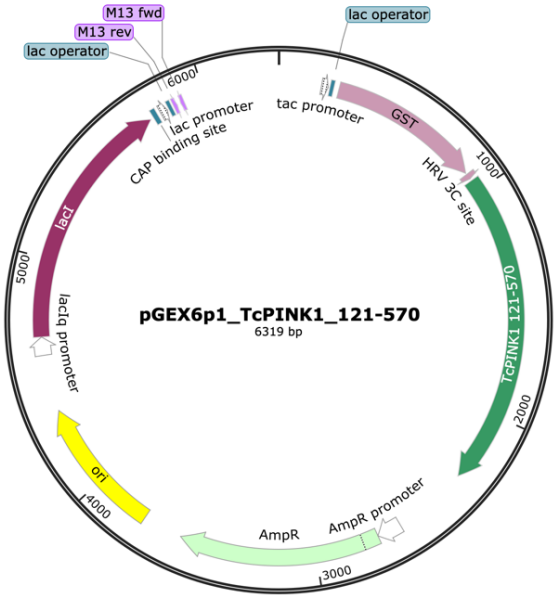

Figure 6. pGEX6p1 vector containing TcPINK1 121-570.

Contains a N-terminal GST tag followed by a HRV 3C cleavage site (Rasool et al 2018).

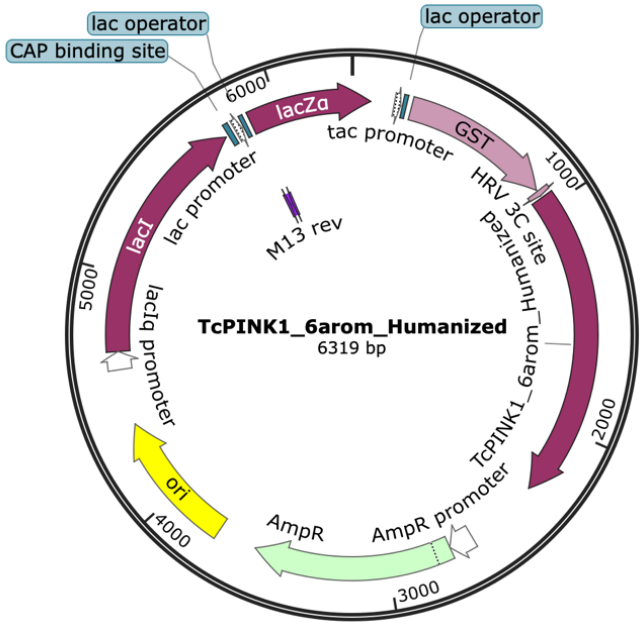

Figure 7. pGEX6p1 vector containing TcPINK1^{humanized}.

Contains a N-terminal GST tag followed by a HRV 3C cleavage site.

2.1.2 Tetraubiquitin expression

The plasmid of tetraubiquitin (Ub_4) was also ordered from GenScript. This plasmid contains the ubiquitin gene repeated four times and contains a N-term GST tag as well as a 3V HRV cleavage site.

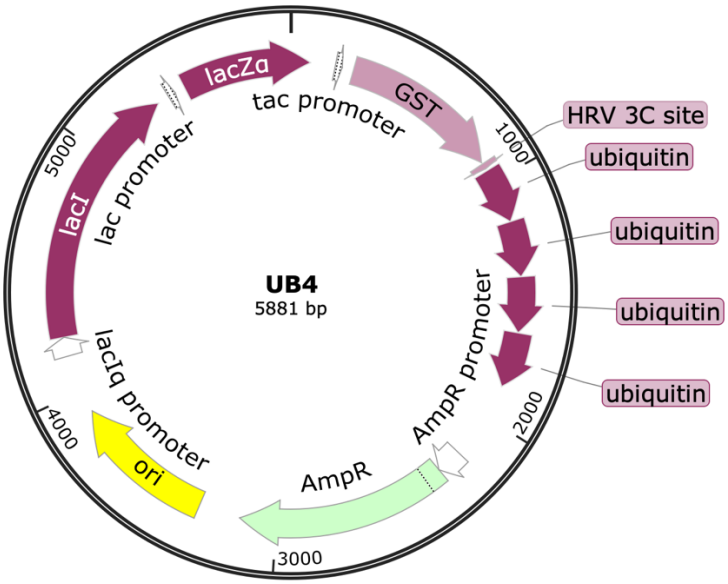

Figure 8. pGEX6p1 vector containing tetra Ubiquitin.

Contains a N-terminal GST tag followed by a HRV 3C cleavage site.

2.2 Protein Growth

A single colony of each co-transformation were used to inoculate a 10 mL starter culture of Lysogeny Broth (LB) with 0.1 mg/mL ampicillin and 0.05 mg/mL of spectinomycin; the cultures were incubated at 37˚C overnight, shaking at 180 rpm. The starter culture was then added to 1 L of LB containing 0.1 mg/mL ampicillin and 0.05 mg/mL and left to grow at 37˚C, shaking at 180 rpm until the optical density at a wavelength of 600 nm (OD_{600}) of the culture reached between a 0.8-1 reading. Once the OD_{600} was reached, the cultures were cooled down to 16˚C, at which point 300 µM of IPTG and 25 µM of $MnCl_2$ were

added. The cultures were then incubated at 16˚C overnight, shaking at 180rpm. The growths were then centrifuged at 3500 rpm for 30 minutes at 4˚C. The resulting pellets were resuspended in 30 mL of lysis buffer consisting of 0.025 mg/mL DNAse, 5 mM $MgCl_2$, 1 mM PMSF, 0.1 mg/mL lysozyme, 0.2% Tween 20, 10% glycerol, in 300 mM NaCl and 50mM Tris-HCl pH 8. The resuspended pellets were sonicated at 4˚C for 20 seconds on-off intervals repeated 8 times.

2.3 Protein Lysis and purification

After cell lysis and sonication, the bacteria were spun down at 15000 rpm for 20 minutes at 4˚C to separate the cell debris and insoluble protein from the soluble fractions. The clarified cell lysate (supernatant) was then incubated for 1 hour at 4˚C on a rotating platform with 2 mL Sepharose 2B resin (GE Healthcare Life Sciences) suspended in 2mL kinase buffer (50 mM Tris, 300 mM NaCl, 3 mM DTT, pH 8.0). After incubation, the protein was passed through a gravity column. The proteins in the lysate which do not have Glutathione S-Transferase (GST) tag were allowed to flow through (FT fraction) the column, leaving only the resin bound to the GST fusion protein. After washing the resin repeatedly with kinase buffer (wash fractions), the protein of interest was eluted off the column using 20 mM glutathione (Bio Basics Canada) and concentrated by centrifugation using 15 kDa Centrifugal Filter Units (Millipore). The resulting protein concentration was measured using the Denovix DS-11 spectrophotometer at 280 nm wavelength absorption with theoretical extinction coefficients and molar masses obtained by inputting the amino acid sequence of the protein into the ProtParam website. The molar mass and extinction coefficient of GST-TcPINK1 were 77494.37 Da and 119180 M^{-1} cm^{-1} and for GST-

TcPINK1^{humanized} they were 77327.22 Da and 105200 M^{-1} cm^{-1}. The eluted protein was incubated with a 1:50 ratio of HRV-3C protease to protein at 4˚C overnight to cleave the GST tag off the protein.

2.4 GST tag cleavage and size exclusion chromatography

The cleaved protein was injected in the Äkta pure (Cytiva) with the S75 HiLoad 16/600 Superdex column (Cytiva) with a 5mL GST trap attached and run at 0.7ml/min in the corresponding kinase buffer to separate GST dimers from the protein. The fractions eluted off the Äkta were further concentrated with the 15 kDa Centrifugal Filter Units (Millipore) according to the manufacturer's instructions.

2.5 Intact protein mass spectrometry

Proteins were diluted to a concentration of 0.5 mg/ml in 0.5% formic acid (F.A.) and 2% acetonitrile (ACN). About 10 μL of the dilution was injected on a Dionex C4 Acclaim 1.0/15 mm column and eluted by a 5-50% ACN gradient at 40 μl/min for 10 minutes. The resulting data was analyzed by Bruker Q-TOF equipped with an Apollo II ion funnel electrospray ionization source. The spectra were analyzed using the Data Analysis software from Bruker, deconvoluted at 10,000 resolution using the maximum entropy method.

2.6 Autophosphorylation assay

Purified and cleaved TcPINK1 was incubated with 2 mM ATP, and 3 mM $MgCl_2$ for 30 minutes at 30˚C to allow for autophosphorylation. The reaction was stopped with a final concentration of 0.1% F.A. and stored in aliquots at -80˚C until further use.

The TcPINK1^{humanized} protein autophosphorylation followed the same protocol as above but left instead at 37˚C for 1 hour.

2.7 In vitro Kinase Assays and SDS gel

Kinase activity assays were performed by adding 5 nM of purified TcPINK1 or 6-aromatic-humanized-PINK1 in 10 second increments to with 100 μM ATP, 100 μM small molecules, 200 μM $MgCl_2$ in kinase buffer. The reactions were left in a 30˚C incubator for 5 minutes for TcPINK1, and at 37˚C for 15 minutes for the TcPINK1^{humanized}. The reactions were stopped with the addition of Laemmli buffer (2% SDS, 0.1% bromophenol blue (Sigma-Aldrich), 10% glycerol, 100 mM DTT) final concentration 1X. The entire reaction was loaded onto a 12.5% Tris-Tricine gel (1 M Tris-HCl pH 8.45, 12.5% acrylamide, 0.1% SDS, 0.1% APS, 0.04% TEMED). The gels were inserted in a gasket filled with SDS running buffer and were run at 120 V for 90 minutes.

2.8 Western Blots

Protein from a 12.5% polyacrylamide gel were transferred onto an Immuno-blot PVDF membrane (Bio-rad) at 45mA overnight in transfer buffer. The membranes were stained with 1% Ponceau and imaged using the ImageQuant LAS 500. The membrane was washed with distilled water and then blocked in 5% BSA diluted in tris buffered saline with

0.1% Tween (TBS-T) for 1 hour. The membrane was briefly rinsed and left to incubate with primary antibody (pUb) at a 1:10,000 dilution in TBS-T for two hours. The membrane was further rinsed three times for 10 minutes with TBS-T before incubating it with a 1:2000 dilution of secondary antibody, anti-rabbit, in TBS-T. The membrane was rinsed three times for 10 minutes in TBS followed by the addition of 1 mL ECL solution (BioRad) to the membrane and visualized on the ImageQuant LAS 500.

2.9 Luminescence based activity assays – Kinase Glo

The Kinase Glo experiment described is a method used to determine the kinase activity of the PINK1 proteins. Comparatively, most assays used to determine the activity of PINK1 are downstream reading of phosphorylation. The Kinase Glo assay does not rely on downstream phosphorylation product of PINK1. The Kinase Glo assay is a direct measurement of the ATP the protein consumes to undergo autophosphorylation and hydrolysis. For this assay, 1 μM TcPINK1 GST-cleaved, and non-phosphorylated was incubated with 10 μM ATP for 5 minutes at 30˚C in kinase buffer. Inhibitor (ranging concentration between 100 μM for PRT062607, PRT060318 and TAK659, 400 μM for JNJ- 7706621, 1300 μM of CYC116) and serial diluted in 4x kinase buffer 12 times, the 13th sample having no kinase (negative control). The kinase buffer consists of 50 mM Tris-HCl pH 7.5, 300 mM NaCl, 1 mM DTT. At 10 second increments, 100 μL of kinase at 1 μM was added to 100 μL 2x kinase buffer with inhibitor and left in a 30˚C incubator. After the 5-minute mark, 200 μL kinase glo was added to stop the reaction at 10 seconds increments as well, ensuring that each reaction was exactly 5 minutes in duration. 100 μL of the sample was then pipetted into 3 wells of an opaque white 96-well plate according

to the loading pattern shown in figure 9. In parallel, an ATP standard was generated ranging from 0 to 100 μM ATP in a 2-fold dilution series. The luminescence was measured using the Orion II Microplate Luminometer and obtained using the Simplicity 4.2 program.

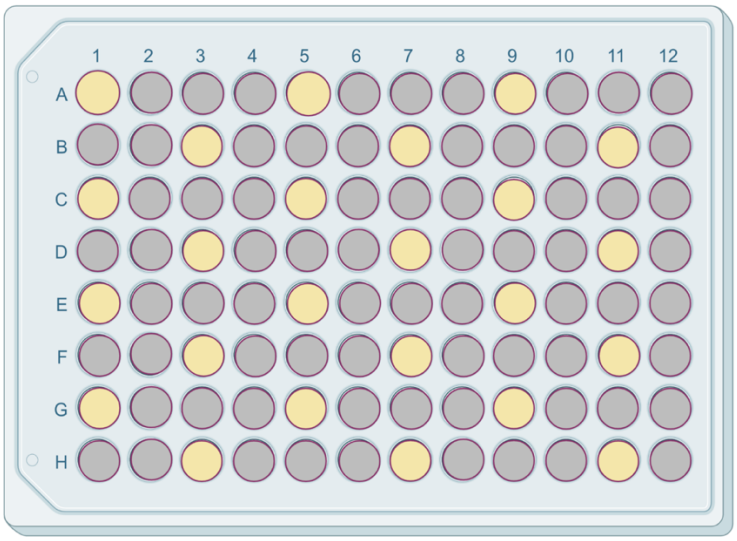

Figure 9. 96-well plate layout for the kinase glo experiments.

This layout was used to decrease the leaking of signal between adjacent wells.

2.10 IC_{50} calculation

For each IC_{50} experiment, a corresponding ATP standard curve ranging from zero to 12.5μM was generated. From the linear equation of the ATP standard curve, every point was back calculated to determine the amount of ATP left in reaction. This number was then divided by the amount of ATP initially present and multiplied by 100 to obtain the percent inhibition. The values were normalized according to the baseline, in this case being kinase reaction with no inhibitor present. The points were then averaged as they were in triplicates and plotted on a non-linear regression graph on GraphPad Prism 7 as the log of the concentration for the x axis and the mean percent inhibition. The IC_{50} value

of the log inhibitor concentration versus the luminescence was generated from the graph. This process was performed twice, once with a free-floating Hill slope, and once by constraining the Hill slope to 1.

2.11 In organello assay (performed by Nathalie Croteau)

HeLa cells were treated with CCCP to induce the accumulation of PINK1 on the OMM. The cells were then separated from their mitochondria by nitrogen cavitation and the mitochondrial fraction was purified from the cell debris. 7.5ug of mitochondria was incubated with 3.75 μg Ub4, 5 mM MgCl2, 0.1 mM ATP and 100 μM of each inhibitor for 5 minutes at 30˚C.

2.12 In silico modelling of ligand-protein interactions

All structural modelling was performed using PyMOL. The crystal structures of TcPINK1 bound to PRT062607 and bound to CYC116 were obtained by Shafqat Rasool and refined by Simon Veyron. The ligands JNJ-7706621 was modelled into the crystal structure of TcPINK1 bound to PRT062607. The modelling of JNJ-7706621 was done using the crystal structure obtained from protein kinase A's catalytic domain (PDB 3AMA). The modelling of PRT060318 was done using the structure of spleen tyrosine kinase (SYK) and PRT060318 (PDB 3FQE). The TcPINK1^{humanized} modelling was performed by manually mutating the 12 amino acids onto the crystal structures of TcPINK1 bound to PRT062607 and CYC116 in PyMOL. The models obtained with PRT060318 and JNJ-7706621 were obtained using the crystal structure backbone of TcPINK1 bound to PRT062607 and the ligand of 3FQE or 3AMA and manually adding the twelve mutations.

3. Research Findings

3.1 Protein growth and expression

Our overall goal is to establish methods to assess the activity of small molecule inhibitors against human PINK1's kinase domain. Kinase assays require protein that remains active after purification, however the HsPINK1 protein is not obtainable for experiments as it is not active when purified from E. coli or insect cells (Woodroof et al 2011). Instead of the HsPINK1 protein, we will thus opt to use the active TcPINK1 insect orthologue, which our laboratory previously used for structural studies (Rasool et al, 2018; 2022). TcPINK1 shares significant sequence homology with HsPINK1, especially in the kinase domain and active site. The chosen construct spans residues from 121-570 of TcPINK1, which corresponds to the cytosolic domain. In addition to wild-type (WT) TcPINK1, we also designed a humanized construct, where 10 mutations were introduced in amino acids lining the TcPINK1 active site ($TcPINK1^{humanized}$). In addition, six aromatic surface exposed residues were mutated into alanine in the humanized construct to increase the solubility of the protein. The two plasmids were transformed into BL21 DE3 E. coli and grown in substantial amount. The protein can be purified as it is tagged with GST (~26 kDa), which binds to glutathione-Sepharose beads. As can be seen in Figure 10, the cleared lysate loaded to show the flow-through show what did not bind to the breads. The protein-bead mix was then washed thoroughly, and remaining proteins were washed off. Finally, the protein was eluted off the beads with glutathione. The elution step was performed in three consecutive steps, as can be seen in the figure, eluting at ~ 76 kDa. A similar trend can be seen in Figure 11, which is the $TcPINK1^{humanized}$ construct. This protein is shown to express readily as well.

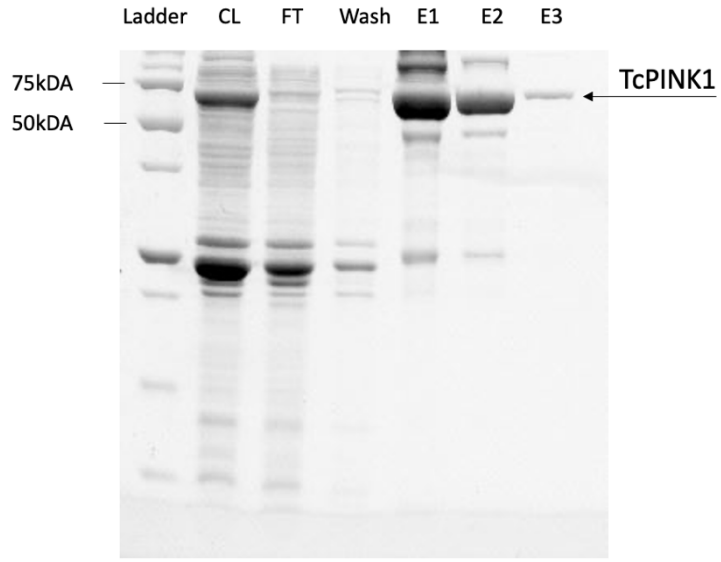

Figure 10. Purification gel of TcPINK1 WT

This purification gel shows an intense band at around 75 kDa, the correct molecular weight of GST-tagged TcPINK1. In the flowthrough (labelled FT) and the wash fractions, the protein of interest did not elute, while the proteins that did not bind the glutathione-Sepharose beads were removed.

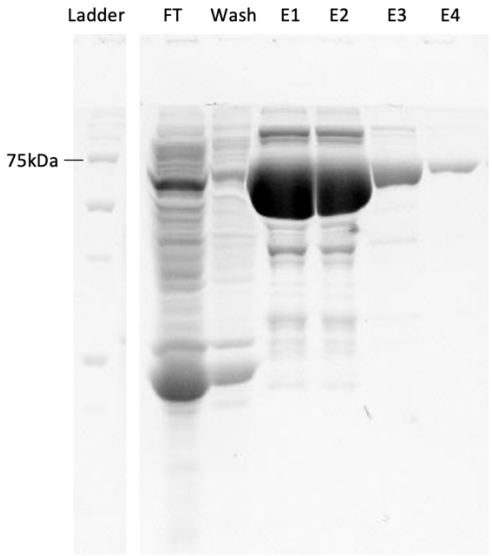

Figure 11. Purification gel of TcPINK1^{humanized}.

This purification gel shows an intense band at around 75 kDa, the correct molecular weight of GST tagged TcPINK1^{humanized}. In the flowthrough (labelled FT) and the wash fractions, the protein of interest did not elute, while the proteins that did not bind the glutathione-Sepharose beads were removed. The ladder provided on the left is from the same gel, but several lanes between the ladder and purification fractions were cut out.

Following affinity purification, the protein elutions were left to incubate overnight with the 3C protease, thus separating the tag from our protein of interest. The proteins were injected on a Superdex75 HiLoad size exclusion chromatography (SEC) column. The chromatogram generated for TcPINK1 WT, Figure 12, and TcPINK1^{humanized} in Figure 13, shows the elution of proteins at different point in the run, monitored using UV absorption.

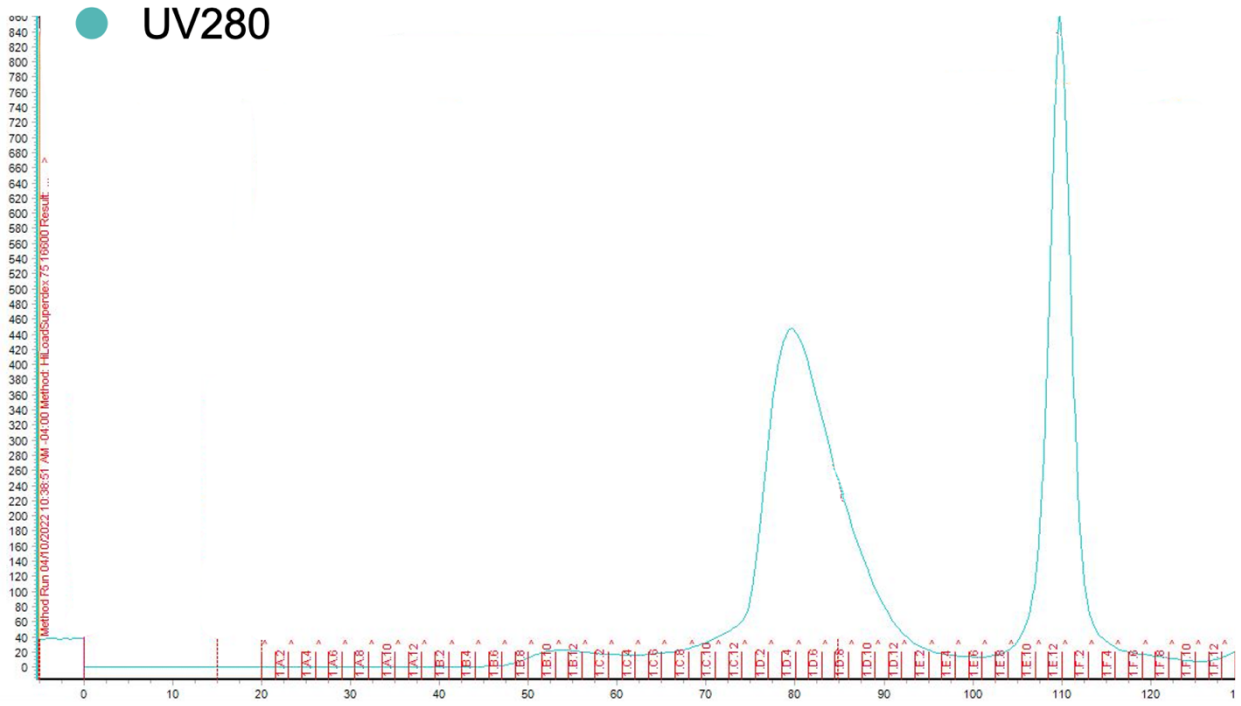

Figure 12. Gel filtration spectrum of TcPINK1.

TcPINK1 is further purified by size exclusion chromatography. The elution fractions are labelled in red at their corresponding volume on the x-axis, while the UV280 is shown on the y axis. In turquoise we see the spectrum for TcPINK1, elution at the 80 mL while the GST fraction is eluting at 110 mL.

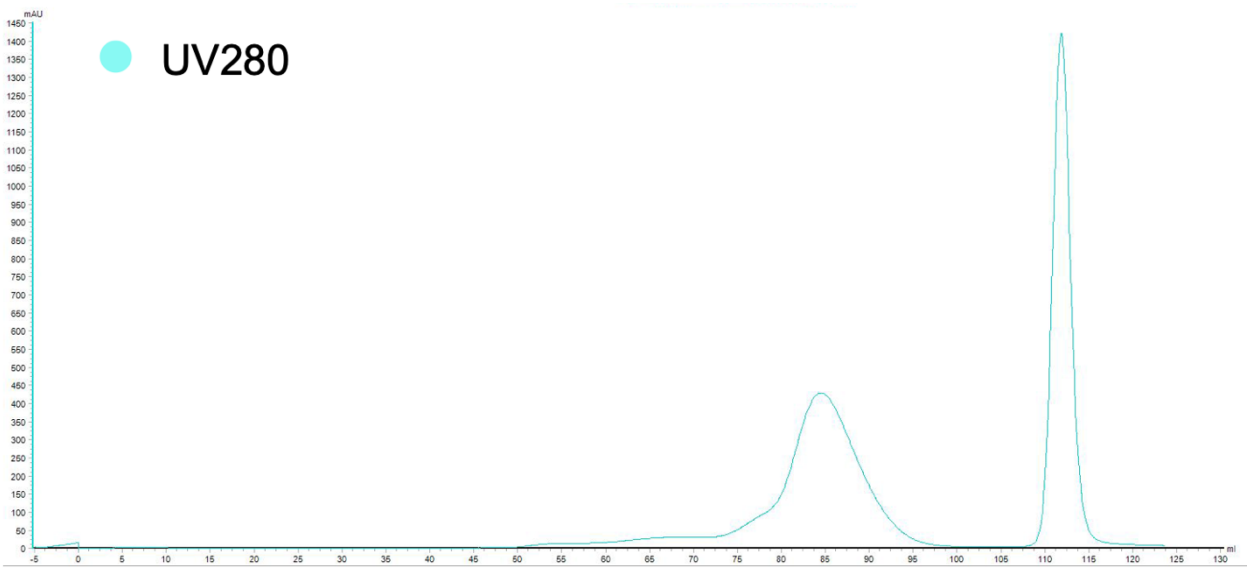

Figure 13. Gel filtration spectrum of TcPINK1^{humanized}.

TcPINK1 is further purified by size exclusion chromatography. The elution fractions are labelled in red at their corresponding volume on the x-axis, while the UV280 is shown on the y axis. In turquoise we see the spectrum for TcPINK1, elution at the 80 mL while the GST fraction is eluting at 110 mL.

The following gel is the SEC fraction of TcPINK1 WT loaded on an SDS gel and is shown in Figure 14. The first fraction after the ladder is an aliquot of what was injected onto the Äkta following overnight 3C cleavage. The first 7 fractions represent TcPINK1, appearing at the cleavage molecular weight of 51.5 kDa, while the 4 right most fractions are the GST fractions.

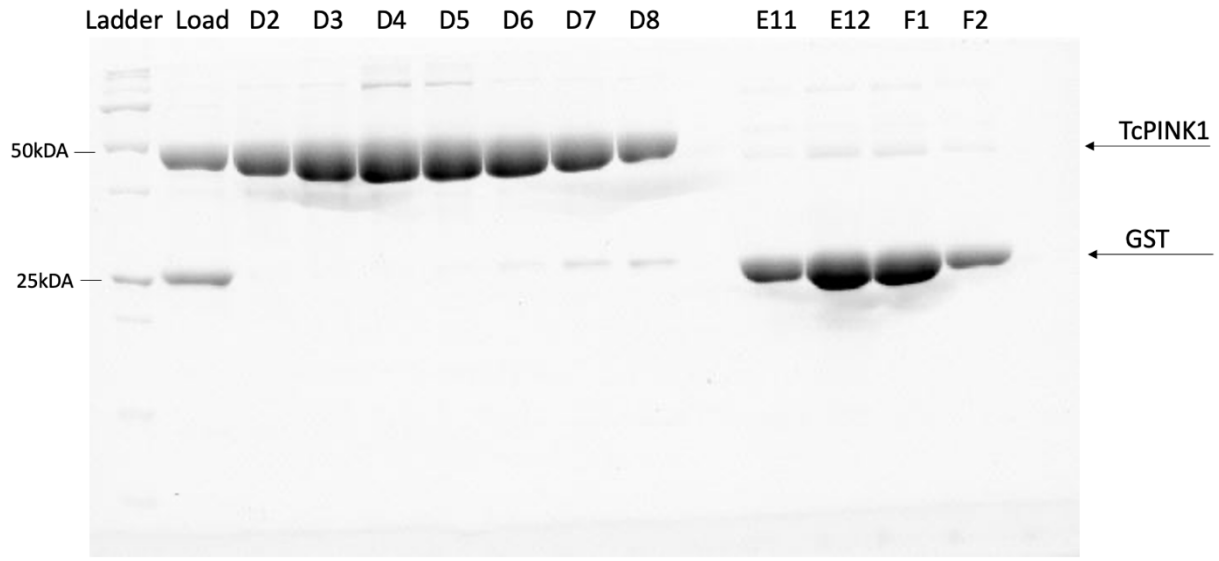

Figure 14. SDS-PAGE gel of SEC fractions.

The gel above are the fractions surrounding 80 and 110 mL from the gel filtration spectrum in Figure 12. The first lane shows the fraction which was loaded onto the Äkta, the lanes D2 through D8 which were at eluted 80 mL are showing a molecular weight of around 50kDa which is expected for TcPINK1. The 4 last lanes, E11 to F2, are the fractions which eluted at 110 mL and contain GST at a molecular weight around 25 kDa.

3.2 In vitro ubiquitin kinase assays with TcPINK1 and in organello

Following the thermal shift screen performed previously by our lab, figure 3, the eight compounds which induced the most stability in TcPINK1 were selected, namely JNJ-in-8, JNJ-7706621, AZD3463, URMC-099, CYC116, CYT387, VE822, and PRT062607. To determine the effect of these compounds, an in vitro ubiquitin kinase assay was performed using purified TcPINK1 WT and tetraubiquitin (Ub_4). Following incubation with ATP, the quantity of pUb produced was assessed using a Western blot. In Figure 15, lanes A and B show the amount of pUb present at 0 minute (baseline signal) or 5 minutes following incubation with ATP and Ub_4, with no inhibitor present (with DMSO carrier). The

subsequent reactions were done at 5 minutes with 100 μM of each corresponding inhibitor.

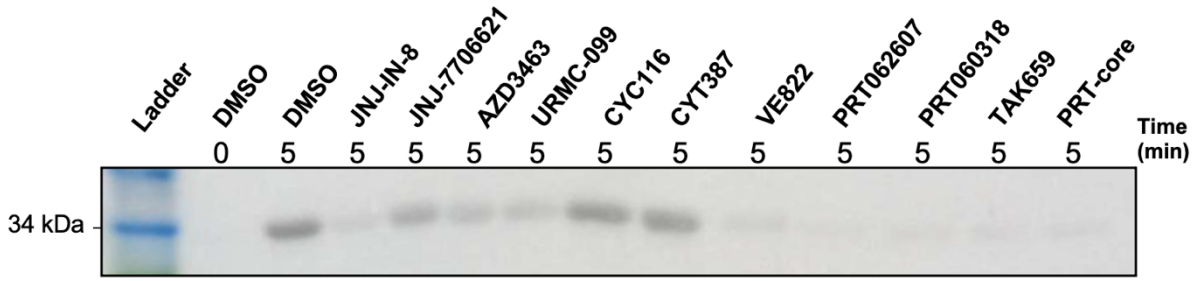

Figure 15. Western blot of pUb with TcPINK1 and several inhibitors.

The lane numbers correspond to the inhibitor in the table on the right of the figure. The higher the intensity of the band, the more pUb was present meaning PINK1 was not inhibited. Absence or diminished intensity of a band compared to the 5 minutes positive control is indicative of inhibition of PINK1's kinase activity by the corresponding inhibitor.

All lanes except for lanes 5 and 6, show a decrease production of pUb signal, indicating inhibition of the PINK1 kinase activity. Out of those active compounds, lanes 1, 7, and 8 show a higher degree of inhibition of TcPINK1 compared to those from lanes 2 to 4. These inhibitors target a variety of different kinases. To determine whether these compounds also inhibit human PINK1, an in organello experiment was performed using mitochondria isolated from HeLa cells treated for 3 hours with CCCP to induce PINK1 accumulation. These mitochondria were then incubated with recombinant Ub_4 in the presence of ATP, followed by a Western blot against pUb (Figure 16). From the original compounds in the Selleckchem library as well as the pan-kinase weak inhibitor staurosporine (lanes 1-9), only inhibitors JNJ-7706621 (lane 2) and PRT062607 (lane 9) inhibited the ubiquitin kinase activity of HsPINK1. By comparing the TcPINK1 and in organello HsPINK1 kinase assays, it appears that PRT062607 is the most potent inhibitor of both PINK1 orthologs.

PRT062607 is an inhibitor of the SYK tyrosine kinase, a kinase involved in its role in B cell lymphoma mediated signalling (Cornall et al., 2000). To determine whether related SYK inhibitors could also inhibit PINK1, we tested the SYK inhibitors PRT060318 and TAK659, as well as the core chemical backbone of PRT062607 lacking the triazole group (racemic PRT-core). All these compounds inhibit the kinase activity of TcPINK1 (Figure 15; lanes 9-11) as well as HsPINK1 (Figure 16; lanes 10-12). Thus, PRT062607 and its derivatives are promising hits for the development of PINK1-selective inhibitors.

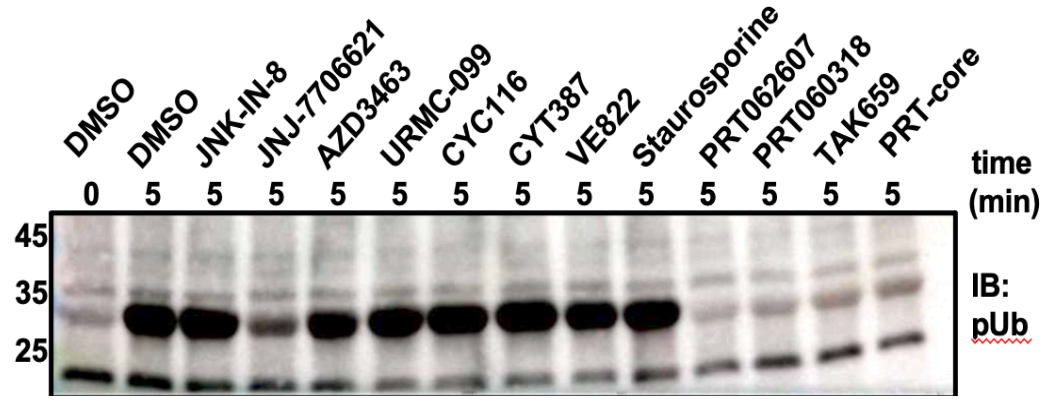

Figure 16. pUb blot of isolated mitochondria with different inhibitors.

The isolated mitochondria were from HeLa cells treated with CCCP therefore had accumulated PINK1 on their OMM. The mitochondria were incubated with 100 μM of each inhibitor listed above, and their amount of pUb present is seen above. The higher the intensity of the band, the more pUb was present meaning PINK1 was not inhibited. Absence or diminished intensity of a band compared to the 5 minutes positive control is indicative of inhibition of PINK1's kinase activity by the corresponding inhibitor.

3.3 Kinase Glo assays

3.3.1 Kinase Glo optimization

The Kinase Glo kit was used as a luminescence-based assay to monitor the consumption of ATP in a kinase reaction. The reagent contains luciferin and luciferase enzyme

compound which will react with remaining ATP in the reaction and emit luminescence. If an inhibitor blocks the kinase activity of PINK1, there will be more luminescence as there is more ATP left after the reaction (Figure 17).

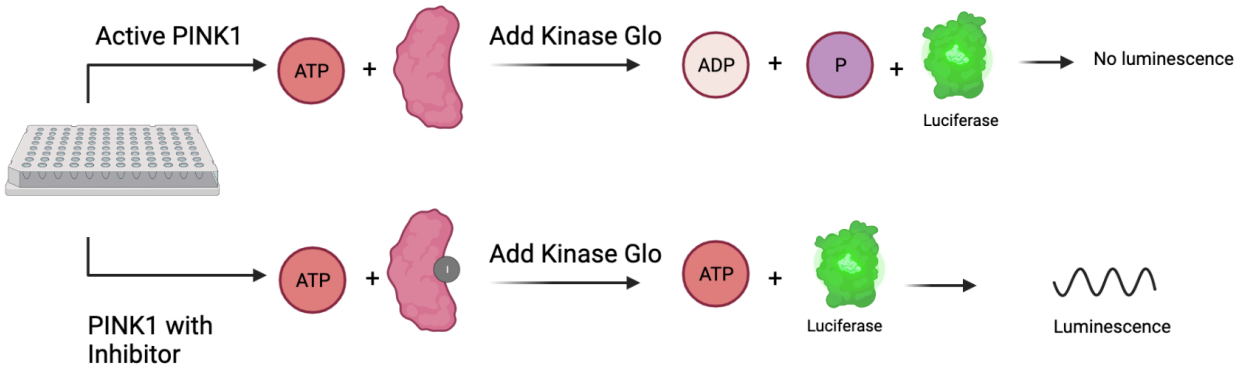

Figure 17. Kinase Glo reaction rationale.

On the first row, active PINK1 mixed with ATP will lead to a generation of adenosine diphosphate (ADP) and deplete levels on ATP. In this case, the luciferase cannot produce any luminescence. On the bottom row, PINK1 is incubated with an inhibitor, thereby not consuming all the ATP. In this case, luciferase enzyme will be able to catalyse the mono-oxygenation of luciferin and emit luminescence which we will measure.

In order to avoid signal leakage between wells, the samples were loaded according to the pattern presented in figure 9. This technique was validated by measuring the luminescence reading with increasing ATP concentration. The following graph, Figure 18, was generated confirming the linear relationship between luminescence and ATP concentration between 0 and 100 μM. Previous experiments that were performed with samples loaded in adjacent wells did not show a linear trend.

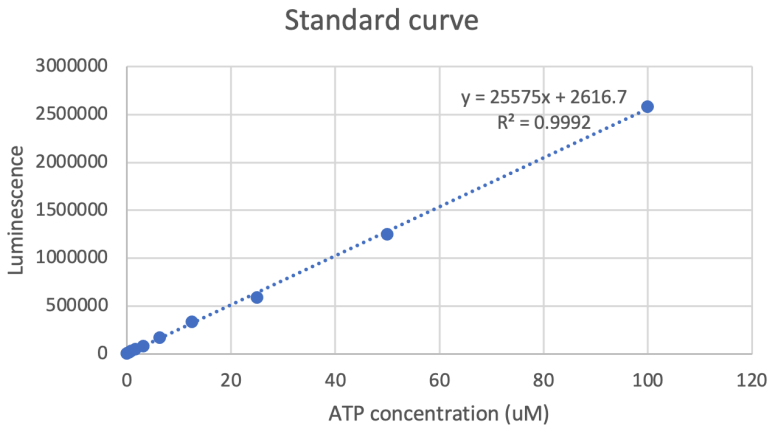

Figure 18. ATP standard curve between 0 and 100 μM.

This standard curve demonstrates a high correlation between the amount of luminescence generated, and the concentration of ATP and is linear.

3.3.2 IC_{50} measurement for TcPINK1

The Kinase Glo assay was used to measure the IC_{50} value of several inhibitors against unphosphorylated TcPINK1. It is to note that each experiment was fitted using two models in Graph Pad Prism 7: once with the Hill coefficient constrained to 1 (no cooperativity; shown on the left) and once with a variable Hill coefficient (shown on the right). The experiment was repeated for TcPINK1 with inhibitors PRT062607, PRT060318, CYC116, JNJ-7706621 and TAK659. Results are shown in Figure 19. The IC50's of the PRT compounds are around 2 μM, while those of CYC116 and JNJ-7706621 are higher, between 30-60 μM. Interestingly, the Hill slope values of all curves expect TAK659 have a tendency towards a value of 2.

A

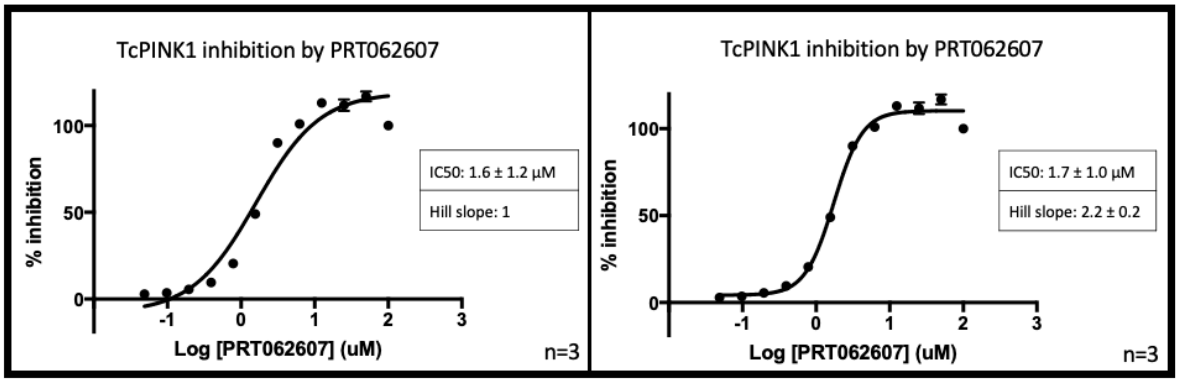
TcPINK1 inhibition by PRT062607
% inhibition
Log [PRT062607] (uM)
IC50: 1.6 ± 1.2 µM
Hill slope: 1
n=3
TcPINK1 inhibition by PRT062607
% inhibition
Log [PRT062607] (uM)
IC50: 1.7 ± 1.0 µM
Hill slope: 2.2 ± 0.2
n=3

B

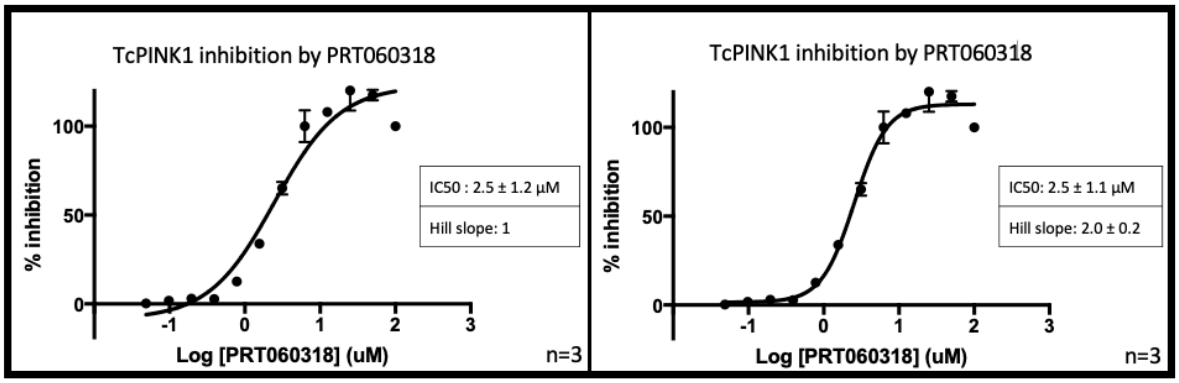
TcPINK1 inhibition by PRT060318
% inhibition
Log [PRT060318] (uM)
IC50 : 2.5 ± 1.2 µM
Hill slope: 1
n=3
TcPINK1 inhibition by PRT060318
% inhibition
Log [PRT060318] (uM)
IC50: 2.5 ± 1.1 µM
Hill slope: 2.0 ± 0.2
n=3

C

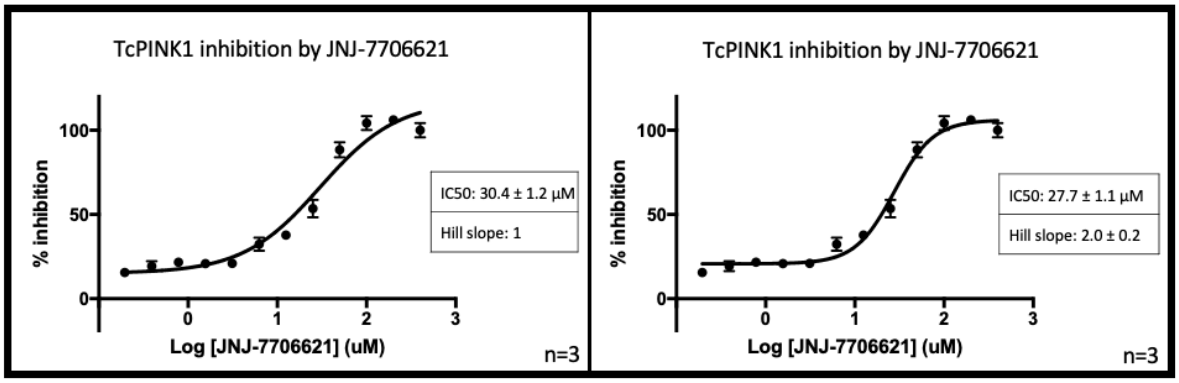
TcPINK1 inhibition by JNJ-7706621
% inhibition
Log [JNJ-7706621] (uM)
IC50: 30.4 ± 1.2 µM
Hill slope: 1
n=3
TcPINK1 inhibition by JNJ-7706621
% inhibition
Log [JNJ-7706621] (uM)
IC50: 27.7 ± 1.1 µM
Hill slope: 2.0 ± 0.2
n=3

D

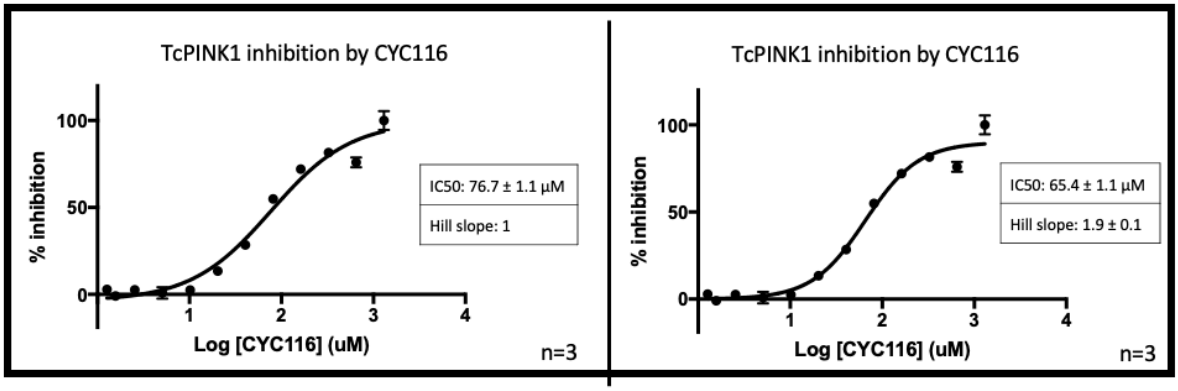
TcPINK1 inhibition by CYC116
% inhibition
Log [CYC116] (uM)
IC50: 76.7 ± 1.1 µM
Hill slope: 1
n=3
TcPINK1 inhibition by CYC116
% inhibition
Log [CYC116] (uM)
IC50: 65.4 ± 1.1 µM
Hill slope: 1.9 ± 0.1
n=3

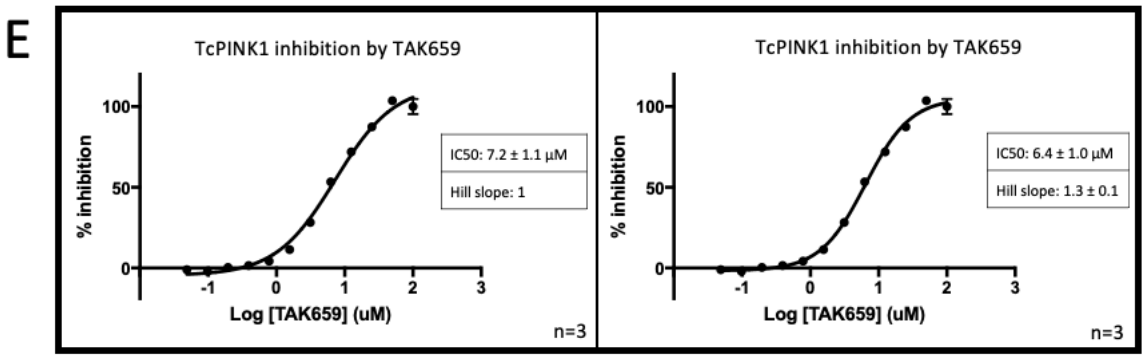

Figure 19. IC_{50} graphs for each inhibitor against TcPINK1.

The graph on the left shows the IC_{50} curve with a Hill slope constrained to 1. On the right, the Hill slope was generated by Graph Pad Prism based on the raw data. Both graphs show the log inhibitor concentration on the x-axis and the percent inhibition of the protein's kinase activity compared to no inhibitor on the y-axis. Each data point is the average of triplicates and the standard error bars are also displayed. (A) IC_{50} of PRT062607. (B) IC_{50} of PRT0620318. (C) IC_{50} of JNJ-7706621. (D) IC_{50} of CYC116. (E) IC_{50} of TAK659.

3.3.3 Monophosphorylated TcPINK1 comparison

The experiments performed above measured the IC_{50} of inhibitors against unphosphorylated TcPINK1. However, PINK1 also autophosphorylates, which enables it to recognize ubiquitin. To determine the impact of autophosphorylation on the potency of inhibition by this class of inhibitors, another IC_{50} was performed against the most potent compound PRT062607. To do so, we needed to generate mono-phosphorylated TcPINK1. TcPINK1 was thus incubated with 1 mM ATP and 2 mM $MgCl_2$ (co-factor of the kinase) for 30 minutes for protein autophosphorylation to occur. As can be seen in Figure 20, the top of the figure shows the unphosphorylated protein obtained from the Äkta purification. On the bottom is an 80 Da shift, representing the addition of one phosphate on our protein, in this case, on Ser205.

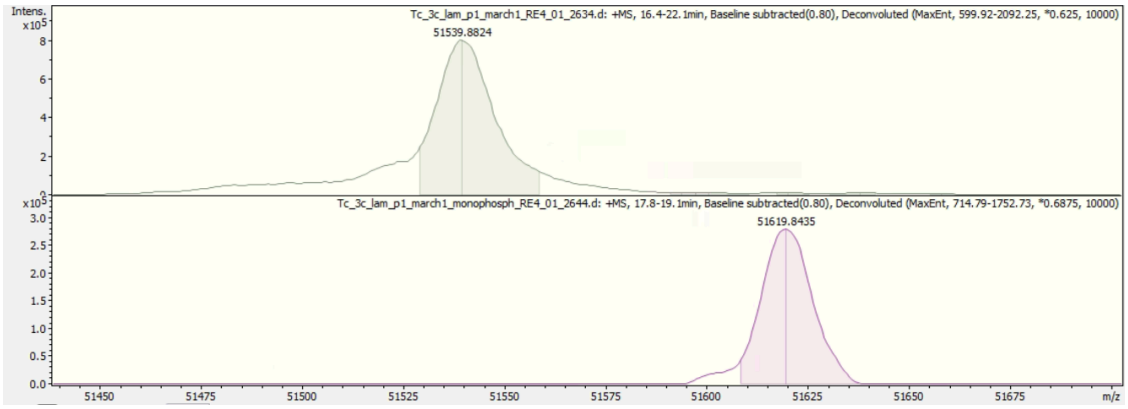

Figure 20. TcPINK1 autophosphorylation assay.

The above is a mass spectrum analysis of TcPINK1 prior to and after an ATP phosphorylation reaction. The x axis shows the mass to charge ratio while the y axis shows the intensity of the signal. The green curve is the MS spectra of GST-cleaved unphosphorylated TcPINK1. The violet MS curve is a kinase reaction left with 10 μM ATP for 30 minutes at 30˚C. The unphosphorylated form of TcPINK1 is 51539 kDa while the monophosphorylated molecular weight of TcPINK1^{humanized} is 51619 kDa. The shift in the purple curve shows complete phosphorylation of the protein after 30 minutes.

The mono-phosphorylated TcPINK1 WT was then tested using the Kinase Glo assay and PRT062607, and an IC_{50} of 2.1 ± 1.1 μM was measured (Figure 21).

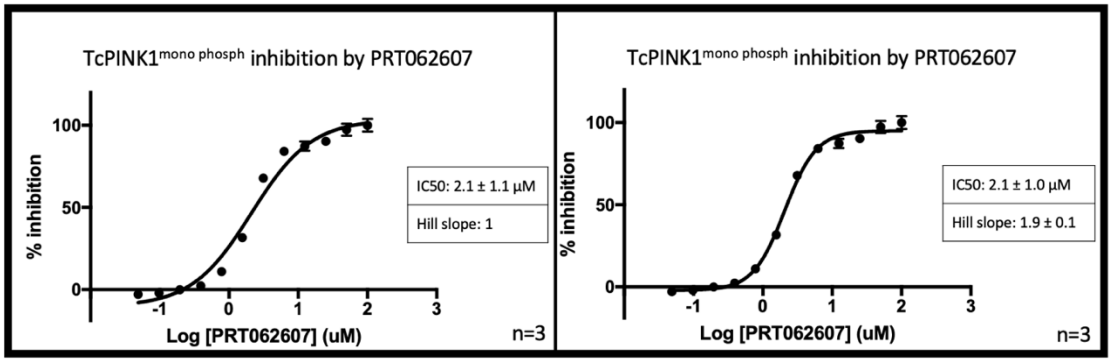

Figure 21. Inhibition of monophosphorylated TcPINK by PRT062607.

The graph on the left shows the IC_{50} curve with a Hill slope constrained to 1. On the right, the Hill slope was generated by Graph Pad Prism based on the raw data. Both graphs show the log inhibitor concentration on the x-axis and the percent inhibition of the protein's kinase activity compared to no inhibitor on the y-axis. Each data point is the average of triplicates and the standard error bars are also displayed.

3.4 Kinase activity of humanized TcPINK1

An autophosphorylation experiment was also performed for TcPINK1^{humanized}. In this case, the protein did not complete autophosphorylation, as shown in the mass spectrometry data in Figure 22, despite having the same reaction conditions as for TcPINK1 WT (Figure 20). This suggests that the humanization mutations reduced the kinase activity of TcPINK1. We then conduced ubiquitin kinase activity assays, and confirmed that TcPINK1^{humanized} is less active than TcPINK1 WT (Figure 23). However, similar activity was observed between TcPINK1^{humanized} at 15 min and TcPINK1 WT at 5 min. We thus used a longer incubation time for the Kinase Glo assay with the TcPINK1^{humanized} construct.

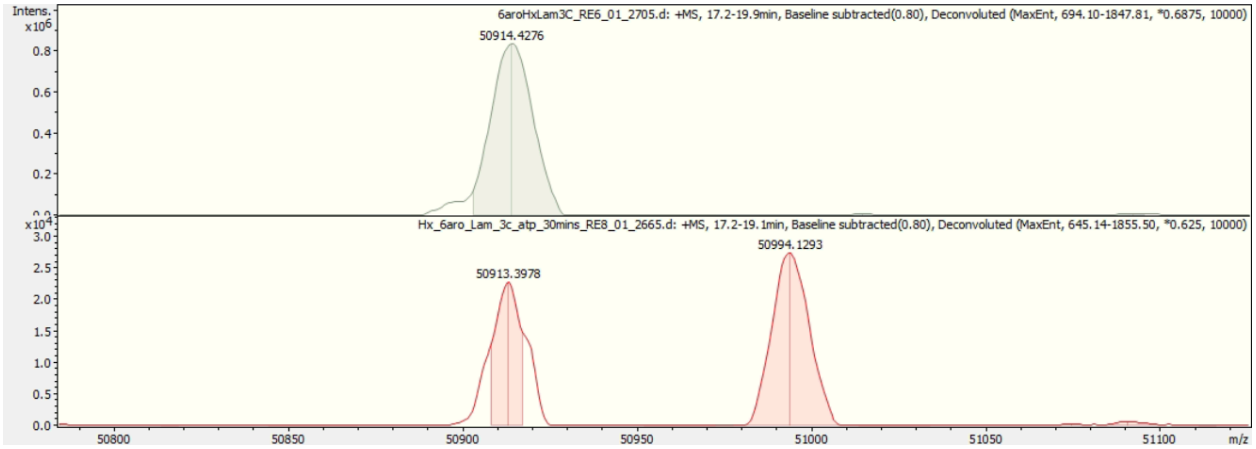

Figure 22. TcPINK1 ^{humanized} autophosphorylation assay.

Mass spectrum analysis of TcPINK1 prior to and after an ATP phosphorylation reaction. The x axis shows the mass to charge ratio while the y axis shows the intensity of the signal. The green curve is the MS spectra of GST-cleaved unphosphorylated TcPINK1 ^{humanized}. The orange MS curve is a kinase reaction left with 10μM ATP for 30 minutes at 37˚C. The unphosphorylated form of TcPINK1 ^{humanized} is 50915 kDa while the monophosphorylated molecular weight of TcPINK1 ^{humanized} is 50994 kDa. The shift in the orange curve shows a portion of the protein remaining unphosphorylated while some is monophosphorylated after the reaction.

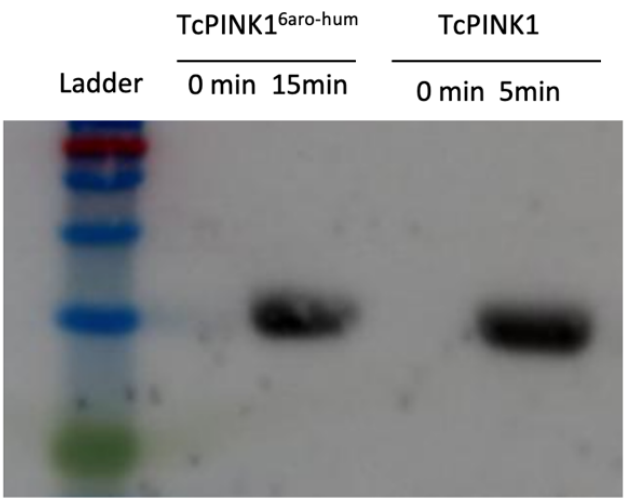

Figure 23. Western blot of pUb with TcPINK1 humanized and TcPINK1.

The blot shows presence of pUb with TcPINK1 ^{humanized} and TcPINK1 following a 15 or 5 minute incubation.

3.5 IC_{50} for TcPINK1 *humanized*

The IC_{50} values of the two most potent TcPINK1 inhibitors were determined for TcPINK1^{humanized}. Figure 24 shows that the IC_{50} for TcPINK1 *humanized* is 1.5 ± 1.1 μM for PRT062607 and 18.1 ± 1.3 μM for PRT060318. By comparison, the IC_{50} of TcPINK1 WT for PRT062607 is about the same (1.7 ± 1.0 μM), but lower for PRT060318 (2.5 ± 1.1 μM) compared to TcPINK1 *humanized*.

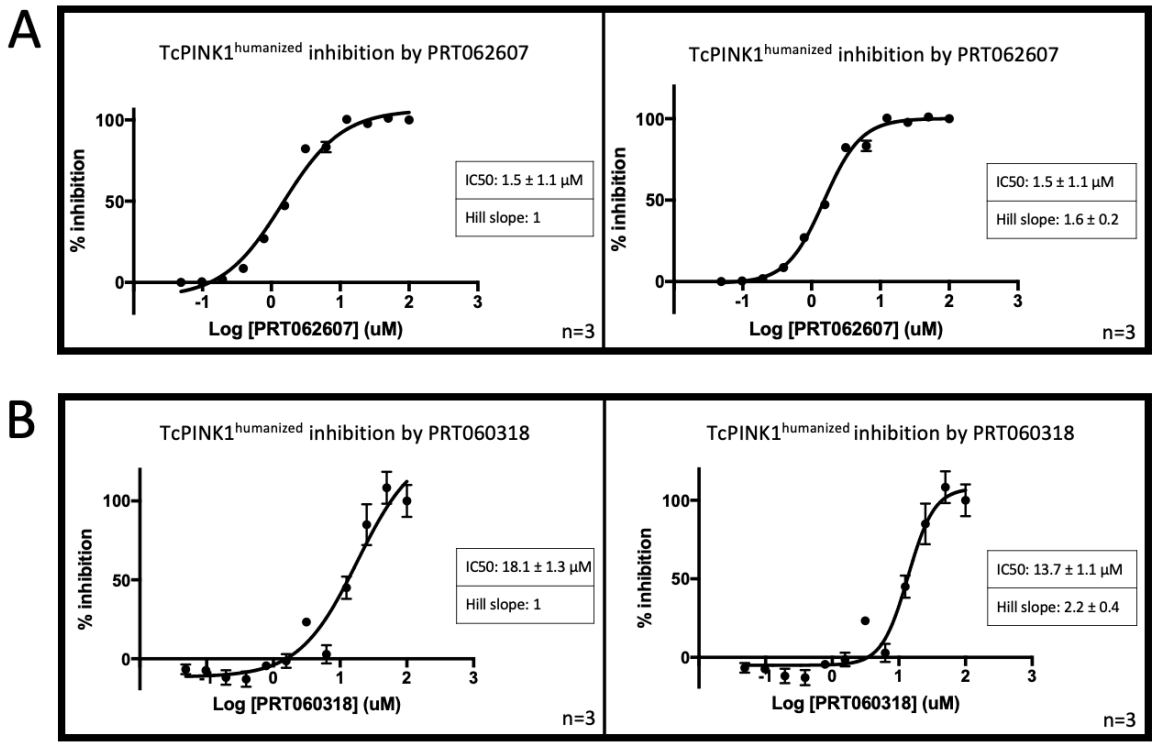

Figure 24. IC_{50} graphs for each inhibitor against TcPINK1^{humanized}.

The graph on the left shows the IC_{50} curve with a Hill slope constrained to 1. On the right, the Hill slope was generated by Graph Pad Prism based on the raw data. Both graphs show the log inhibitor concentration on the x-axis and the percent inhibition of the protein's kinase activity compared to no inhibitor on the y-axis. Each data point is the average of triplicates and the standard error bars are also displayed. (A) IC_{50} of PRT062607. (B) IC_{50} of PRT0620318.

3.6 Crystal structures of TcPINK1 bound to inhibitors

3.6.1 Crystal structure of TcPINK1 with PRT062607

The crystal structure of TcPINK1 bound to PRT062607 was obtained by Shafqat Rasool, a previous member of the lab, and refined by Dr Simon Veyron (Figures 25). From this structure, we can determine key interactions that the ligand makes with the protein to exert its inhibitory effect. Superposition of the PRT062607-bound TcPINK1 on the AMP-PN-bound TcPINK1 shows that the two molecules occupy the same site, explaining why PRT062607 acts as ATP-competitive inhibitor (Figure 26). Importantly, there are two

hydrogen bonds formed by the oxygen and nitrogen of residues Tyr297 and Lys295, respectively, which correspond to the hinge region of the kinase domain (Figure 27). As previously mentioned, this hinge region is important as it contributes to ATP recognition. Furthermore, the nitrogen coming off the cyclohexane forms a salt bridge with the aspartate of the “DFG” motif of the kinase. Typically, DFG motifs are important for mediating the catalysis of the protein and promotes ATP binding by coordinating the Mg^{2+} ion bound. Inhibition of the DFG motif has previously been used to inhibit kinases (Peng et al., 2013). In addition, we also observe a long-distance hydrogen bond between the triazole nitrogen and the side-chain of Asn300. However, this interaction probably does not contribute much to the potency of PRT062607, since PRT060318 lacks the triazole groups and has a similar potency.

Figure 25. Crystal structure of TcPINK1 bound to PRT062607.

PRT062607 is shown in turquoise, with nitrogen shown in dark blue.

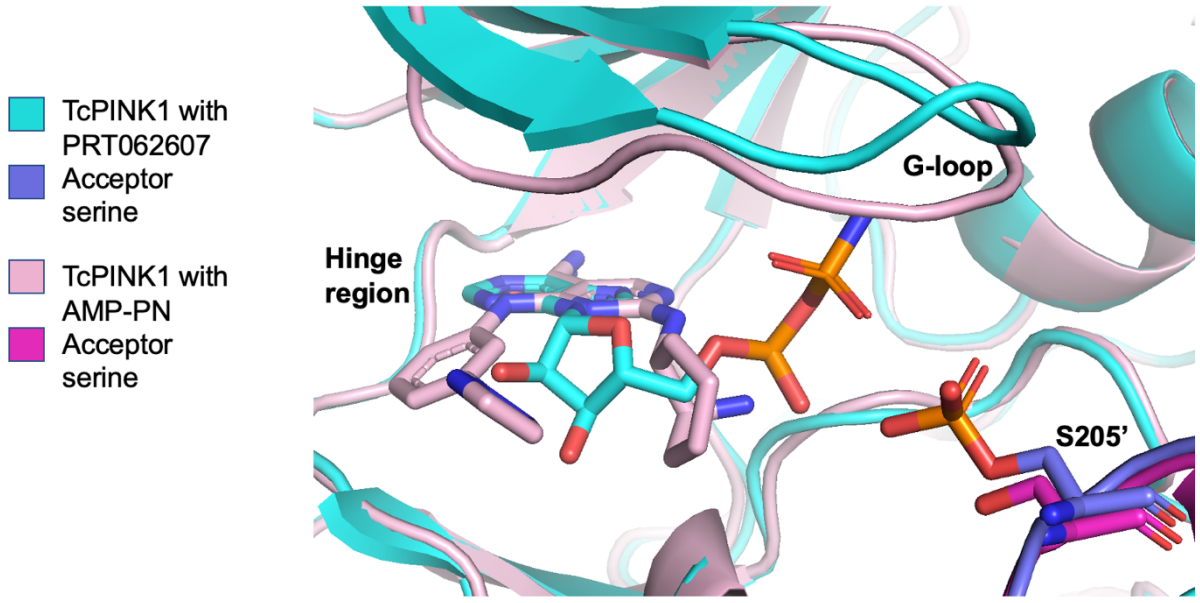

Figure 26. Superposition of AMP-PN and PRT062607 in the ATP binding pocket of TcPINK1.

Superposition of both structures, both ligands are sitting in the same pocket of TcPINK1. The ligands are sitting against the hinge regions of the protein on the left size of the structure. The S205 of the opposing moiety, referred to as S205', can be seen protruding into the pocket on the bottom right-hand side of the figure. This demonstrate that both structures are in the autophosphorylation dimeric state. The G-loop formed on top of the ligands is in the DFG-in conformation for TcPINK1 bound AMP-PN, demonstrating the protein is readily to mediate phosphoryl transfer. The G-loop of the TcPINK1 bound PRT062607 seems to be adopting a conformation similar to the of the DFG-in motif.

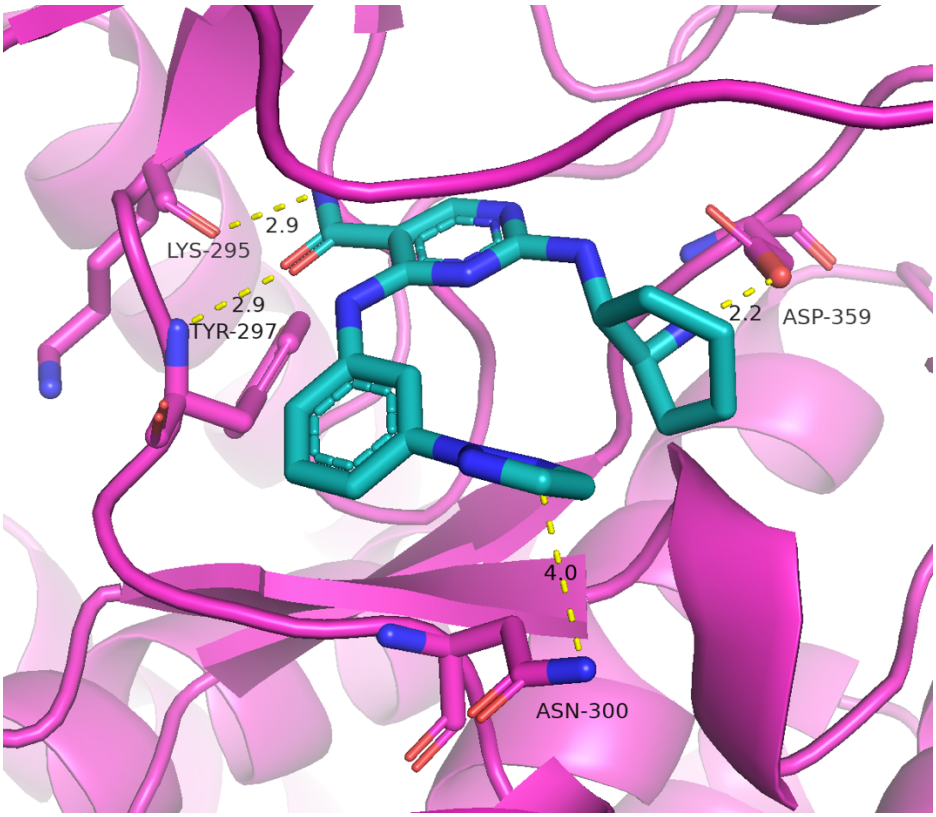

Figure 27. Interactions between TcPINK1 and PRT062607.

PRT062607 is shown in turquoise, with nitrogen shown in dark blue, and oxygens shown in red. There are two hydrogen bonds formed between residues Tyr297 and Lys295 PINK1 and a salt bridge formation with Asp359. There is also a hydrogen bond between the triazole nitrogen and the side-chain of Asn300. Bond lengths are shown in angstrom.

3.6.2 Crystal structure of TcPINK1 with CYC116

The crystal structure of TcPINK1 bound to CYC116 was also obtained and is shown in Figure 28. This weak inhibitor (IC_{50} ~ 70 μM) also occupies the ATP binding site. In this structure, we can see that the tertiary amine group on the azole ring of CYC116 forms a salt bridge with the Asp side-chain of the DFG motif (Figure 29), similarly to PRT062607. CYC116 also forms two hydrogen bonds with the hinge region, specifically with the backbone amide and carbonyl oxygen of residue Tyr297. This hydrogen bond length is

however 3.8 Å, while in TcPINK1, it is 2.9 Å. This could explain why CYC116 is not as potent of an inhibitor compared to PRT062607.

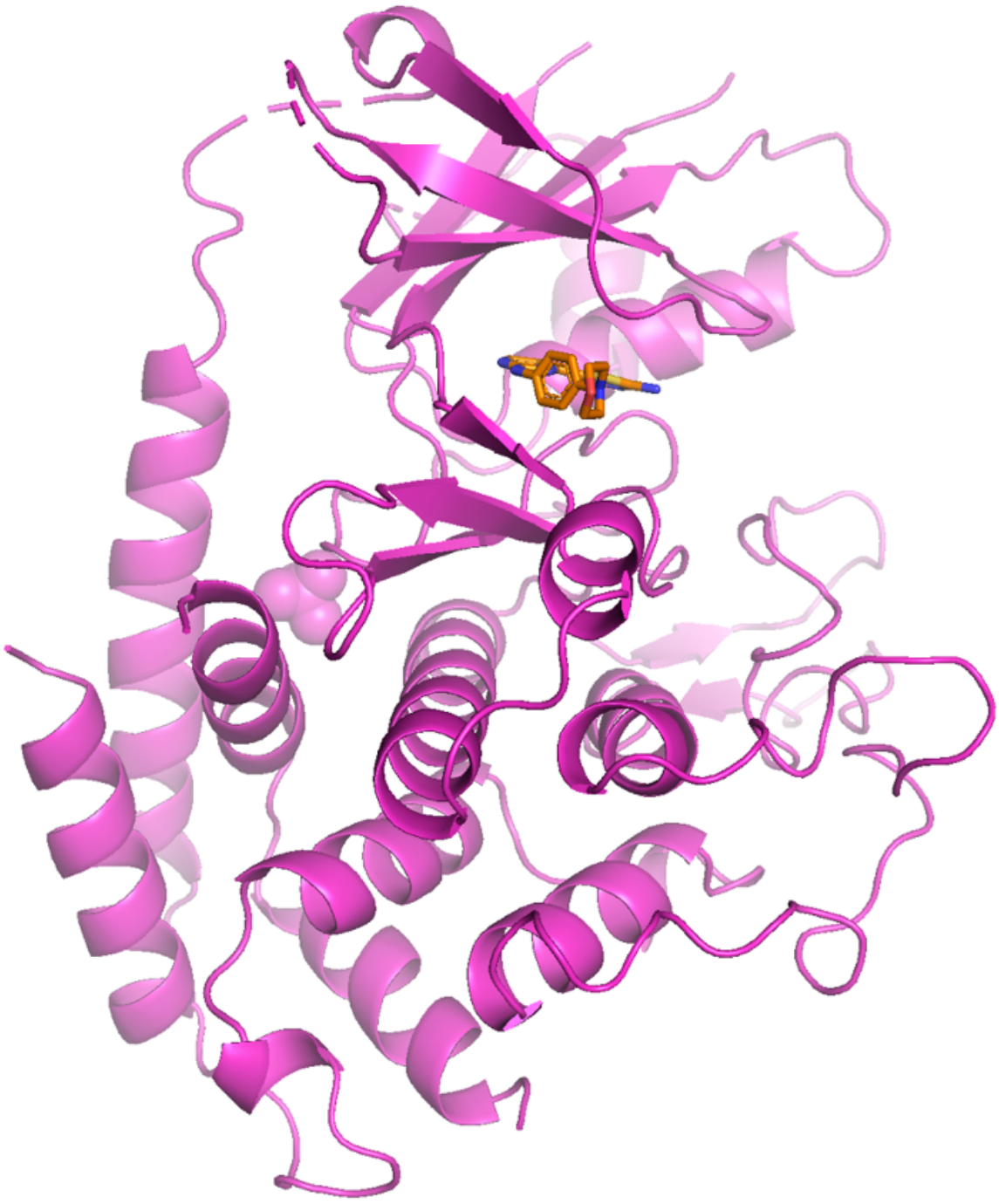

Figure 28. Crystal structure of TcPINK1 bound to CYC116.

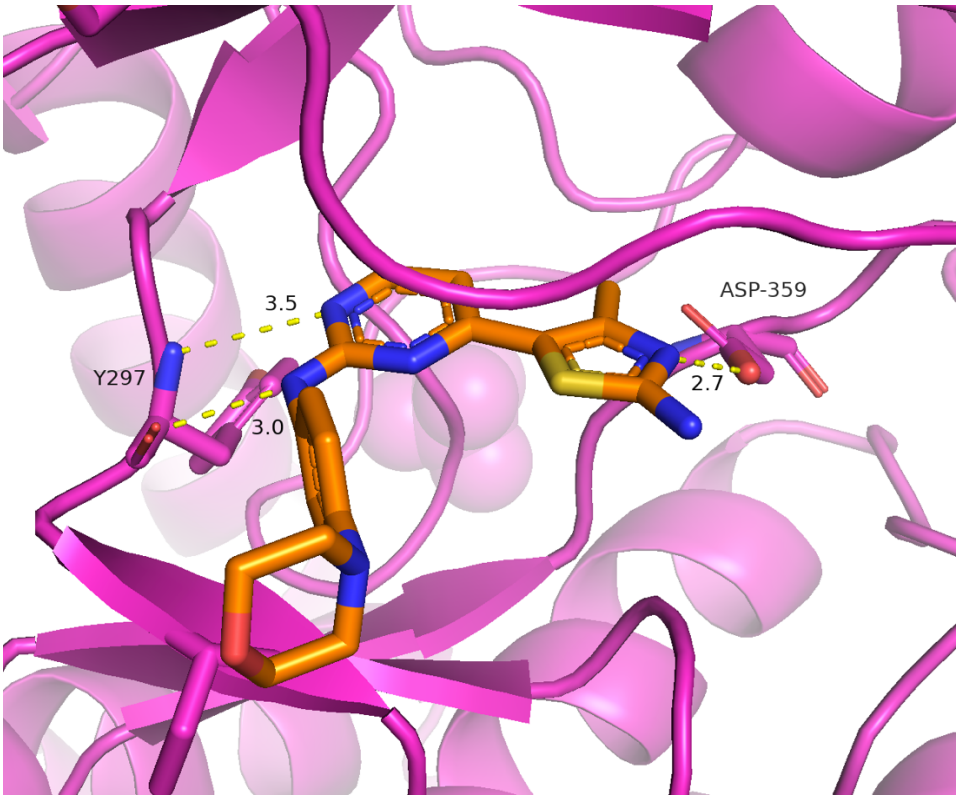

Figure 29. Interactions between TcPINK1 and CYC116.

CYC116 is shown in orange, nitrogens are shown in dark blue, and oxygens are shown in red. There are two hydrogen bonds formed with residue Tyr297 of PINK1, and a salt bridge formation with Asp359. Bond lengths are shown in angstrom.

3.7 In silico modelling of inhibitors bound to PINK1

3.7.1. In silico modelling with TcPINK1

In silico modelling is a great method to determine potential interactions between ligands and protein for which crystal structures cannot been obtained. To understand how PRT060318 might interact with TcPINK1, the structure of TcPINK1 bound to PRT062607 was superposed on the structure of SYK with PRT060318 (Figure 30). The resulting hybrid structure shows the same interactions between TcPINK1 and PRT060318 as with

PRT062607, notably at Asp359 of the DFG motif, and two hydrogen bond formations with Y297 and K295 of the hinge region. This is consistent with the two inhibitors having the same potency against TcPINK1 (IC_{50} ~ 1-2 μM).

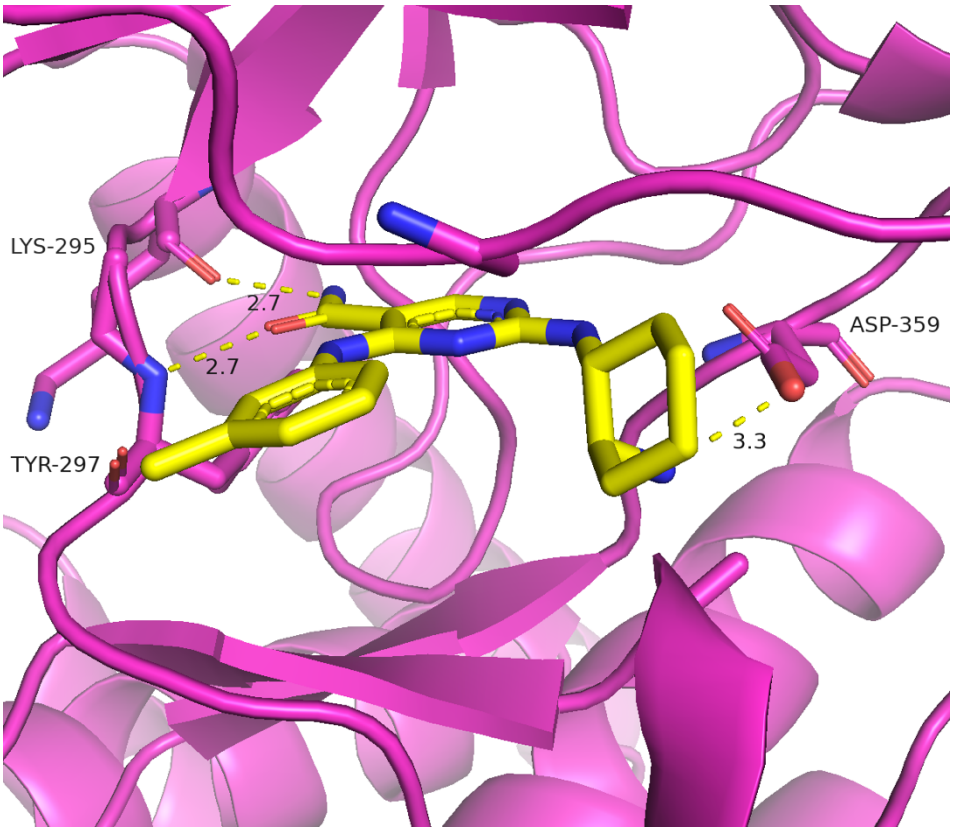

Figure 30. Model of TcPINK1 with PRT060318.

PRT060318 is shown in yellow, nitrogens are shown in dark blue, and oxygens are shown in red. The PRT060318 structure was taken from PDB 3FQE. There are two hydrogen bonds formed between residues Tyr297 and Lys295 PINK1 and a salt bridge formation with Asp359. Bond lengths are shown in angstrom.

Similarly, the structure of TcPINK1 was superposed with that of the catalytic domain of protein kinase A (PKA) bound to the Aurora kinase inhibitor JNJ-7706621, which also inhibits PINK1 (IC_{50} ~ 30 μM) . This modeled structure reveals three hydrogen bonding between JNJ-7706621 and the hinge domain of TcPINK1 (Figure 31). More specifically, the inhibitor forms two hydrogen bonds with Y297 and one hydrogen bond with K295, the

same amino acids targeted by PRT062607, PRT060318 and CYC116. However, JNJ-7706621 does not interact with Asp359, which may explain its weaker IC_{50} compared to the PRT062607 compound and related derivatives.

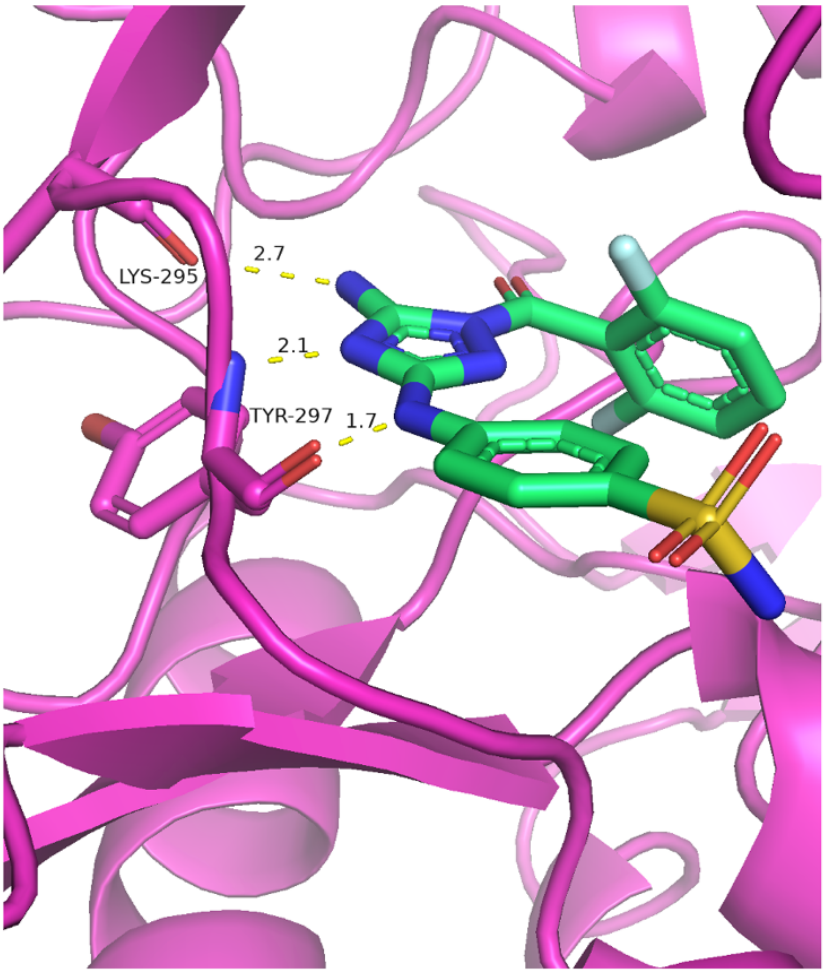

Figure 31. Model of TcPINK1 with JNJ-7706621.

JNJ-7706621 is shown in green, nitrogens are shown in dark blue, and oxygens are shown in red. The JNJ-7706621 structure was taken from PDB 3AMA.There are three hydrogen bonds formed between residues Tyr297 and Lys295 PINK1. Bond lengths are shown in angstrom.

3.7.2 In silico modeling with TcPINK1*humanized*

All the above inhibitors were modeled again with the insertion of twelve humanizing mutations in order to determine whether there are structural differences between the two which could account for the increase in IC_{50}'s between the two proteins for PRT060318 (5- to 7-fold difference). Figure 32 shows the model of the humanized protein with PRT062607 and reveals that all the interactions are maintained despite the insertions of the dozen mutations.

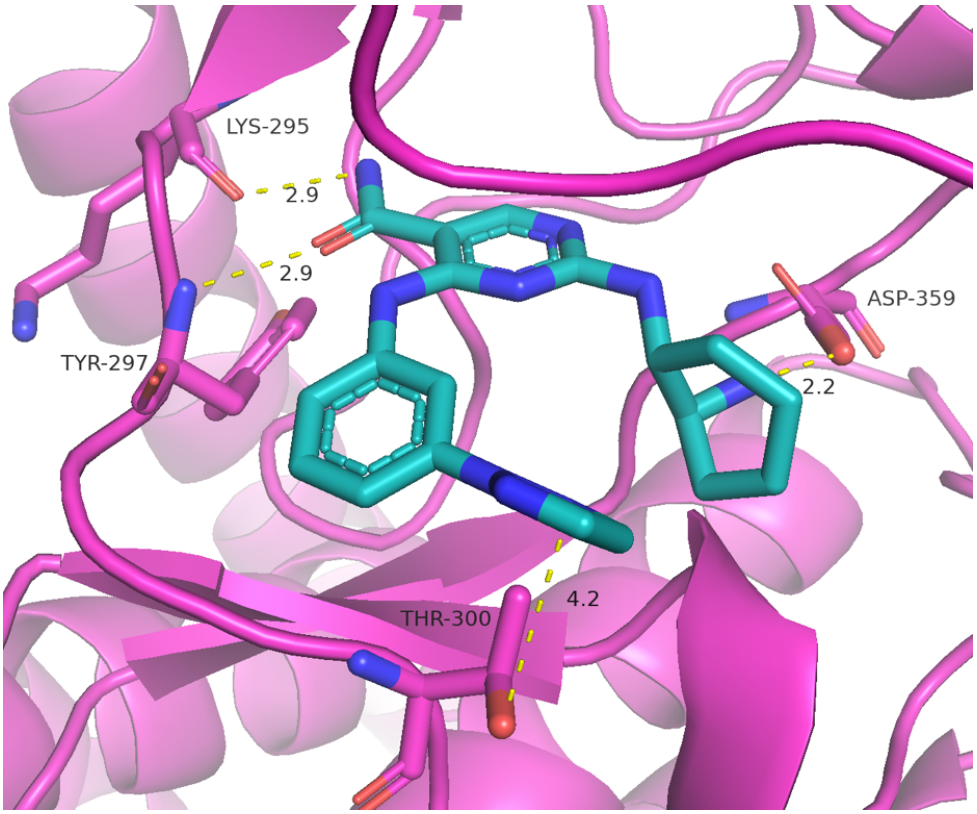

Figure 32. Model of 6aromatic humanized TcPINK1 with PRT062607.

PRT062607is shown in turquoise, nitrogens are shown in dark blue, and oxygens are shown in red. The PRT062607 structure was taken from the structure with TcPINK1, shown in figure 25. There are two hydrogen bonds formed between residues Tyr297 and Lys295 PINK1 and a salt bridge formation with Asp359. The humanized protein has a threonine at residue 300 compares to asparagine in TcPINK1, the bond length is a little further to allow for interactions from this in silico model, obtaining a crystal structure of the humanized protein with PRT062607 would help determine if there is a bond formation or not. Bond lengths are shown in angstrom.

As for PRT060318, the structure with TcPINK^{humanized} also shows the same three interactions, two at the hinge domain and one and the DFG motif. Notably, PRT060318 does not have a triazole group, and thus does not interact with Thr300 in TcPINK^{humanized} (nor with Asn300 in WT TcPINK1).

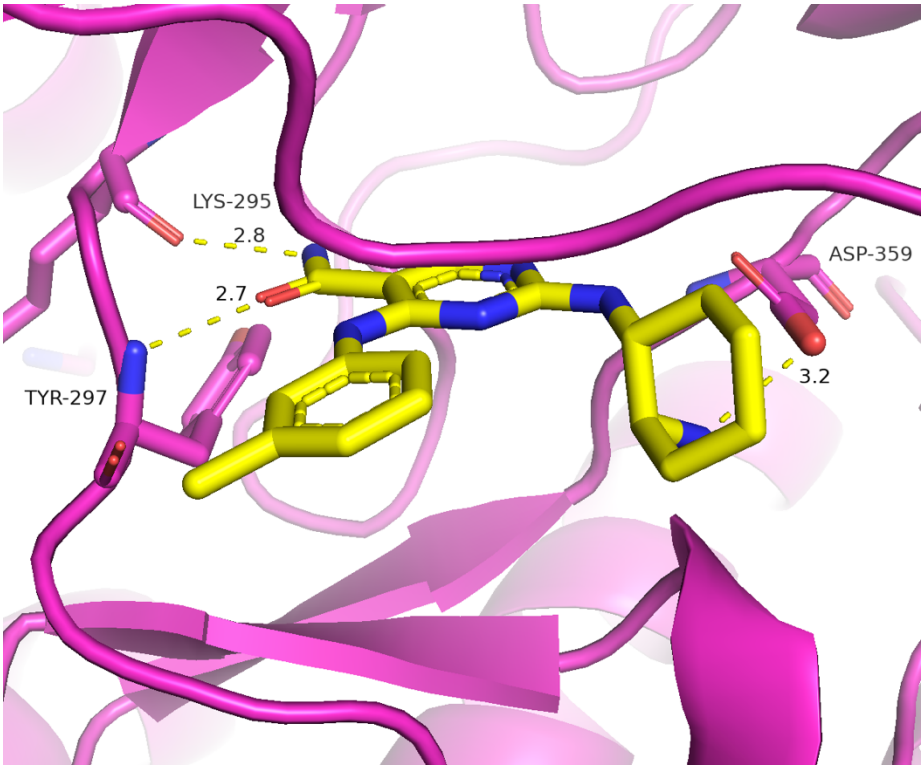

Figure 33. Model of TcPINK1 ^{humanized} with PRT060318.

PRT060318 is shown in yellow, nitrogens are shown in dark blue, and oxygens are shown in red. The PRT060318 structure was taken from PDB 3FQE. There are two hydrogen bonds formed between residues Tyr297 and Lys295 PINK1 and a salt bridge formation with Asp359. Bond lengths are shown in angstrom.

The structure with CYC116 also shows the same hydrogen bonding with Y297 and Lys295, and a salt bridge formed with the DFG motif (Figure 34).

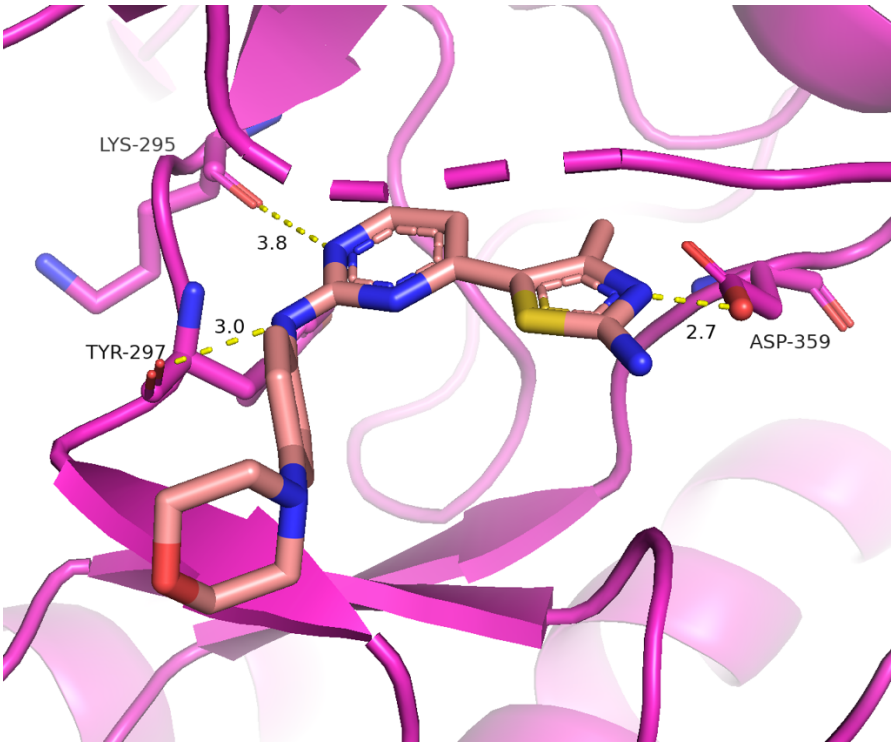

Figure 34 Model of TcPINK1^{humanized} with CYC116.

CYC116 is shown in pink, nitrogens are shown in dark blue, and oxygens are shown in red. The CYC116 structure was taken from the structure with TcPINK1, shown in figure 28. There are two hydrogen bonds formed between residues Tyr297 and Lys295 PINK1 and a salt bridge formation with Asp359. Bond lengths are shown in angstrom.

Finally, the structure of the TcPINK1^{humanized} with JNJ-7706621 shows the same three hydrogen bonding with the hinge region as with the TcPINK1 protein (Figure 35).

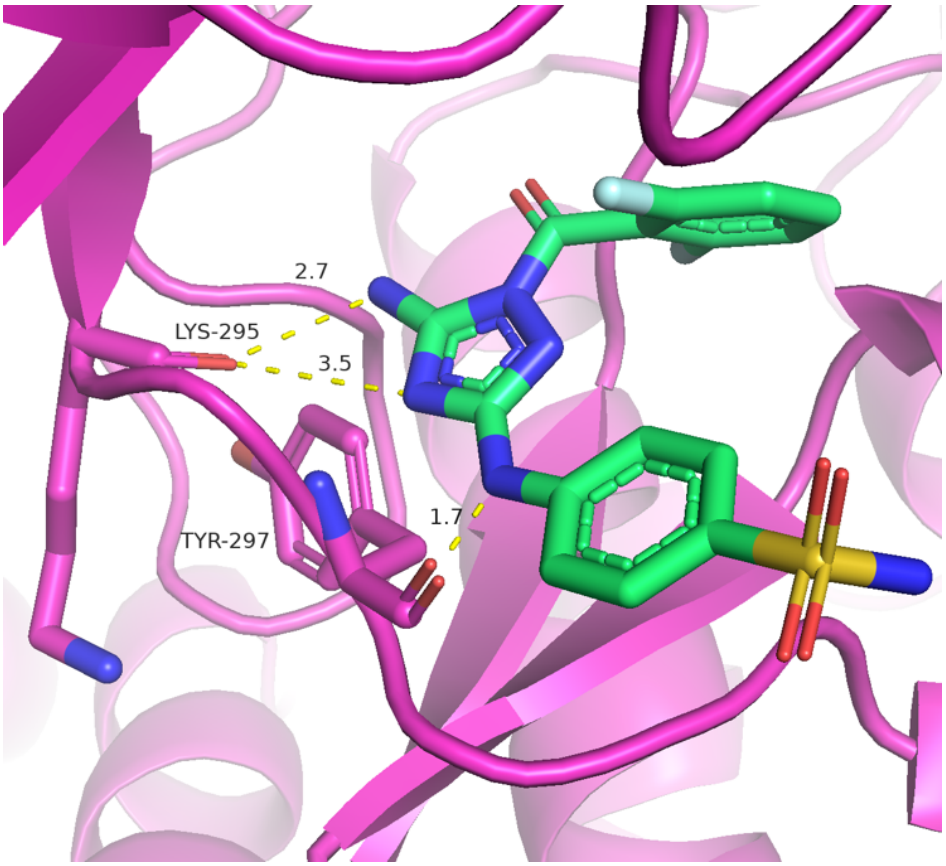

Figure 35. Model of TcPINK1^{humanized} with JNJ-7706621.

JNJ-7706621 is shown in green, nitrogens are shown in dark blue, and oxygens are shown in red. The JNJ-7706621 structure was taken from PDB 3AMA. There are three hydrogen bonds formed between residues Tyr297 and Lys295 PINK1.

In conclusion, the measurements of the IC_{50} alongside the crystal structures and modeling have revealed several key residues within PINK1 which to mediate the potency of inhibitors. The difference in potency between CYC116 and the PRT compounds is likely due to the longer bond formation with the hinge region of the protein, resulting in weaker interactions. PRT062607 forms hydrogen bonds 2.9 Å with Lys295 and Tyr297 while CYC116 form 3.8 and 3 Å bonds to the same amino acids respectively. Comparatively, JNJ-7706621 forms 3 hydrogen bonds with the hinge region, at 1.7, 2.1 and 2.7 Å and

thus forms tighter interactions compared to CYC116. This notion is also reflected in the IC_{50} values as CYC116's IC_{50} is 76.7 ± 1.1 μM while JNJ-7706621's is 30.4 ± 1.2 μM. The difference in the IC_{50} between PRT062607 and PRT060318 is potentially due to the lack of the triazole on the PRT060318, which would interact with residue N300T (one of the twelve mutations). In TcPINK1, this change in IC_{50} is not seen between the PRT compounds, indicating that N300 in TcPINK1 might not be as important in ligand binding/mediating interactions as its counterpart in HsPINK1.

4. Discussion

PINK1 is an important ubiquitin kinase required for the clearance of damaged mitochondria and is an important potential therapeutic target for the treatment of PD. Currently, there is a lack of small molecules which can target PINK1, which makes it a novel avenue. The goal of this project has been the characterization of several inhibitors against TcPINK1, and the development of an alternative humanized construct to investigate human selectivity. Consequently, the small molecule inhibitors identified in a TSA screen were tested against TcPINK1 in order to identify residues and determine the mode of inhibition of these inhibitors. As seen in figure 15, several compounds that were identified as stabilizers of TcPINK1 inhibit TcPINK1, and a Western blot in Figure 16 revealed that some of the hits also inhibit HsPINK1. Among those, only PRT062607 and its derivatives were potent inhibitors of both TcPINK1 and HsPINK1.

To further develop potent and selective inhibitors of PINK1, it was important to narrow down the hits obtained to those which are the most potent against PINK1. Therefore, to quantitively determine their potency, the IC_{50}'s of the inhibitors were measured and compared. The Kinase Glo assay provides a more precise measurement of IC_{50}'s and of kinase activity as it does not rely on the presence of an end-product, but rather the consumption of ATP. A summary of the values obtained is shown in Table 1. The assays used both unphosphorylated and phosphorylated forms of the protein to determine whether autophosphorylation at S205 would affect the IC_{50}, but we found no significant differences between the two for PRT062607.

Table 1 Summary table of IC_{50}'s at variable Hill coefficients of different inhibitors against TcPINK1 and TcPINK1^{humanized}

Compound	Protein	IC_{50} ± S.E. (μM) (Hill = 1)	IC_{50} ± S.E. (μM) (variable)	Hill ± S.E.
PRT062607	TcPINK1	1.6 ± 1.2	1.7 ± 1.0	2.2 ± 0.2
PRT060318	TcPINK1	2.5 ± 1.2	2.5 ± 1.1	2.0 ± 0.2
JNJ-7706621	TcPINK1	30.4 ± 1.2	27.7 ± 1.1	2.0 ± 0.2
CYC116	TcPINK1	76.7 ± 1.1	65.4 ± 1.1	1.5 ± 0.2
TAK659	TcPINK1	7.2 ± 1.1	6.4 ± 1.0	1.3 ± 0.1
PRT062607	Phospho-TcPINK1	2.1 ± 1.1	2.1 ± 1.0	1.9 ± 0.1
PRT062607	TcPINK1^{humanized}	1.5 ± 1.1	1.5 ± 1.1	1.6 ± 0.2
PRT060318	TcPINK1^{humanized}	18.1 ± 1.3	13.7 ± 1.1	2.2 ± 0.4

Using the Kinase Glo data obtained without inhibitor, I was also able to estimate the catalytic efficiency of ATP hydrolysis by PINK1. Table 2 shows that the rate of catalysis of unphosphorylated and phosphorylated TcPINK1 are 1.82 and 1.94 min^{-1}. This indicates that autophosphorylation does not affect the rate of ATP hydrolysis. However, the catalytic efficiency of TcPINK1^{humanized} is 0.59 min^{-1}, about 3-fold lower than TcPINK1. To compensate for the slower rate of catalysis, the TcPINK1^{humanized} protein was incubated in reactions for 15 minutes instead of 5 minutes. Another factor to consider is that autophosphorylation will also take place under our assay conditions. “Futile” ATP hydrolysis rate is slower than the rate of autophosphorylation, which was measured to be 43.5 min^{-1} (Rasool et al. 2022). With an autophosphorylation K_m of 6.7 μM and enzyme concentration of 1 μM, the initial reaction velocity will be equal to 6 μM/min, and thus most

TcPINK1 will be autophosphorylated in 5 min at ATP concentrations above the K_m for ATP (around 70-80 μM).

Table 2 k_{cat} comparison between TcPINK1 unphosphorylated, monophosphorylated and TcPINK1^{humanized} unphosphorylated

Protein	k_{cat} (min^{-1})
TcPINK1 unphosphorylated	1.82
TcPINK1 monophosphorylated	1.94
TcPINK1^{humanized} unphosphorylated	0.59

The kinase glo assay was then used to measure the IC_{50}'s of the inhibitors with the unphosphorylated protein (Table 1). The IC_{50} for PRT062607 was measured to be 1.6 ± 1.2 μM, making it the most potent of the inhibitors tested and a candidate for further drug development, followed by PRT060318 with an IC_{50} of 2.5 ± 1.2 μM for TcPINK1. PRT062607 and PRT060318 were originally discovered as a spleen tyrosine kinase (SYK) inhibitor with an IC_{50} of 1 nM (Coffey et al., 2012). SYK is known for its role in B cell lymphoma mediated signalling (Cornall et al., 2000). Despite its relatively high potency for PINK1, PRT062607 is not specific for PINK1, with tyrosine kinases being the main targets, with IC_{50}'s in the nanomolar range for SYK (1 nM), FGR 81 nM), and MLK1 (88 nM) (Coffey et al., 2012). In the literature, PRT060318 is also a potent inhibitor of SYK at 4 nM. Both inhibitors prevent thrombocytopenia and thrombosis in transgenic mouse models (Reilly et al., 2011). In vitro studies of both PRT062607 and PRT060318 reveal that they are inhibit chemokine secretion and leukemia cell

migration after B-cell receptor activation, acting as antagonist to the chronic lymphocytic leukemia (CLL) cell survival (Hoellenriegel et al., 2012). These compounds are currently being investigated as therapeutics for CLL, B-cell malignancies and autoimmune disorders. A phase 2 clinical trial was completed for PRT062607 however results of the trial are not posted. SYK inhibitors are developed to treat hematological malignancies and rheumatoid arthritis, currently SYK inhibitor fostamatinib is FDA approved for use in patient with chronic immune thrombocytopenia (Mullard, 2018). PRT062607 thus needs to be modified in order to gain more specificity towards PINK1 and to eliminate any off-target effects against tyrosine kinases. Strategies to improve the target specificity of PRT062607 are provided later in this discussion. Given their high potency against PINK1, they serve as good small molecules for the development of more specific compounds.

Comparatively, the IC_{50} of CYC116 against TcPINK1 was 76.7 ± 1.1 μM. CYC116 inhibits the Aurora Ser/Thr kinases (A, B and C) and the vascular endothelial growth factor receptor 2 in vitro and has been shown to delay tumour growth in vivo mice model (Wang et al., 2010). CYC116 was undergoing phase I clinical trials in cancer patients with solid tumors, but the trial was terminated in 2021 for undisclosed reasons. CYC116 is able to inhibit TcPINK1, but not as potently as the PRT compounds, which is why CYC116 will not be used for further inhibitor development.

The IC_{50} of TAK659 for TcPINK1 is 7.2 ± 1.1 μM. This compound was originally found to reversible inhibit of SYK at 3 nM and FMS-like tyrosine kinase 3 (FLTK3) (Lam et al.,

2016). Similarly to the PRT compounds, TAK659 also inhibits CLL proliferation after B-cell receptor activation in cells (Purroy et al., 2017). TAK659 is currently in phase 2 trials for acute myelogenous leukemia treatment (Phillips et al., 2019).

The IC_{50} of JNJ-7706621 against TcPINK1 is 30.4 ± 1.2 μM. This compound is a dual inhibitor of cyclin dependent kinases (CDK1 and CDK2) and Aurora kinases (Emanuel et al., 2005), which are two Ser/Thr kinases. In human cancer cells, JNJ-7706621 was able to inhibit cell growth and proliferation and at high concentration, induce cytotoxicity of the cells. Further studies demonstrate the same inhibitory activity of the compounds in human melanoma mouse models (Lin et al., 2005).

Here, we characterized a number of inhibitors against TcPINK1, using kinase assays and structural analysis, despite being characterized as potent against TcPINK1, we could not assume that these compounds would have the same effect on HsPINK1. Therefore, it is deemed necessary to test these compounds against HsPINK1 in some way. As aforementioned, HsPINK1 will not express nor remain active when purified from bacteria, thus requiring an alternative path to determine whether these compounds also inhibited HsPINK1. This was tested by an in organello assay with isolated mitochondria from cells treated with CCCP to accumulate PINK1 on their OMM. In these in organello assays, we measured the amount of end-product generation, which is a downstream measurement of PINK1's whole kinase activity. In contrast, the IC_{50} assays are performed with no Ub, and are a direct measurement of the amount of ATP PINK1 uses to carry out its activity.

Therefore, despite being a good experiment to test whether the inhibitors do affect HsPINK1, it is not the best way to measure IC_{50} of ATP competitive molecules.

Given the previous work done with these compounds, we know that they bind the ATP domain of PINK1 and act as a competitive inhibitor of ATP (Truong, 2019). Therefore, the ATP binding domain of TcPINK1 was switched with that of HsPINK1. This will permit specifically to determine the potency against the human protein and give more precise results with the Kinase Glo experiment. However, prior to performing the experiments, it is important to determine whether the TcPINK1^{humanized} construct was active and able to carry out PINK1's kinase activity.

The first experiment was to determine whether TcPINK1^{humanized} could autophosphorylate itself. The autophosphorylation assay shown in Figure 22 demonstrated that the humanized protein was indeed able to autophosphorylate. However, when comparing the TcPINK1 and TcPINK1^{humanized}, it is revealed that the humanized protein has a slower autophosphorylation mechanism compared to wild type TcPINK1. This constraint was considered in the later kinase glo studies, an equivalent time was substituted, going from 5 minutes to 15 minutes.

The second step was to determine whether the TcPINK1^{humanized} was able to phosphorylate its substrate ubiquitin. In Figure 23, we can see from the pUb blot that the TcPINK1^{humanized} was indeed able to phosphorylate Ub in the 15 minutes time scale found. Therefore, we have confirmed that the humanized protein is indeed a good alternative to

measure the inhibitors against. The IC_{50} of PRT062607 and PRT060318 have thus far been measured with the humanized protein and are represented in Table 1, comparing the IC_{50}'s of each inhibitor against the two proteins.

Structural difference between the humanized protein and TcPINK1 can be seen as their respective IC_{50} for PRT060318 were indeed different. In the case of PRT062607, the IC_{50} was 1.5 ± 1.1 μM (similar to TcPINK1 WT) and with PRT060318, it was 18.1 ± 1.3 μM (5- to 7-fold lower than for TcPINK1 WT). Despite this difference, there was no visible structural difference between TcPINK1 and TcPINK1^{humanized} and ligand interactions. However, the humanizing mutations clearly reduce the k_{cat} of TcPINK1 ATP hydrolysis by 3-fold, which indeed confirms that the ATP-binding site of the two proteins differ. The crystal structure between ligand and the humanized protein might help elucidate this difference as the in silico modelling does not point to any major differences. Of note, the triazole group of PRT062607 is close to Asn300, which corresponds to Thr324 in human. This mutation D300N in TcPINK1^{humanized}, close to the hinge region, could indeed lead to a rearrangement that reduces the catalytic efficiency of the construct, and also affect the energetics of inhibitor binding. For PRT062607, the interaction is retained, perhaps because the triazole is able to better interact with Thr than with Asn. However, these differences are subtle, and we cannot exclude that the differences could arise from the change in incubation time for KinaseGlo between WT and humanized TcPINK1.

Given our current understanding of the PINK1 protein, we have been working under the assumption that there is no cooperativity between inhibitors and the kinase, as PINK1

only has one binding pocket for ATP. Interestingly, when the Hill slope was not constrained to 1, it tended to sway towards a value of 2 (Table 1). The Hill slope is the measurement of cooperativity between the binding of a ligand and the chance for another ligand to bind the protein. A historic example of this would be hemoglobin, a protein which has 4 binding pockets for oxygen. The binding of one oxygen increased the likelihood that another oxygen would bind and so forth by increasing the affinity of the other sites for the ligand. In our case, this would potentially mean that the binding of one inhibitor molecule would induce the binding of another one and decrease ATP hydrolysis in both subunits. Since PINK1 only has one binding site, it is possible that the binding occurs in a dimer state, meaning the binding of one ligand can increase the affinity of the opposing PINK1 to bind a ligand as well. In this case, we would consider the dimerized form of the protein as our multiunit higher order complex. It is currently understood from SEC spectra that PINK1 tends to mostly form a monomer. However, it is important to investigate whether ligands induce a stable dimeric PINK1 complex in solution. To further investigate this avenue, we will measure use the analytical ultracentrifuge (AUC) to determine the state of PINK1 in solution. This could have potential implications for the development of paradoxical agonists. If the protein travels as a dimer, the binding of a ligand might not necessarily influence the opposing kinase to bind ATP and activate. If the protein travels primarily as a monomer, as is most likely the case, then binding of an inhibitor at the ATP domain may induce dimerization, which occurs with the BRAF kinase mentioned previously. It is worth noting that PINK1, when bound to another PINK1 or to Ub cannot bind ATP due to steric restriction to the binding site. In other words, ATP needs to bind the PINK1 active *before* PINK1 binds the substrate. If the ligand would bind one moiety

and induce the formation of a dimer, then the opposing PINK1 would be held in this dimer conformation and be unable to bind an ATP molecule and will then be inhibited.

Despite being able to inhibit PINK1, the above-mentioned inhibitors are not ideal for use in cells as they are even more potent against a number of other kinases and thus their use in cells could impact many pathways. There are three proposed approaches to make the PRT backbone more specific against human PINK1. Firstly, PINK1 has a conserved amino acid residue Cys166 in the glycine-rich loop of HsPINK1 which is unique and not present in any other kinases which bind PRT (Figure 36). This cysteine can be targeted by a chemical warhead placed on the cyclohexane group which would extend into the ATP binding pocket and form a covalent bond with Cys166. Secondly, the Asp366 of HsPINK1 is also conserved amongst PINK1, but not amongst the other kinases such as SYK and JAK2 which bind PRT. The addition of an amine or hydroxyl group insertion on the cyclohexane ring would form an interaction with Asp366 and thus could improve selectivity between the kinases. Thirdly, a boronic acid derivative could be used to target the autophosphorylation site Ser228 in HsPINK1 (S205 in TcPINK1) and induce and maintain dimerization.

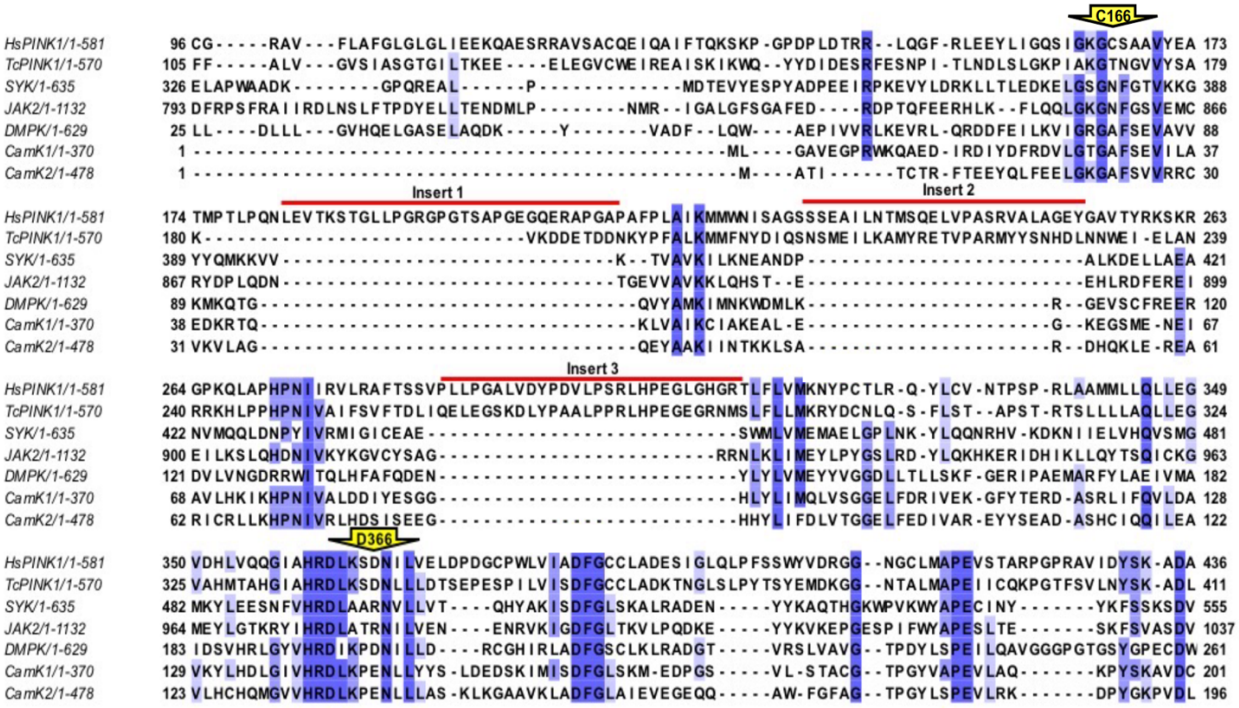

Figure 36. Comparison of sequences between PINK1 and tyrosine kinases.

C166 and D366 are present in PINK1 but are not found in any of the kinases which bind PRT062607, PRT060318 or TAK659.

The inhibitors PRT062607 and CYC116 crystallized with TcPINK1 revealed many interactions between the inhibitors and the protein. The structure of the TcPINK1-PRT062607 complex showed that main chain atoms in residues Tyr297 and Lys295 from TcPINK1 were forming hydrogen bonds with the drug, and the sidechain of Asp359 was forming a salt bridge with a positively charged amino group on the cyclohexane ring. These residues in TcPINK1 are important as they reside within the DFG motif and the hinge region which are important for the recognition and catalysis of ATP by the kinase. However, additional interactions should be mediated to confer more selectivity towards PINK1.

5. Conclusion

PINK1 is an important kinase involved in the very distinct and critical mitochondrial clearance pathway in mitochondria. Dysfunction of this protein and the downstream proteins involved in MQC cause early onset forms of PD. Therefore, a potential therapeutic strategy emerges from the pharmacological activation of this protein to remedy the accumulation of damaged mitochondria and prevent neuronal loss. One way to identify activator is to exploit the ability of certain inhibitor to paradoxically activate the kinase through stabilization of the kinase and induction of dimerization or allosteric changes in the kinase. In order to find such compounds, a thermal shift assay was performed, and multiple compounds were identified to bind TcPINK1. Quantification of their IC_{50}'s revealed that PRT062607 was the most potent inhibitor of TcPINK1. Further studies in organello confirmed that this compound also inhibited HsPINK1. Despite being unable to purify and use recombinant HsPINK1, another method was used to counter this issue. Since the crystal structure revealed that these inhibitors bound to the ATP binding domain of TcPINK1, we sought to humanize this region of TcPINK1 by inserting several mutations. The humanized construct was thus created and used for further characterization of the compounds. So far, we have found slight differences between the humanized and insect construct as the IC_{50} of inhibitors, such as PRT060318, were different. This vector will be used to continue studying the interactions of ligand to the humanized PINK1.

Given the IC_{50}'s and this new translation model, there are several additional experiments which could be done to further our investigation into a paradoxical agonist of PINK1, and

towards a better in vitro model for experiments. The next steps of this project are to determine whether PINK1 does form a dimer in solution with and without ligands to determine if cooperativity is a factor which should be considered in the future. There are many strategies that are left to explore in order to design a more potent and selective inhibitor of PINK1 while minimizing any chance of off target effects. This novel inhibitor can then be used in cells and animals PD models such as in rats. Finally, determining the crystal structure of the humanized TcPINK1 in complex with the ligands will allow us to have a better understanding of the intricate differences between this domain in the orthologues. Moreover, this humanized PINK1 could potentially be further humanized by changing certain domain and comparing solubility and stability.

In conclusion, these experiments have been helpful in characterizing the potency of several compounds against TcPINK1, and against a humanized alternative of PINK1. This provides both a new therapeutic and experimental avenue to design compounds selective and potent against PINK1 and provides a new way to approach the issues revolving around the use of HsPINK1.

6. References List (in alphabetical order)

Abeliovich, A., Schmitz, Y., Farinas, I., Choi-Lundberg, D., Ho, W. H., Castillo, P. E., Shinsky, N., Verdugo, J. M., Armanini, M., Ryan, A., Hynes, M., Phillips, H., Sulzer, D., & Rosenthal, A. (2000). Mice lacking alpha-synuclein display functional deficits in the nigrostriatal dopamine system. *Neuron*, *25*(1), 239-252. https://doi.org/10.1016/s0896-6273(00)80886-7

Attwood, M. M., Fabbro, D., Sokolov, A. V., Knapp, S., & Schioth, H. B. (2021). Trends in kinase drug discovery: targets, indications and inhibitor design. *Nat Rev Drug Discov*, *20*(11), 839-861. https://doi.org/10.1038/s41573-021-00252-y

Bender, A., Krishnan, K. J., Morris, C. M., Taylor, G. A., Reeve, A. K., Perry, R. H., Jaros, E., Hersheson, J. S., Betts, J., Klopstock, T., Taylor, R. W., & Turnbull, D. M. (2006). High levels of mitochondrial DNA deletions in substantia nigra neurons in aging and Parkinson disease. *Nat Genet*, *38*(5), 515-517. https://doi.org/10.1038/ng1769

Bereczki, D. (2010). The description of all four cardinal signs of Parkinson's disease in a Hungarian medical text published in 1690. *Parkinsonism Relat Disord*, *16*(4), 290-293. https://doi.org/10.1016/j.parkreldis.2009.11.006

Berridge, M. J. (1998). Neuronal calcium signaling. *Neuron*, *21*(1), 13-26. https://doi.org/10.1016/s0896-6273(00)80510-3

Betarbet, R., Canet-Aviles, R. M., Sherer, T. B., Mastroberardino, P. G., McLendon, C., Kim, J. H., Lund, S., Na, H. M., Taylor, G., Bence, N. F., Kopito, R., Seo, B. B., Yagi, T., Yagi, A., Klinefelter, G., Cookson, M. R., & Greenamyre, J. T. (2006). Intersecting pathways to neurodegeneration in Parkinson's disease: effects of the pesticide rotenone on DJ-1, alpha-synuclein, and the ubiquitin-proteasome system. *Neurobiol Dis*, *22*(2), 404-420. https://doi.org/10.1016/j.nbd.2005.12.003

Botta, M. (2014). New frontiers in kinases: special issue. *ACS Med Chem Lett*, *5*(4), 270. https://doi.org/10.1021/ml500071m

Braak, H., Ghebremedhin, E., Rub, U., Bratzke, H., & Del Tredici, K. (2004). Stages in the development of Parkinson's disease-related pathology. *Cell Tissue Res*, *318*(1), 121-134. https://doi.org/10.1007/s00441-004-0956-9

Brix, J., Dietmeier, K., & Pfanner, N. (1997). Differential recognition of preproteins by the purified cytosolic domains of the mitochondrial import receptors Tom20, Tom22, and Tom70. *J Biol Chem*, *272*(33), 20730-20735. https://doi.org/10.1074/jbc.272.33.20730

Burke, W. J., Kumar, V. B., Pandey, N., Panneton, W. M., Gan, Q., Franko, M. W., O'Dell, M., Li, S. W., Pan, Y., Chung, H. D., & Galvin, J. E. (2008). Aggregation of alpha-synuclein by DOPAL, the monoamine oxidase metabolite of dopamine. *Acta Neuropathol*, *115*(2), 193-203. https://doi.org/10.1007/s00401-007-0303-9

Burman, J. L., Pickles, S., Wang, C., Sekine, S., Vargas, J. N. S., Zhang, Z., Youle, A. M., Nezich, C. L., Wu, X., Hammer, J. A., & Youle, R. J. (2017). Mitochondrial fission facilitates the selective mitophagy of protein aggregates. *J Cell Biol*, *216*(10), 3231-3247. https://doi.org/10.1083/jcb.201612106

Cardona, F., Sanchez-Mut, J. V., Dopazo, H., & Perez-Tur, J. (2011). Phylogenetic and in silico structural analysis of the Parkinson disease-related kinase PINK1. *Hum Mutat*, *32*(4), 369-378. https://doi.org/10.1002/humu.21444

Caumont-Sarcos, A., Moulin, C., Poinot, L., Guiard, B., van der Laan, M., & Ieva, R. (2020). Transmembrane Coordination of Preprotein Recognition and Motor Coupling by the Mitochondrial Presequence Receptor Tim50. *Cell Rep*, *30*(9), 3092-3104 e3094. https://doi.org/10.1016/j.celrep.2020.02.031

Chang, D., Nalls, M. A., Hallgrimsdottir, I. B., Hunkapiller, J., van der Brug, M., Cai, F., International Parkinson's Disease Genomics, C., andMe Research, T., Kerchner, G. A., Ayalon, G., Bingol, B., Sheng, M., Hinds, D., Behrens, T. W., Singleton, A. B., Bhangale, T. R., & Graham, R. R. (2017). A meta-analysis of genome-wide association studies identifies 17 new Parkinson's disease risk loci. *Nat Genet*, *49*(10), 1511-1516. https://doi.org/10.1038/ng.3955

Cheng, S., & Niv, M. Y. (2010). Molecular dynamics simulations and elastic network analysis of protein kinase B (Akt/PKB) inactivation. *J Chem Inf Model*, *50*(9), 1602-1610. https://doi.org/10.1021/ci100076j

Clark, I. E., Dodson, M. W., Jiang, C., Cao, J. H., Huh, J. R., Seol, J. H., Yoo, S. J., Hay, B. A., & Guo, M. (2006). Drosophila pink1 is required for mitochondrial function and interacts genetically with parkin. *Nature*, *441*(7097), 1162-1166. https://doi.org/10.1038/nature04779

Coffey, G., DeGuzman, F., Inagaki, M., Pak, Y., Delaney, S. M., Ives, D., Betz, A., Jia, Z. J., Pandey, A., Baker, D., Hollenbach, S. J., Phillips, D. R., & Sinha, U. (2012). Specific inhibition of spleen tyrosine kinase suppresses leukocyte immune function and inflammation in animal models of rheumatoid arthritis. *J Pharmacol Exp Ther*, *340*(2), 350-359. https://doi.org/10.1124/jpet.111.188441

Contin, M., & Martinelli, P. (2010). Pharmacokinetics of levodopa. *J Neurol*, *257*(Suppl 2), S253-261. https://doi.org/10.1007/s00415-010-5728-8

Conway, K. A., Lee, S. J., Rochet, J. C., Ding, T. T., Williamson, R. E., & Lansbury, P. T., Jr. (2000). Acceleration of oligomerization, not fibrillization, is a shared property of both alpha-synuclein mutations linked to early-onset Parkinson's disease: implications for pathogenesis and therapy. *Proc Natl Acad Sci U S A*, *97*(2), 571-576. https://doi.org/10.1073/pnas.97.2.571

Cookson, M. R. (2010). The role of leucine-rich repeat kinase 2 (LRRK2) in Parkinson's disease. *Nat Rev Neurosci*, *11*(12), 791-797. https://doi.org/10.1038/nrn2935

Cornall, R. J., Cheng, A. M., Pawson, T., & Goodnow, C. C. (2000). Role of Syk in B-cell development and antigen-receptor signaling. *Proc Natl Acad Sci U S A*, *97*(4), 1713-1718. https://doi.org/10.1073/pnas.97.4.1713

Cotzias, G. C., Papavasiliou, P. S., & Gellene, R. (1969). Modification of Parkinsonism--chronic treatment with L-dopa. *N Engl J Med*, *280*(7), 337-345. https://doi.org/10.1056/NEJM196902132800701

Dar, A. C., & Shokat, K. M. (2011). The evolution of protein kinase inhibitors from antagonists to agonists of cellular signaling. *Annu Rev Biochem*, *80*, 769-795. https://doi.org/10.1146/annurev-biochem-090308-173656

Dauer, W., & Ho, C. C. (2010). The biology and pathology of the familial Parkinson's disease protein LRRK2. *Mov Disord*, *25 Suppl 1*, S40-43. https://doi.org/10.1002/mds.22717

Dauer, W., & Przedborski, S. (2003). Parkinson's disease: mechanisms and models. *Neuron*, *39*(6), 889-909. https://doi.org/10.1016/s0896-6273(03)00568-3

de Brito, O. M., & Scorrano, L. (2008). Mitofusin 2 tethers endoplasmic reticulum to mitochondria. *Nature*, *456*(7222), 605-610. https://doi.org/10.1038/nature07534

Deas, E., Plun-Favreau, H., Gandhi, S., Desmond, H., Kjaer, S., Loh, S. H., Renton, A. E., Harvey, R. J., Whitworth, A. J., Martins, L. M., Abramov, A. Y., & Wood, N. W. (2011). PINK1 cleavage at position A103 by the mitochondrial protease PARL. *Hum Mol Genet*, *20*(5), 867-879. https://doi.org/10.1093/hmg/ddq526

Diao, J., Burre, J., Vivona, S., Cipriano, D. J., Sharma, M., Kyoung, M., Sudhof, T. C., & Brunger, A. T. (2013). Native alpha-synuclein induces clustering of synaptic-vesicle mimics via binding to phospholipids and synaptobrevin-2/VAMP2. *Elife*, *2*, e00592. https://doi.org/10.7554/eLife.00592

Dick, F. D., De Palma, G., Ahmadi, A., Scott, N. W., Prescott, G. J., Bennett, J., Semple, S., Dick, S., Counsell, C., Mozzoni, P., Haites, N., Wettinger, S. B., Mutti, A., Otelea, M., Seaton, A., Soderkvist, P., Felice, A., & Geoparkinson study, g. (2007). Environmental risk factors for Parkinson's disease and parkinsonism: the Geoparkinson study. *Occup Environ Med*, *64*(10), 666-672. https://doi.org/10.1136/oem.2006.027003

Dzamko, N., Inesta-Vaquera, F., Zhang, J., Xie, C., Cai, H., Arthur, S., Tan, L., Choi, H., Gray, N., Cohen, P., Pedrioli, P., Clark, K., & Alessi, D. R. (2012). The IkappaB kinase family phosphorylates the Parkinson's disease kinase LRRK2 at Ser935 and Ser910 during Toll-like receptor signaling. *PLoS One*, *7*(6), e39132. https://doi.org/10.1371/journal.pone.0039132

Emanuel, S., Rugg, C. A., Gruninger, R. H., Lin, R., Fuentes-Pesquera, A., Connolly, P. J., Wetter, S. K., Hollister, B., Kruger, W. W., Napier, C., Jolliffe, L., & Middleton, S. A. (2005). The in vitro and in vivo effects of JNJ-7706621: a dual inhibitor of cyclin-dependent kinases and aurora kinases. *Cancer Res*, *65*(19), 9038-9046. https://doi.org/10.1158/0008-5472.CAN-05-0882

Erecinska, M., & Silver, I. A. (1989). ATP and brain function. *J Cereb Blood Flow Metab*, *9*(1), 2-19. https://doi.org/10.1038/jcbfm.1989.2

Fabbro, D., Cowan-Jacob, S. W., & Moebitz, H. (2015). Ten things you should know about protein kinases: IUPHAR Review 14. *Br J Pharmacol*, *172*(11), 2675-2700. https://doi.org/10.1111/bph.13096

Fedorov, O., Muller, S., & Knapp, S. (2010). The (un)targeted cancer kinome. *Nat Chem Biol*, *6*(3), 166-169. https://doi.org/10.1038/nchembio.297
Fedorov, O., Niesen, F. H., & Knapp, S. (2012). Kinase inhibitor selectivity profiling using differential scanning fluorimetry. *Methods Mol Biol*, *795*, 109-118. https://doi.org/10.1007/978-1-61779-337-0_7
Ferguson, F. M., & Gray, N. S. (2018). Kinase inhibitors: the road ahead. *Nat Rev Drug Discov*, *17*(5), 353-377. https://doi.org/10.1038/nrd.2018.21
Gloeckner, C. J., Schumacher, A., Boldt, K., & Ueffing, M. (2009). The Parkinson disease-associated protein kinase LRRK2 exhibits MAPKKK activity and phosphorylates MKK3/6 and MKK4/7, in vitro. *J Neurochem*, *109*(4), 959-968. https://doi.org/10.1111/j.1471-4159.2009.06024.x
Greene, A. W., Grenier, K., Aguileta, M. A., Muise, S., Farazifard, R., Haque, M. E., McBride, H. M., Park, D. S., & Fon, E. A. (2012). Mitochondrial processing peptidase regulates PINK1 processing, import and Parkin recruitment. *EMBO Rep*, *13*(4), 378-385. https://doi.org/10.1038/embor.2012.14
Greene, J. C., Whitworth, A. J., Kuo, I., Andrews, L. A., Feany, M. B., & Pallanck, L. J. (2003). Mitochondrial pathology and apoptotic muscle degeneration in Drosophila parkin mutants. *Proc Natl Acad Sci U S A*, *100*(7), 4078-4083. https://doi.org/10.1073/pnas.0737556100
Grimes, D., Gordon, J., Snelgrove, B., Lim-Carter, I., Fon, E., Martin, W., Wieler, M., Suchowersky, O., Rajput, A., Lafontaine, A. L., Stoessl, J., Moro, E., Schoffer, K., Miyasaki, J., Hobson, D., Mahmoudi, M., Fox, S., Postuma, R., Kumar, H., . . . Canadian Nourological Sciences, F. (2012). Canadian Guidelines on Parkinson's Disease. *Can J Neurol Sci*, *39*(4 Suppl 4), S1-30. https://doi.org/10.1017/s031716710001516x
Guo, C., Sun, L., Chen, X., & Zhang, D. (2013). Oxidative stress, mitochondrial damage and neurodegenerative diseases. *Neural Regen Res*, *8*(21), 2003-2014. https://doi.org/10.3969/j.issn.1673-5374.2013.21.009
Guzman, J. N., Sanchez-Padilla, J., Wokosin, D., Kondapalli, J., Ilijic, E., Schumacker, P. T., & Surmeier, D. J. (2015). Corrigendum: Oxidant stress evoked by pacemaking in dopaminergic neurons is attenuated by DJ-1. *Nature*, *521*(7552), 380. https://doi.org/10.1038/nature14487
Hall-Jackson, C. A., Eyers, P. A., Cohen, P., Goedert, M., Boyle, F. T., Hewitt, N., Plant, H., & Hedge, P. (1999). Paradoxical activation of Raf by a novel Raf inhibitor. *Chem Biol*, *6*(8), 559-568. https://doi.org/10.1016/s1074-5521(99)80088-x
Hardy, J. (2010). Genetic analysis of pathways to Parkinson disease. *Neuron*, *68*(2), 201-206. https://doi.org/10.1016/j.neuron.2010.10.014
Hoellenriegel, J., Coffey, G. P., Sinha, U., Pandey, A., Sivina, M., Ferrajoli, A., Ravandi, F., Wierda, W. G., O'Brien, S., Keating, M. J., & Burger, J. A. (2012). Selective, novel spleen tyrosine kinase (Syk) inhibitors suppress chronic lymphocytic leukemia B-cell activation and migration. *Leukemia*, *26*(7), 1576-1583. https://doi.org/10.1038/leu.2012.24
Ibanez, P., Lesage, S., Lohmann, E., Thobois, S., De Michele, G., Borg, M., Agid, Y., Durr, A., Brice, A., & French Parkinson's Disease Genetics Study, G. (2006). Mutational analysis of the PINK1 gene in early-onset parkinsonism in Europe and North Africa. *Brain*, *129*(Pt 3), 686-694. https://doi.org/10.1093/brain/awl005
Jin, S. M., Lazarou, M., Wang, C., Kane, L. A., Narendra, D. P., & Youle, R. J. (2010). Mitochondrial membrane potential regulates PINK1 import and proteolytic destabilization by PARL. *J Cell Biol*, *191*(5), 933-942. https://doi.org/10.1083/jcb.201008084
Jin, S. M., & Youle, R. J. (2013). The accumulation of misfolded proteins in the mitochondrial matrix is sensed by PINK1 to induce PARK2/Parkin-mediated mitophagy of polarized mitochondria. *Autophagy*, *9*(11), 1750-1757. https://doi.org/10.4161/auto.26122
Kasemsuk, C., Oyama, G., & Hattori, N. (2017). Management of impulse control disorders with deep brain stimulation: A double-edged sword. *J Neurol Sci*, *374*, 63-68. https://doi.org/10.1016/j.jns.2017.01.019
Kitada, T., Asakawa, S., Hattori, N., Matsumine, H., Yamamura, Y., Minoshima, S., Yokochi, M., Mizuno, Y., & Shimizu, N. (1998). Mutations in the parkin gene cause autosomal recessive juvenile parkinsonism. *Nature*, *392*(6676), 605-608. https://doi.org/10.1038/33416
Kondapalli, C., Kazlauskaite, A., Zhang, N., Woodroof, H. I., Campbell, D. G., Gourlay, R., Burchell, L., Walden, H., Macartney, T. J., Deak, M., Knebel, A., Alessi, D. R., & Muqit, M. M. (2012). PINK1 is activated by mitochondrial membrane potential depolarization and stimulates Parkin E3 ligase

activity by phosphorylating Serine 65. *Open Biol*, *2*(5), 120080. https://doi.org/10.1098/rsob.120080
Kumar, A., Tamjar, J., Waddell, A. D., Woodroof, H. I., Raimi, O. G., Shaw, A. M., Peggie, M., Muqit, M. M., & van Aalten, D. M. (2017). Structure of PINK1 and mechanisms of Parkinson's disease-associated mutations. *Elife*, *6*. https://doi.org/10.7554/eLife.29985
Lam, B., Arikawa, Y., Cramlett, J., Dong, Q., de Jong, R., Feher, V., Grimshaw, C. E., Farrell, P. J., Hoffman, I. D., Jennings, A., Jones, B., Matuszkiewicz, J., Miura, J., Miyake, H., Natala, S. R., Shi, L., Takahashi, M., Taylor, E., Wyrick, C., . . . Nie, Z. (2016). Discovery of TAK-659 an orally available investigational inhibitor of Spleen Tyrosine Kinase (SYK). *Bioorg Med Chem Lett*, *26*(24), 5947-5950. https://doi.org/10.1016/j.bmcl.2016.10.087
Langston, J. W. (1987). MPTP: insights into the etiology of Parkinson's disease. *Eur Neurol*, *26 Suppl 1*, 2-10. https://doi.org/10.1159/000116349
Langston, J. W. (2017). The MPTP Story. *J Parkinsons Dis*, *7*(s1), S11-S19. https://doi.org/10.3233/JPD-179006
Lavoie, H., Li, J. J., Thevakumaran, N., Therrien, M., & Sicheri, F. (2014). Dimerization-induced allostery in protein kinase regulation. *Trends Biochem Sci*, *39*(10), 475-486. https://doi.org/10.1016/j.tibs.2014.08.004
Lazarou, M., Jin, S. M., Kane, L. A., & Youle, R. J. (2012). Role of PINK1 binding to the TOM complex and alternate intracellular membranes in recruitment and activation of the E3 ligase Parkin. *Dev Cell*, *22*(2), 320-333. https://doi.org/10.1016/j.devcel.2011.12.014
Lazarou, M., Sliter, D. A., Kane, L. A., Sarraf, S. A., Wang, C., Burman, J. L., Sideris, D. P., Fogel, A. I., & Youle, R. J. (2015). The ubiquitin kinase PINK1 recruits autophagy receptors to induce mitophagy. *Nature*, *524*(7565), 309-314. https://doi.org/10.1038/nature14893
Lesage, S., Ibanez, P., Lohmann, E., Pollak, P., Tison, F., Tazir, M., Leutenegger, A. L., Guimaraes, J., Bonnet, A. M., Agid, Y., Durr, A., Brice, A., & French Parkinson's Disease Genetics Study, G. (2005). G2019S LRRK2 mutation in French and North African families with Parkinson's disease. *Ann Neurol*, *58*(5), 784-787. https://doi.org/10.1002/ana.20636
Li, J. Q., Tan, L., & Yu, J. T. (2014). The role of the LRRK2 gene in Parkinsonism. *Mol Neurodegener*, *9*, 47. https://doi.org/10.1186/1750-1326-9-47
Lin, R., Connolly, P. J., Huang, S., Wetter, S. K., Lu, Y., Murray, W. V., Emanuel, S. L., Gruninger, R. H., Fuentes-Pesquera, A. R., Rugg, C. A., Middleton, S. A., & Jolliffe, L. K. (2005). 1-Acyl-1H-[1,2,4]triazole-3,5-diamine analogues as novel and potent anticancer cyclin-dependent kinase inhibitors: synthesis and evaluation of biological activities. *J Med Chem*, *48*(13), 4208-4211. https://doi.org/10.1021/jm050267e
Liu, Z., Galemmo, R. A., Jr., Fraser, K. B., Moehle, M. S., Sen, S., Volpicelli-Daley, L. A., DeLucas, L. J., Ross, L. J., Valiyaveettil, J., Moukha-Chafiq, O., Pathak, A. K., Ananthan, S., Kezar, H., White, E. L., Gupta, V., Maddry, J. A., Suto, M. J., & West, A. B. (2014). Unique functional and structural properties of the LRRK2 protein ATP-binding pocket. *J Biol Chem*, *289*(47), 32937-32951. https://doi.org/10.1074/jbc.M114.602318
Lucking, C. B., Durr, A., Bonifati, V., Vaughan, J., De Michele, G., Gasser, T., Harhangi, B. S., Meco, G., Denefle, P., Wood, N. W., Agid, Y., Brice, A., French Parkinson's Disease Genetics Study, G., & European Consortium on Genetic Susceptibility in Parkinson's, D. (2000). Association between early-onset Parkinson's disease and mutations in the parkin gene. *N Engl J Med*, *342*(21), 1560-1567. https://doi.org/10.1056/NEJM200005253422103
Madero-Perez, J., Fdez, E., Fernandez, B., Lara Ordonez, A. J., Blanca Ramirez, M., Gomez-Suaga, P., Waschbusch, D., Lobbestael, E., Baekelandt, V., Nairn, A. C., Ruiz-Martinez, J., Aiastui, A., Lopez de Munain, A., Lis, P., Comptdaer, T., Taymans, J. M., Chartier-Harlin, M. C., Beilina, A., Gonnelli, A., . . . Hilfiker, S. (2018). Parkinson disease-associated mutations in LRRK2 cause centrosomal defects via Rab8a phosphorylation. *Mol Neurodegener*, *13*(1), 3. https://doi.org/10.1186/s13024-018-0235-y
Maries, E., Dass, B., Collier, T. J., Kordower, J. H., & Steece-Collier, K. (2003). The role of alpha-synuclein in Parkinson's disease: insights from animal models. *Nat Rev Neurosci*, *4*(9), 727-738. https://doi.org/10.1038/nrn1199
Martin, I., Dawson, V. L., & Dawson, T. M. (2011). Recent advances in the genetics of Parkinson's disease. *Annu Rev Genomics Hum Genet*, *12*, 301-325. https://doi.org/10.1146/annurev-genom-082410-101440

McLelland, G. L., Goiran, T., Yi, W., Dorval, G., Chen, C. X., Lauinger, N. D., Krahn, A. I., Valimehr, S., Rakovic, A., Rouiller, I., Durcan, T. M., Trempe, J. F., & Fon, E. A. (2018). Mfn2 ubiquitination by PINK1/parkin gates the p97-dependent release of ER from mitochondria to drive mitophagy. *Elife*, *7*. https://doi.org/10.7554/eLife.32866

Mullard, A. (2018). FDA approves first-in-class SYK inhibitor. *Nat Rev Drug Discov*, *17*(6), 385. https://doi.org/10.1038/nrd.2018.96

Narendra, D., Tanaka, A., Suen, D. F., & Youle, R. J. (2008). Parkin is recruited selectively to impaired mitochondria and promotes their autophagy. *J Cell Biol*, *183*(5), 795-803. https://doi.org/10.1083/jcb.200809125

Narendra, D. P., Jin, S. M., Tanaka, A., Suen, D. F., Gautier, C. A., Shen, J., Cookson, M. R., & Youle, R. J. (2010). PINK1 is selectively stabilized on impaired mitochondria to activate Parkin. *PLoS Biol*, *8*(1), e1000298. https://doi.org/10.1371/journal.pbio.1000298

Okatsu, K., Kimura, M., Oka, T., Tanaka, K., & Matsuda, N. (2015). Unconventional PINK1 localization to the outer membrane of depolarized mitochondria drives Parkin recruitment. *J Cell Sci*, *128*(5), 964-978. https://doi.org/10.1242/jcs.161000

Okatsu, K., Sato, Y., Yamano, K., Matsuda, N., Negishi, L., Takahashi, A., Yamagata, A., Goto-Ito, S., Mishima, M., Ito, Y., Oka, T., Tanaka, K., & Fukai, S. (2018). Structural insights into ubiquitin phosphorylation by PINK1. *Sci Rep*, *8*(1), 10382. https://doi.org/10.1038/s41598-018-28656-8

Okatsu, K., Uno, M., Koyano, F., Go, E., Kimura, M., Oka, T., Tanaka, K., & Matsuda, N. (2013). A dimeric PINK1-containing complex on depolarized mitochondria stimulates Parkin recruitment. *J Biol Chem*, *288*(51), 36372-36384. https://doi.org/10.1074/jbc.M113.509653

Ordureau, A., Sarraf, S. A., Duda, D. M., Heo, J. M., Jedrychowski, M. P., Sviderskiy, V. O., Olszewski, J. L., Koerber, J. T., Xie, T., Beausoleil, S. A., Wells, J. A., Gygi, S. P., Schulman, B. A., & Harper, J. W. (2014). Quantitative proteomics reveal a feedforward mechanism for mitochondrial PARKIN translocation and ubiquitin chain synthesis. *Mol Cell*, *56*(3), 360-375. https://doi.org/10.1016/j.molcel.2014.09.007

Orr, A. L., Rutaganira, F. U., de Roulet, D., Huang, E. J., Hertz, N. T., Shokat, K. M., & Nakamura, K. (2017). Long-term oral kinetin does not protect against alpha-synuclein-induced neurodegeneration in rodent models of Parkinson's disease. *Neurochem Int*, *109*, 106-116. https://doi.org/10.1016/j.neuint.2017.04.006

Ozelius, L. J., Senthil, G., Saunders-Pullman, R., Ohmann, E., Deligtisch, A., Tagliati, M., Hunt, A. L., Klein, C., Henick, B., Hailpern, S. M., Lipton, R. B., Soto-Valencia, J., Risch, N., & Bressman, S. B. (2006). LRRK2 G2019S as a cause of Parkinson's disease in Ashkenazi Jews. *N Engl J Med*, *354*(4), 424-425. https://doi.org/10.1056/NEJMc055509

Paisan-Ruiz, C., Jain, S., Evans, E. W., Gilks, W. P., Simon, J., van der Brug, M., Lopez de Munain, A., Aparicio, S., Gil, A. M., Khan, N., Johnson, J., Martinez, J. R., Nicholl, D., Marti Carrera, I., Pena, A. S., de Silva, R., Lees, A., Marti-Masso, J. F., Perez-Tur, J., . . . Singleton, A. B. (2004). Cloning of the gene containing mutations that cause PARK8-linked Parkinson's disease. *Neuron*, *44*(4), 595-600. https://doi.org/10.1016/j.neuron.2004.10.023

Pandey, S., & Srivanitchapoom, P. (2017). Levodopa-induced Dyskinesia: Clinical Features, Pathophysiology, and Medical Management. *Ann Indian Acad Neurol*, *20*(3), 190-198. https://doi.org/10.4103/aian.AIAN_239_17

Papa, F. R., Zhang, C., Shokat, K., & Walter, P. (2003). Bypassing a kinase activity with an ATP-competitive drug. *Science*, *302*(5650), 1533-1537. https://doi.org/10.1126/science.1090031

Park, J., Lee, S. B., Lee, S., Kim, Y., Song, S., Kim, S., Bae, E., Kim, J., Shong, M., Kim, J. M., & Chung, J. (2006). Mitochondrial dysfunction in Drosophila PINK1 mutants is complemented by parkin. *Nature*, *441*(7097), 1157-1161. https://doi.org/10.1038/nature04788

Patil, C., & Walter, P. (2001). Intracellular signaling from the endoplasmic reticulum to the nucleus: the unfolded protein response in yeast and mammals. *Curr Opin Cell Biol*, *13*(3), 349-355. https://doi.org/10.1016/s0955-0674(00)00219-2

Peng, Y. H., Shiao, H. Y., Tu, C. H., Liu, P. M., Hsu, J. T., Amancha, P. K., Wu, J. S., Coumar, M. S., Chen, C. H., Wang, S. Y., Lin, W. H., Sun, H. Y., Chao, Y. S., Lyu, P. C., Hsieh, H. P., & Wu, S. Y. (2013). Protein kinase inhibitor design by targeting the Asp-Phe-Gly (DFG) motif: the role of the DFG motif in the design of epidermal growth factor receptor inhibitors. *J Med Chem*, *56*(10), 3889-3903. https://doi.org/10.1021/jm400072p

Ping, H. X., & Shepard, P. D. (1996). Apamin-sensitive Ca(2+)-activated K+ channels regulate pacemaker activity in nigral dopamine neurons. *Neuroreport*, *7*(3), 809-814. https://doi.org/10.1097/00001756-199602290-00031
Poewe, W. (2008). Non-motor symptoms in Parkinson's disease. *Eur J Neurol*, *15 Suppl 1*, 14-20. https://doi.org/10.1111/j.1468-1331.2008.02056.x
Purroy, N., Carabia, J., Abrisqueta, P., Egia, L., Aguilo, M., Carpio, C., Palacio, C., Crespo, M., & Bosch, F. (2017). Inhibition of BCR signaling using the Syk inhibitor TAK-659 prevents stroma-mediated signaling in chronic lymphocytic leukemia cells. *Oncotarget*, *8*(1), 742-756. https://doi.org/10.18632/oncotarget.13557
Puschmann, A. (2013). Monogenic Parkinson's disease and parkinsonism: clinical phenotypes and frequencies of known mutations. *Parkinsonism Relat Disord*, *19*(4), 407-415. https://doi.org/10.1016/j.parkreldis.2013.01.020
Rasool, S., Soya, N., Truong, L., Croteau, N., Lukacs, G. L., & Trempe, J. F. (2018). PINK1 autophosphorylation is required for ubiquitin recognition. *EMBO Rep*, *19*(4). https://doi.org/10.15252/embr.201744981
Rasool, S., & Trempe, J. F. (2018). New insights into the structure of PINK1 and the mechanism of ubiquitin phosphorylation. *Crit Rev Biochem Mol Biol*, *53*(5), 515-534. https://doi.org/10.1080/10409238.2018.1491525
Rasool, S., Veyron, S., Soya, N., Eldeeb, M. A., Lukacs, G. L., Fon, E. A., & Trempe, J. F. (2022). Mechanism of PINK1 activation by autophosphorylation and insights into assembly on the TOM complex. *Mol Cell*, *82*(1), 44-59 e46. https://doi.org/10.1016/j.molcel.2021.11.012
Reilly, M. P., Sinha, U., Andre, P., Taylor, S. M., Pak, Y., Deguzman, F. R., Nanda, N., Pandey, A., Stolla, M., Bergmeier, W., & McKenzie, S. E. (2011). PRT-060318, a novel Syk inhibitor, prevents heparin-induced thrombocytopenia and thrombosis in a transgenic mouse model. *Blood*, *117*(7), 2241-2246. https://doi.org/10.1182/blood-2010-03-274969
Riederer, P., Berg, D., Casadei, N., Cheng, F., Classen, J., Dresel, C., Jost, W., Kruger, R., Muller, T., Reichmann, H., Riess, O., Storch, A., Strobel, S., van Eimeren, T., Volker, H. U., Winkler, J., Winklhofer, K. F., Wullner, U., Zunke, F., & Monoranu, C. M. (2019). alpha-Synuclein in Parkinson's disease: causal or bystander? *J Neural Transm (Vienna)*, *126*(7), 815-840. https://doi.org/10.1007/s00702-019-02025-9
Rizzuto, R., & Pozzan, T. (2006). Microdomains of intracellular Ca2+: molecular determinants and functional consequences. *Physiol Rev*, *86*(1), 369-408. https://doi.org/10.1152/physrev.00004.2005
Roskoski, R., Jr. (2022). Properties of FDA-approved small molecule protein kinase inhibitors: A 2022 update. *Pharmacol Res*, *175*, 106037. https://doi.org/10.1016/j.phrs.2021.106037
Schapira, A. H., Cooper, J. M., Dexter, D., Jenner, P., Clark, J. B., & Marsden, C. D. (1989). Mitochondrial complex I deficiency in Parkinson's disease. *Lancet*, *1*(8649), 1269. https://doi.org/10.1016/s0140-6736(89)92366-0
Schubert, A. F., Gladkova, C., Pardon, E., Wagstaff, J. L., Freund, S. M. V., Steyaert, J., Maslen, S. L., & Komander, D. (2017). Structure of PINK1 in complex with its substrate ubiquitin. *Nature*, *552*(7683), 51-56. https://doi.org/10.1038/nature24645
Sekine, S., Wang, C., Sideris, D. P., Bunker, E., Zhang, Z., & Youle, R. J. (2019). Reciprocal Roles of Tom7 and OMA1 during Mitochondrial Import and Activation of PINK1. *Mol Cell*, *73*(5), 1028-1043 e1025. https://doi.org/10.1016/j.molcel.2019.01.002
Shiba-Fukushima, K., Imai, Y., Yoshida, S., Ishihama, Y., Kanao, T., Sato, S., & Hattori, N. (2012). PINK1-mediated phosphorylation of the Parkin ubiquitin-like domain primes mitochondrial translocation of Parkin and regulates mitophagy. *Sci Rep*, *2*, 1002. https://doi.org/10.1038/srep01002
Shimura, H., Hattori, N., Kubo, S., Mizuno, Y., Asakawa, S., Minoshima, S., Shimizu, N., Iwai, K., Chiba, T., Tanaka, K., & Suzuki, T. (2000). Familial Parkinson disease gene product, parkin, is a ubiquitin-protein ligase. *Nat Genet*, *25*(3), 302-305. https://doi.org/10.1038/77060
Sian-Hulsmann, J., Monoranu, C., Strobel, S., & Riederer, P. (2015). Lewy Bodies: A Spectator or Salient Killer? *CNS Neurol Disord Drug Targets*, *14*(7), 947-955. https://doi.org/10.2174/1871527314666150317225659

Siddiqui, A., Rane, A., Rajagopalan, S., Chinta, S. J., & Andersen, J. K. (2016). Detrimental effects of oxidative losses in parkin activity in a model of sporadic Parkinson's disease are attenuated by restoration of PGC1alpha. *Neurobiol Dis*, *93*, 115-120. https://doi.org/10.1016/j.nbd.2016.05.009
Silvestri, L., Caputo, V., Bellacchio, E., Atorino, L., Dallapiccola, B., Valente, E. M., & Casari, G. (2005). Mitochondrial import and enzymatic activity of PINK1 mutants associated to recessive parkinsonism. *Hum Mol Genet*, *14*(22), 3477-3492. https://doi.org/10.1093/hmg/ddi377
Sim, C. H., Gabriel, K., Mills, R. D., Culvenor, J. G., & Cheng, H. C. (2012). Analysis of the regulatory and catalytic domains of PTEN-induced kinase-1 (PINK1). *Hum Mutat*, *33*(10), 1408-1422. https://doi.org/10.1002/humu.22127
Sinemet. (1974). *Drug Ther Bull*, *12*(21), 83-84. https://www.ncbi.nlm.nih.gov/pubmed/4617660
Singleton, A. B., Farrer, M., Johnson, J., Singleton, A., Hague, S., Kachergus, J., Hulihan, M., Peuralinna, T., Dutra, A., Nussbaum, R., Lincoln, S., Crawley, A., Hanson, M., Maraganore, D., Adler, C., Cookson, M. R., Muenter, M., Baptista, M., Miller, D., . . . Gwinn-Hardy, K. (2003). alpha-Synuclein locus triplication causes Parkinson's disease. *Science*, *302*(5646), 841. https://doi.org/10.1126/science.1090278
Song, S., Jang, S., Park, J., Bang, S., Choi, S., Kwon, K. Y., Zhuang, X., Kim, E., & Chung, J. (2013). Characterization of PINK1 (PTEN-induced putative kinase 1) mutations associated with Parkinson disease in mammalian cells and Drosophila. *J Biol Chem*, *288*(8), 5660-5672. https://doi.org/10.1074/jbc.M112.430801
Steger, M., Diez, F., Dhekne, H. S., Lis, P., Nirujogi, R. S., Karayel, O., Tonelli, F., Martinez, T. N., Lorentzen, E., Pfeffer, S. R., Alessi, D. R., & Mann, M. (2017). Systematic proteomic analysis of LRRK2-mediated Rab GTPase phosphorylation establishes a connection to ciliogenesis. *Elife*, *6*. https://doi.org/10.7554/eLife.31012
Striessnig, J., Koschak, A., Sinnegger-Brauns, M. J., Hetzenauer, A., Nguyen, N. K., Busquet, P., Pelster, G., & Singewald, N. (2006). Role of voltage-gated L-type Ca2+ channel isoforms for brain function. *Biochem Soc Trans*, *34*(Pt 5), 903-909. https://doi.org/10.1042/BST0340903
Surmeier, D. J. (2007). Calcium, ageing, and neuronal vulnerability in Parkinson's disease. *Lancet Neurol*, *6*(10), 933-938. https://doi.org/10.1016/S1474-4422(07)70246-6
Szabadkai, G., Simoni, A. M., Bianchi, K., De Stefani, D., Leo, S., Wieckowski, M. R., & Rizzuto, R. (2006). Mitochondrial dynamics and Ca2+ signaling. *Biochim Biophys Acta*, *1763*(5-6), 442-449. https://doi.org/10.1016/j.bbamcr.2006.04.002
Tasaki, T., Sriram, S. M., Park, K. S., & Kwon, Y. T. (2012). The N-end rule pathway. *Annu Rev Biochem*, *81*, 261-289. https://doi.org/10.1146/annurev-biochem-051710-093308
Thomas, B., & Beal, M. F. (2007). Parkinson's disease. *Hum Mol Genet*, *16 Spec No. 2*, R183-194. https://doi.org/10.1093/hmg/ddm159
Thomas, R. E., Andrews, L. A., Burman, J. L., Lin, W. Y., & Pallanck, L. J. (2014). PINK1-Parkin pathway activity is regulated by degradation of PINK1 in the mitochondrial matrix. *PLoS Genet*, *10*(5), e1004279. https://doi.org/10.1371/journal.pgen.1004279
Tolosa, E., Garrido, A., Scholz, S. W., & Poewe, W. (2021). Challenges in the diagnosis of Parkinson's disease. *Lancet Neurol*, *20*(5), 385-397. https://doi.org/10.1016/S1474-4422(21)00030-2
Trempe, J. F., & Fon, E. A. (2013). Structure and Function of Parkin, PINK1, and DJ-1, the Three Musketeers of Neuroprotection. *Front Neurol*, *4*, 38. https://doi.org/10.3389/fneur.2013.00038
Udell, C. M., Rajakulendran, T., Sicheri, F., & Therrien, M. (2011). Mechanistic principles of RAF kinase signaling. *Cell Mol Life Sci*, *68*(4), 553-565. https://doi.org/10.1007/s00018-010-0520-6
Unoki, M., & Nakamura, Y. (2001). Growth-suppressive effects of BPOZ and EGR2, two genes involved in the PTEN signaling pathway. *Oncogene*, *20*(33), 4457-4465. https://doi.org/10.1038/sj.onc.1204608
Valente, E. M., Abou-Sleiman, P. M., Caputo, V., Muqit, M. M., Harvey, K., Gispert, S., Ali, Z., Del Turco, D., Bentivoglio, A. R., Healy, D. G., Albanese, A., Nussbaum, R., Gonzalez-Maldonado, R., Deller, T., Salvi, S., Cortelli, P., Gilks, W. P., Latchman, D. S., Harvey, R. J., . . . Wood, N. W. (2004). Hereditary early-onset Parkinson's disease caused by mutations in PINK1. *Science*, *304*(5674), 1158-1160. https://doi.org/10.1126/science.1096284
Valente, E. M., Salvi, S., Ialongo, T., Marongiu, R., Elia, A. E., Caputo, V., Romito, L., Albanese, A., Dallapiccola, B., & Bentivoglio, A. R. (2004). PINK1 mutations are associated with sporadic early-onset parkinsonism. *Ann Neurol*, *56*(3), 336-341. https://doi.org/10.1002/ana.20256

Van Laar, V. S., & Berman, S. B. (2009). Mitochondrial dynamics in Parkinson's disease. *Exp Neurol*, *218*(2), 247-256. https://doi.org/10.1016/j.expneurol.2009.03.019

Vranas, M., Lu, Y., Rasool, S., Croteau, N., Krett, J. D., Sauve, V., Gehring, K., Fon, E. A., Durcan, T. M., & Trempe, J. F. (2022). Selective localization of Mfn2 near PINK1 enables its preferential ubiquitination by Parkin on mitochondria. *Open Biol*, *12*(1), 210255. https://doi.org/10.1098/rsob.210255

Wang, C., Ko, H. S., Thomas, B., Tsang, F., Chew, K. C., Tay, S. P., Ho, M. W., Lim, T. M., Soong, T. W., Pletnikova, O., Troncoso, J., Dawson, V. L., Dawson, T. M., & Lim, K. L. (2005). Stress-induced alterations in parkin solubility promote parkin aggregation and compromise parkin's protective function. *Hum Mol Genet*, *14*(24), 3885-3897. https://doi.org/10.1093/hmg/ddi413

Wang, S., Midgley, C. A., Scaerou, F., Grabarek, J. B., Griffiths, G., Jackson, W., Kontopidis, G., McClue, S. J., McInnes, C., Meades, C., Mezna, M., Plater, A., Stuart, I., Thomas, M. P., Wood, G., Clarke, R. G., Blake, D. G., Zheleva, D. I., Lane, D. P., . . . Fischer, P. M. (2010). Discovery of N-phenyl-4-(thiazol-5-yl)pyrimidin-2-amine aurora kinase inhibitors. *J Med Chem*, *53*(11), 4367-4378. https://doi.org/10.1021/jm901913s

Wilson, C. J., & Callaway, J. C. (2000). Coupled oscillator model of the dopaminergic neuron of the substantia nigra. *J Neurophysiol*, *83*(5), 3084-3100. https://doi.org/10.1152/jn.2000.83.5.3084

Woodroof, H. I., Pogson, J. H., Begley, M., Cantley, L. C., Deak, M., Campbell, D. G., van Aalten, D. M., Whitworth, A. J., Alessi, D. R., & Muqit, M. M. (2011). Discovery of catalytically active orthologues of the Parkinson's disease kinase PINK1: analysis of substrate specificity and impact of mutations. *Open Biol*, *1*(3), 110012. https://doi.org/10.1098/rsob.110012

Wu, D., Qu, L., Fu, Y., Li, J., Jiang, L., Chen, X., Guo, M., Chen, Z., Chen, L., & Chen, Y. (2016). Expression and purification of the kinase domain of PINK1 in Pichia pastoris. *Protein Expr Purif*, *128*, 67-72. https://doi.org/10.1016/j.pep.2016.08.010

Yamano, K., & Youle, R. J. (2013). PINK1 is degraded through the N-end rule pathway. *Autophagy*, *9*(11), 1758-1769. https://doi.org/10.4161/auto.24633

Zimprich, A., Biskup, S., Leitner, P., Lichtner, P., Farrer, M., Lincoln, S., Kachergus, J., Hulihan, M., Uitti, R. J., Calne, D. B., Stoessl, A. J., Pfeiffer, R. F., Patenge, N., Carbajal, I. C., Vieregge, P., Asmus, F., Muller-Myhsok, B., Dickson, D. W., Meitinger, T., . . . Gasser, T. (2004). Mutations in LRRK2 cause autosomal-dominant parkinsonism with pleomorphic pathology. *Neuron*, *44*(4), 601-607. https://doi.org/10.1016/j.neuron.2004.11.005